Инженерная школа ядерных технологий
Направление подготовки 14.04.02 Ядерные физика и технологии
Научно-образовательный центр международного ядерного образования и карьерного сопровождения иностранных студентов ТПУ

МАГИСТЕРСКАЯ ДИССЕРТАЦИЯ

Тема работы

Когерентное излучение последовательностей сгустков заряженных частиц на современных ускорителях

УДК 621.384.6:539.12.2-18

Студент

Группа	ФИО	Подпись	Дата
0АМ1М	Токтаганова Маржан Мейрамхановна		

Руководитель ВКР

Должность	ФИО	Ученая степень, звание	Подпись	Дата
Научный сотрудник ИШФВП	Шкитов Д.А.	к.ф.-м.н.		

Консультант

Должность	ФИО	Ученая степень, звание	Подпись	Дата
Старший научный сотрудник МНОЛ РО, ИЯТШ	Шевелев М.В.	к.ф.-м.н.		

КОНСУЛЬТАНТЫ ПО РАЗДЕЛАМ:

По разделу «Финансовый менеджмент, ресурсоэффективность и ресурсосбережение»

Должность	ФИО	Ученая степень, звание	Подпись	Дата
Доцент ОСГН ШИП	Меньшикова Е.В.	к.ф.н.		

По разделу «Социальная ответственность»

Должность	ФИО	Ученая степень, звание	Подпись	Дата
Доцент ОЯТЦ ИЯТШ	Передерин Ю.В.	к.т.н		

ДОПУСТИТЬ К ЗАЩИТЕ:

Руководитель ООП	ФИО	Ученая степень, звание	Подпись	Дата
Nuclear medicine / Ядерная медицина	Верхотурова В.В.	к.и.н.		

Томск – 2023 г.

TOMSK POLYTECHNIC UNIVERSITY | **ТОМСКИЙ ПОЛИТЕХНИЧЕСКИЙ УНИВЕРСИТЕТ**

School of Nuclear Science & Engineering
Field of training: 14.04.02 Nuclear Science and Technology
Specialization: Nuclear medicine
Research and Training Centre for International Nuclear Education and Career, School of Nuclear Engineering

MASTER THESIS

Topic of research work
Coherent radiation of charged particles bunch trains at modern accelerators

UDC 621.384.6:539.12.2-18

Student

Group	Full name	Signature	Date
0AM1M	Marzhan M. Toktaganova		

Scientific supervisor

Position	Full name	Academic degree, academic rank	Signature	Date
Researcher	Dmitry A. Shkitov	PhD		

Adviser

Position	Full name	Academic degree, academic rank	Signature	Date
Senior Research Fellow	Mikhail V. Shevelev	PhD		

ADVISERS:

Section "Financial Management, Resource Efficiency and Resource Saving"

Position	Full name	Academic degree, academic rank	Signature	Date
Associate Professor	Ekaterina V. Menshikova	PhD		

Section "Social Responsibility"

Position	Full name	Academic degree, academic rank	Signature	Date
Associate Professor	Yuriy V. Perederin	PhD		

ADMITTED TO DEFENSE:

Programme Director	Full name	Academic degree, academic rank	Signature	Date
Nuclear medicine	Vera V. Verkhoturova	PhD		

Tomsk – 2023

LEARNING OUTCOMES

Competence code	Competence name
Universal competences	
UC(U)-1	Ability to make critical analysis of problem-based situations using the systems analysis approach, and generate decisions and action plans.
UC(U)-2	Ability to run a project at all life-cycle stages.
UC(U)-3	Ability to organize and lead the teamwork and generate a team strategy to achieve the target goal.
UC(U)-4	Ability to use modern communication technologies to realize academic and professional interaction.
UC(U)-5	Ability to analyze and account for cultural diversity in the process of intercultural interaction.
UC(U)-6	Ability to set and pursue individual and professional activity priorities and ways to modify professional activity based on the self-esteem.
General professional competences	
GPC(U)-1	Ability to formulate goals and objectives of the research study, select assessment criteria, identify priorities for solving problems.
GPC(U)-2	Ability to apply modern research methods, evaluate and present the results of the performed research.
GPC(U)-3	Ability to present research outcomes in the form of articles, reports, scientific reports and presentations using computer layout systems and office software packages.
Professional competences	
PC(U)-1	Ability to maintain medical and technical documentation related to medico-physical aspects of radiation therapy, interventional radiology and radionuclide diagnostics and therapy.
PC(U)-2	Ability to ensure radiation safety of personnel, public, and the environment, to carry out monitoring of radiation exposure levels of patients, personnel, public, and the environment.
PC(U)-3	Ability to operate and maintain equipment and tools applied for the medical use of radiation.
PC(U)-4	Ability to manage the quality of physical and technical aspects within radiation therapy, diagnostics, interventional radiology and radionuclide diagnostics and therapy departments in accordance with the specific equipment requirements, regulatory requirements and staffing of a medical organization.
PC(U)-5	Ability to conduct and organize dosimetry planning, clinical dosimetry, quality assurance procedures for radiotherapy, interventional radiology, and radionuclide diagnostics and therapy.
PC(U)-6	Ability to apply knowledge of natural sciences, fundamental laws in the field of nuclear physics and technology, clinical and radiation standards, hygienic measures in nuclear medicine, which is sufficient to study issues associated with medical physics using modern equipment and information technology relying on the latest Russian and international experience.
PC(U)-7	Ability to develop reference books, tables and software containing data for clinical use in dosimetric planning of radiation therapy, radionuclide diagnostics and therapy.
PC(U)-8	Ability to take part in the design and physical and technical equipment development for radiation therapy, diagnostics, interventional radiology and radionuclide diagnostics and therapy, and radiation safety divisions.
PC(U)-9	Ability to conduct training sessions and develop instructional materials for the training courses within the cycle of professional training programs (bachelor degree programs).

APPROVED BY:
Program Director
_____ Verkhoturova V.V.
«____» _____ 2023

ASSIGNMENT
for the Graduation Thesis completion

In the form:

Master Thesis

For a student:

Group	Full name
0AM1M	Marzhan M. Toktaganova

Topic of research work:

Development and testing of the individual dosimetric phantom of the upper limb

Approved by the order of the Director of School of Nuclear Science & Engineering (date, number):	№ 30-89/c dated January 30, 2023

Deadline for completion of Master Thesis:	06.06.2023

TERMS OF REFERENCE:

Initial date for research work: *(the name of the object of research or design; performance or load; mode of operation (continuous, periodic, cyclic, etc.); type of raw material or material of the product; requirements for the product, product or process; special requirements to the features of the operation of the object or product in terms of operational safety, environmental impact, energy costs; economic analysis, etc.)*	The purpose of this work is to develop a method for diagnosing electron bunch trains based on coherent radiation interferometry.

List of the issues to be investigated, designed and developed *(analytical review of literary sources with the purpose to study global scientific and technological achievements in the target field, formulation of the research purpose, design, construction, determination of the procedure for research, design, and construction, discussion of the research work results, formulation of additional sections to be developed; conclusions).*	In accordance with the purpose of the work, the following tasks were set: 1. Develop the concept of the method; 2. To develop the mathematical formalism underlying the method; 3. Create a software to simulate the detector's signal function; 4. Compare the experimental data and the results of modeling the detector signal function to test the mathematical model and the created software; 5. Reveal and describe the regularities of the influence of the beam parameters on the characteristics of the detector signal function.
List of graphic material *(with an exact indication of mandatory drawings)*	Presentation

Advisors to the sections of the Master Thesis
(with indication of sections)

Section	Advisor
Accelerator Experimental Data Consultation	Mikhail V. Shevelev
Financial Management, Resource Efficiency and Resource Saving	Ekaterina V. Menshikova
Social Responsibility	Yuriy V. Perederin

Date of issuance of the assignment for Master Thesis completion according to the schedule	13.03.2023

Assignment issued by a scientific supervisor / advisor (if any):

Position	Full name	Academic degree, academic status	Signature	Date
Researcher	Dmitry A. Shkitov	PhD		

Assignment accepted for execution by a student:

Group	Full name	Signature	Date
0AM1M	Marzhan M. Toktaganova		

School of Nuclear Science & Engineering
Field of training (specialty): 14.04.02 Nuclear Science and Technology
Specialization: Nuclear medicine

Level of education: Master degree program
Research and Training Centre for International Nuclear Education and Career, School of Nuclear Engineering
Period of completion: spring semester 2022/2023 academic year

Form of presenting the work:

Master Thesis

SCHEDULED ASSESSMENT CALENDAR
for the Master Thesis completion

Deadline for completion of Master's Graduation Thesis:	06.06.2023

Assessment date	Title of section (module) / type of work (research)		Maximum score for the section (module)
4.02.2023	1.	Drafting and approval of terms of reference	4
8.02.2023	2.	Choice of research direction	4
20.02.2023	3.	Selection and study of materials on the topic	13
22.02.2023	4.	Scheduling of research work	3
8.03.2023	5.	Formation of the theoretical base	14
21.03.2023	6.	Creation of a program code for calculating an interferogram by an analytical method	14
3.04.2023	7.	Creation of a program code for calculating interferograms by a numerical method	14
7.04.2023	8.	Control of created programs	4
13.04.2023	9.	Simulation of interferograms from real bunches	6
15.04.2023	10.	Comparison of the obtained results	2
19.04.2023	11.	Analysis of regularities in the influence of bunch parameters on radiation characteristics	4
23.04.2023	12.	Quality control of work performance and consulting the contractor	4
29.04.2023	13.	Drawing up an explanatory note to the program code	6
06.05.2023	14.	Preparing for defense	8

COMPILED BY:
Scientific supervisor:

Position	Full name	Academic degree, academic status	Signature	Date
Researcher	Dmitry A. Shkitov	PhD		

Adviser

Position	Full name	Academic degree, academic rank	Signature	Date
Senior Research Fellow	Mikhail V. Shevelev	PhD		

APPROVED BY:

Program Director	Full name	Academic degree, academic status	Signature	Date
Nuclear medicine	Vera V. Verkhoturova	PhD		

TASK FOR SECTION
«FINANCIAL MANAGEMENT, RESOURCE EFFICIENCY AND RESOURCE SAVING»

To the student:

Group	Full name
0AM1M	Marzhan M. Toktaganova

School	School of Nuclear Science & Engineering	Division	Research and Training Centre for International Nuclear Education and Career
Degree	Master	Educational Program	14.04.02 Nuclear Science and Technology / Nuclear medicine

Input data to the section «Financial management, resource efficiency and resource saving»:	
1. Resource cost of scientific and technical research (STR): material and technical, energetic, financial and human	– Material costs – 41003 rub. – Salary costs – 111333 rub. – Labor tax – 30171 rub. – Overhead – 33400 rub. – Other direct costs – 105 rub. – STR budget – 216012 rub.
2. Expenditure rates and expenditure standards for resources	– Electricity costs – 5,8 rub per 1 kW
3. Current tax system, tax rates, charges rates, discounting rates and interest rates	– Labor tax – 27,1 %; – Overhead costs – 30%;
The list of subjects to study, design and develop:	
1. Assessment of commercial and innovative potential of STR	– comparative analysis with other researches in this field;
2. Development of charter for scientific-research project	– SWOT-analysis;
3. Scheduling of STR management process: structure and timeline, budget, risk management	– calculation of working hours for project; – creation of the time schedule of the project; – calculation of scientific and technical research budget;
4. Resource efficiency	– integral indicator of resource efficiency for the developed project.
A list of graphic material *(with list of mandatory blueprints):*	
1. Competitiveness analysis	
2. SWOT- analysis	
3. Gantt chart and budget of scientific research	
4. Assessment of resource, financial and economic efficiency of STR	
5. Potential risks	

Date of issue of the task for the section according to the schedule	

Task issued by adviser:

Position	Full name	Scientific degree, rank	Signature	Date
Associate Professor	Ekaterina V. Menshikova	PhD		

The task was accepted by the student:

Group	Full name	Signature	Date
0AM1M	Marzhan M. Toktaganova		

TASK FOR SECTION
"SOCIAL RESPONSIBILITY"

To the student:

Group	Full name
0AM1M	Marzhan M. Toktaganova

School	School of Nuclear Science & Engineering	Division	Research and Training Centre for International Nuclear Education and Career
Degree	Master	Educational Program	14.04.02 Nuclear Science and Technology / Nuclear medicine

Subject FQW:

Development and testing of the individual dosimetric phantom of the upper limb

Initial data for the section "Social responsibility":

1. Characteristics of the research object (substance, material, device, algorithm, technique, working area) and its scope	Object of study: model of coherent transition radiation from electron bunch trains Scope: accelerator beam diagnostics

List of questions to be researched, designed and developed:

1. Legal and organizational security issues: - special (typical for the operation of the research object, the projected working area) legal norms of labor legislation; -organizational measures for the layout of the working area.	– SP 2.2.3670-20 Sanitary and epidemiological requirements for working conditions; – SanPiN 2.6.1.2523-09 Radiation safety standards NRB-99/2009; – SanPiN 1.2.3685-21 Hygienic standards and requirements for ensuring the safety and (or) harmlessness of environmental factors for humans; – other.
2. Industrial safety: **2.1. Analysis of the identified harmful and dangerous factors** **2.2. Rationale for mitigation measures**	Harmful and dangerous factors: – noise; – illumination; – microclimate; – electrical safety; – fire and explosion safety; – electromagnetic fields; – radiation safety.
3. Safety in emergencies:	– selection and description of a typical emergency; – justification of measures to prevent emergencies; – the order of actions in the event of an emergency.

Date of issue of the task for the section on a line chart	

The assignment was given by the consultant:

Position	Full name	Academic degree, title	Signature	Date
Associate Professor	Yuriy V. Perederin	PhD		

The student accepted the assignment:

Group	Full name	Signature	Date
0AM1M	Marzhan M. Toktaganova		

ABSTRACT

This master's thesis consists of 158 pages, 45 figures, 30 tables, 76 references and 4 appendices.

The purpose of this thesis is to development of a method for diagnosing of electron bunch trains based on coherent radiation interferometry. The study is based on computer simulations made in Wolfram Language, developed through a broad theoretical study and also analysis and comparison model on real data experiments

Key words: diagnostics of electron beams, interferometry, polarization radiation, form factor of electron bunch trains, autocorrelation function.

CONTENTS

INTRODUCTION

Particle accelerators, since their inception in the 1930s, have undergone significant metamorphoses, going from serving as laboratory horses to wide and dense integration into a number of critically important fields for humans and mankind in medicine, industry, the agricultural sector, as well as fundamental science [1]. As an example, let's consider the areas of application of accelerator technologies in medicine. According to the IAEA report [2], there are currently about 30,000 particle accelerators in the world. If you look at the work [3], it turns out that about 50% of this amount is used for medical purposes. Speaking of applied medicine, one of the most obvious directions for using accelerators is radiotherapy using various types of ionizing radiation [4], obtaining radioisotopes for diagnostics and treatment (tomography, medical imaging) [5]. Often, with the development of accelerator technology, new areas of medical research begin to develop. In the 1980s, for example, synchrotron radiation found its application in angiography - diagnostics of human coronary arteries in X-ray beams with the introduction of iodine-containing contrast [6]. Now, the direction of using synchrotron radiation in mammography, bronchography, with the introduction of xenon as a contrast agent is actively developing [7, 8]. Less obvious, but still indirectly related to accelerator technology, is the use of digital radiography, a direct descendant of high-energy photon detectors at accelerators. Next, we will talk about the use of accelerators in areas of research medicine, such as biomedicine [9], biochemistry [10], pharmacology [10], genetics [11], as well as the production of new materials with certain characteristics [11]. The previously mentioned synchrotron radiation, as well as the radiation obtained in free electron lasers, currently breaks all records in terms of luminosity and duration of the resulting radiation pulses [12]. These advances make it possible not only to consider matter on increasingly smaller scales, but also to resolve atto- and femtosecond time processes [13]. Thus, it is possible to study the structure of biological objects [14], decipher the protein structure [15], study the properties of new pharmacological preparations [16], visualize the structures of implants [17], etc. The last point is about the industrial direction of using electron

accelerators, which is directly related to medicine - the sterilization of medical equipment and medical substances by accelerated electron beams, which today seriously competes with traditional complexes based on cobalt gamma sources [18]. Now, having pointed out the special position of accelerators in the field of medicine and nuclear medicine in particular, let us say a few words about the importance and relevance of the diagnostics of accelerated beams.

As it was said, over the past 90 years, technologies for obtaining accelerated beams have developed so much that they required the creation of a separate area of science - accelerator physics and technology. Each new technology made it possible either to obtain beams with the required characteristics or to make the process of their acceleration more convenient in structural, technological or financial terms. Accordingly, the variety of characteristics of accelerated beams, as well as the design features of a particular machine, require a variety of diagnostic approaches and methods. Thus, the development of detectors for accelerators finds its application in any place where there is something that accelerates particles. If we talk about research in the field of fundamental science, for example, particle colliders, then diagnostics in itself is an even more significant stage than acceleration. So, Let's repeat once again - where there is an accelerator, there are also people who are engaged in beam diagnostics. A large database of accelerator centers is presented on the IAEA portal [19], where everyone can evaluate the geographical coverage and get acquainted with the basic characteristics of accelerators around the world.

As for the group of Tomsk Polytechnic University (TPU), it deals with the methods of diagnostics of accelerated particles in the gigahertz, terahertz, optical and ultraviolet frequency ranges, based on the polarization mechanisms of radiation generation. In Russia, similar studies are carried out by groups from the INP. Budker (Novosibirsk), the Kurchatov Institute (Moscow), the Joint Institute for Nuclear Research (Dubna), the Troitsk Branch of the P. N. Lebedev Physics Institute, as well as a number of other scientific teams. Of the foreign organizations working on similar topics, we mention DESY (Germany), KEK (Japan) and INFN (Italy). In addition, for the last 5 years in Russia, as well as throughout the world, work has

been actively carried out to create installations of the "megascience" class [20]. SoDecree of the President of the Russian Federation of July 25, 2019 No. 356 "On measures to develop synchrotron and neutron research and research infrastructure in the Russian Federation" developedDecree of the Government of the Russian Federation of March 16, 2020 No. 287 "On Approval of the Federal Scientific and Technical Program for the Development of Synchrotron and Neutron Research and Research Infrastructure for 2019–2027" [21]. This document, among other things, briefly describes the state and development of developments on the designated topic, and also approves the program for the construction of a number of accelerator complexes. Among those that correlate with this work are the Siberian Ring Photon Source (SKIF) projects in Novosibirsk, the Russian Photon Source (RIF) synchrotron project on Russky Island, and the Synchrotron-Laser (SILA) synchrotron source in Protvino, also the document refers to the modernization of the Kurchatov accelerator complex. The amount of funding for the program is138318.04 million rubles [21]. The program takes into account the costs of training personnel and specialists of accelerator equipment. We are talking about hundreds and hundreds of people, including specialists in the field of beam diagnostics. At the moment, INP them. Budker is developing a method for registering SKIF beams using Cherenkov radiators - devices that use Cherenkov radiation (which is coherent by definition), which is a special case of polarization radiation. Thus, beam diagnostics remain relevant andin demand, at least in Russia.

The excitement around the fourth generation synchrotrons and free electron lasers is associated with the special characteristics of the resulting electromagnetic radiation, which we mentioned in the paragraph on the use of particle accelerators in medicine. These characteristics directly depend on the parameters of the electron beams. Roughly speaking, if very short but densely following beams are obtained, it will be possible to resolve a fast-flowing process, for example, that occurs in human cells. Thus, modern science establishes a request for obtaining ultrashort sequences of infected particles. An example of technologies for their production, as well as research in this direction, can be found in articles [22, 23, 24, 25]. It is natural that

these beams, like any technological innovation, require the creation of new approaches to diagnostics. At this stage, problems begin with the lack of a sufficient number of them. And here we are gradually approaching the statement of the purpose of the work.

Let us denote it as the development of a method for diagnosing sequences of electron bunches based on coherent radiation interferometry.

In accordance with the goal, we set the following tasks

1.   Formulate the idea of the method;

2.   Develop the mathematical formalism underlying it;

3.   Based on the created formalism, write software for modeling the detector signal function;

4.   To compare the experimental data and the results of modeling the detector signal function to test the mathematical model, and the generated code;

5.   Reveal and describe the regularities of the influence of the beam parameters on the characteristics of the detector signal function.

Section 1 of this work will be devoted to solving the first three problems, section 2 - the fourth, and section 3 - the fifth, respectively.

The object of study in this work is taken to be radiation arising in the presence of charged particles and some inhomogeneity of space, while the subject is considered to be coherent transition radiation from a sequence of electron bunches.

The choice of transition radiation from electrons as a standard in the development of the method is due to the presence of several code blanks for modeling, the greatest study by the author, as well as a large amount of experimental data available in the arsenal of the research group, inherited from experiments on LUCX conducted in 2019 and on the TPU microtron. Nevertheless, we can talk about the universality of the method, in the sense that the principles underlying it, as well as the modeling tools developed in the work, are applicable for calculating a number of characteristics of other types of radiation, where by appearance we mean generation mechanisms.

Interferometry, or rather the use of interferometers in the study of wave processes, originates in the experiments of Jung and Fresnel, which took place at the turn of the 18th and 19th centuries. In this sense, the physical phenomena that are behind the developed technology are well known, and the mathematics behind the method model is understandable to anyone who has mastered the direct and inverse Fourier transform. Historically, interferometry has been associated with radiation in the optical frequency range, as the most visual and intuitive.For example, in optics, interferometry is a generally accepted method for measuring small angular sizes (for example, the angular sizes of stars) [26].As applied to accelerator technology and technologies, namely, to beam diagnostics, interference detectors find their niche where the beam sizes turn out to be small compared to the wavelength of the observed photon radiation, i.e. where the beams radiate coherently in the desired range [26].An example of practical implementation is an interferometer developed at the KEK Photon Factory (Japan) operating on visible synchrotron radiation for measuring the transverse intensity distribution of an electron beam with a size of about 10 μm [26]. Articles were also found by the authordescribing the method for measuring the longitudinal dimensions of single beams using interferometers [27, 28, 29, 30]. This work, in addition to dimensions, focuses on the diagnostics of the parameters of the electron beam associated with its grouping, i.e. with the parameters that appear when the beam is a sequence of bunches. Among these parameters, we will mention the number and distance between clusters in the sequence as the most obvious ones, but we will not limit ourselves to them. In itself, the creation of a method carries an element of novelty. The tasks solved in the work are highly specialized, and, consequently, the programming tools created to solve them are unique. The formalism of the mathematical model describing the structure of the beam in the course of work is supplemented by several new refinements. For example,

Among the factors of practical significance, we single out the comparative simplicity of the method, its accuracy, the ability to make the method non-destructive, the possibility of using the method for diagnosing the periodic structure

of the beam, depending on the tools used and the installation scheme, the possibility of applying to a wide class of radiation and spectral ranges. There is a certain catch in the last statement, since different radiation ranges, different settings and different nature of radiation will dictate their requirements for equipment and the design of the measuring system. For example, the choice of a broadband or narrowband detector will affect both the cost, sensitivity, complexity / ease of operation, and the very results obtained during the measurements. The requirement for equipment protection, process automation, the presence / absence of optical tables, etc.

The author spoke several times with intermediate results of the work at international student and scientific conferences. A list of conferences and related publications is provided in Appendix A.

To solve the problems of the main part, we used, in the order of using the solutions:

- construction of a physical model and formalization of mathematical expressions;

- computer simulation to simulate the physical process;

- comparison of the model and experimental data;

- analysis and synthesis of patterns of signal change when varying the values of the parameters of electron beams in a computer model.

1 The concept and mathematical formalism of the interferometry method

The chapter is devoted to the formation of the theoretical and instrumental base of the method of interferometry of transition radiation generated from sequences of electron bunches of various configurations.

In paragraph 1.1, a detailed description of the objects and phenomena presented in the work is given, and it is also considered how these objects and phenomena are related in the context of the proposed methodology, forming the reader's general idea of the concept of the method. In particular, the definition of an electron beam, a sequence of electron bunches, their uniformity and non-uniformity, polarization radiation, transition and diffraction radiation, coherence and incoherence of radiation, near and far wave zone of radiation observation, interferometry, interferogram and autocorrelation function is given.

Section 1.2 is intended to describe and develop the mathematical formalism of the autocorrelation function model, with a detailed analysis of each of its components: the interference factor, the detector sensitivity function, and the full spectral-angular distribution of transition and diffraction radiation. Special attention is paid to the consistent derivation of the expression of the latter, starting from the mathematical expression for the simplest structure of the perturbing field source - a single electron bunch, to more and more complex structures that take into account all possible spatial parameters of the sequence. In addition, it is considered how the mathematical expression of the signal intensity changes in the case of ultrarelativistic particle velocity. Approximations, assumptions and limits of applicability of the proposed mathematical model are highlighted.

Section 1.3 is devoted to the demonstration of software tools created to solve the problems of modeling the signal intensity function on the interferogram, individual components of its expression and three-dimensional visualization of some physical processes described in paragraph 1.1. The functionality of the created programs is given. The nuances associated with the process of writing code are clarified, different approaches to solving the problem are demonstrated, designed to balance the time spent on modeling and the accuracy of calculations.

Section 1.4 offers an alternative method for calculating the form factor when the distribution of particles in a sequence of electron bunches cannot be or is difficult to describe by an analytical formula.

1.1 Concepts and physical foundations of the radiation interferometry method

Let us describe a method for diagnosing sequences of electron bunches based on coherent radiation interferometry. Before that, we will give a definition of the sequence of electron bunches, coherent radiation and interferometry, and also consider how these objects and phenomena are related in the context of the proposed methodology.

Let us consider an electron beam flying in an accelerating path consisting of a single electron bunch. In the model, the object is a cloud of electrons, subject to a certain spatial distribution, flying in a certain direction of the accelerating path. Now let's imagine a sequence of several such clusters spaced at the same distance from each other. In this case, we can speak of a uniform sequence of electron bunches. If there is some difference in the parameters of the bunches (their sizes, the distribution of electrons inside the bunches, average energy) or the distance between them, then one speaks of an uneven sequence. Let us also not forget that the electron beam has a Coulomb field.

Let us now assume that the electron beam flies through the output channel of the accelerating tract to the air or to the space of the vacuum chamber, and a metal target is placed on its path. The energy of the incident electrons and their Coulomb fields (the total field of the beam) in this case will be redistributed in space and matter - radiation of a different nature will appear in different wavelength ranges λ (or frequencies ν). More details about under what conditions and what kind of radiation will be observed can be found in the article [31].

For the method of diagnostics of electron beams developed in this work, the radiation associated with the polarization of the substance is significant. Polarization radiation is historically divided into Cherenkov, transition and diffraction. Cherenkov radiation arises during the polarization of atoms inside a substance, i.e. in a homogeneous medium, and diffraction and transition on its surface, in the

presence of some inhomogeneity of space, with the difference that in the case of transition radiation the particle crosses the target, and in the case of diffraction radiation it passes in the immediate vicinity, at a distance less than or equal to the effective Coulomb radius $\gamma\lambda$, where γ is the Lorentz factor of the bunch, the function of the velocity v of electrons incident on the target: $\gamma = \frac{1}{\sqrt{1-v^2/c^2}}$, as if hitting the target with its field. It is worth noting that the formalism that combined radiation into one class was developed not so long ago, with special merit in this area of research groups of the Tomsk and Moscow schools. More details about the union can be found in the dissertation of A. S. Konkov [32].

This work will focus mainly on transition radiation, due to its greatest study by the author and a number of code blanks for the implementation of modeling left over from the time of writing the bachelor's thesis. Nevertheless, the mathematical apparatus of the developed technique is described in such a way that it is easily adjusted not only to a certain type of radiation, but also takes into account specific devices and materials involved in real measurements.

So, let us recall that transition radiation occurs when a charged particle crosses some inhomogeneity of space, for example, the boundary of two media with different permittivities ε_1 and ε_2. The history of research on transition radiation dates back to 1945, when it was theoretically predicted by V. L. Ginzburg and I. M. Frank. [33]. Experimentally discovered in 1959 [34]. There are different models that describe the interaction of incident particles, their fields, target atoms, and, ultimately, induced transition radiation [32]. As a rule, they all come down to the problem of calculating the system of Maxwell equations. Here we will talk about the mechanism of the appearance of transition radiation, in the form in which it is described by the model (method) of polarization surface currents by V. E. Pafomov [35], since this approach is the most familiar to the author. In this model, the target atoms are positively charged nuclei and negatively charged electron shells. The Coulomb field of the incident electron also carries a negative charge. Under the action of this field, the electron shells of the target atoms begin to shift in a certain

direction, forming an electric dipole with the atomic nucleus. And further, since the Coulomb field of incident particles is not static either in time or space, the target dipoles begin to oscillate - dynamic polarization occurs and surface currents are formed. From the course of classical electrodynamics, it is known that the movement of charges along curvilinear trajectories creates electromagnetic waves. Thus, the target material serves as a radiation source.

Let us make a reservation that further the author gives himself the freedom to juggle hikes, using in one case the laws of geometric optics (as, for example, in describing the formalism of the form factor), which are inherently closer to the virtual photon model [36], and in the other case, to talk about radiation in terms of wave concepts, for example, when describing the interference pattern, radiation phase, etc., giving preference to the most convenient option.

Let us consider how transition radiation propagates in space. Both the "forward" transition radiation, which always propagate along the direction of the particles incident on the target, and the "backward" transition radiation, which propagate in the direction opposite to the direction of the incident particles movement, are distinguished [37] (Figure 1).
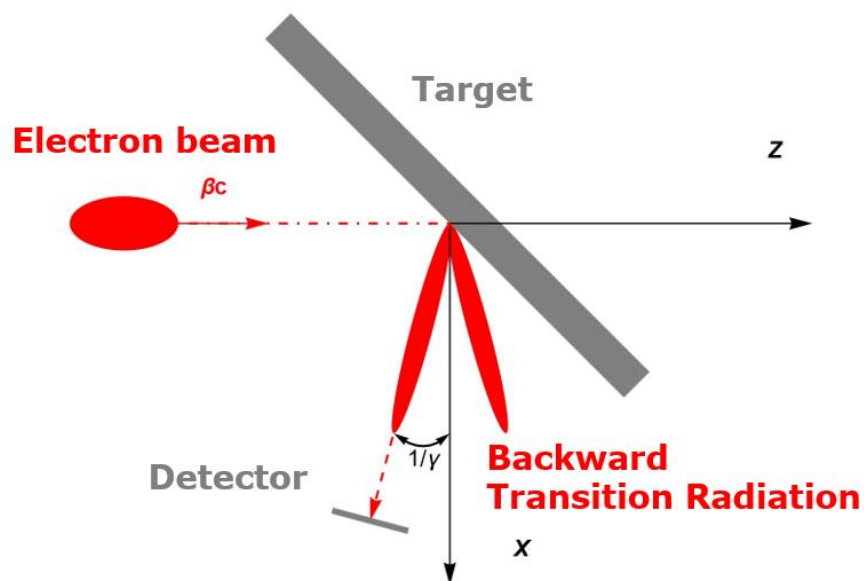

Figure 1 - Scheme of generation of transition radiation "back"

In addition, backward radiation, in contrast to forward radiation, depends on the angle of the target. In experiments, they mainly work with transition radiation "backward", in order to avoid the contribution of the signal from the beam of flying particles, and for reasons of keeping the detector in working condition. In what follows, speaking of transition radiation, only backward transition radiation will be understood.

Under the propagation of radiation in space, the author, as an experimental physicist, understands more not how the radiation actually propagates in space, but what the measuring device shows him. In this formulation, we can say the following - the functions that describe the spatial signal from the radiation change, depending on the distance from the center of the target to the point of observation. These distances are allocated certain zones. A distinction is made between the near zone, where the distance from the target to the observation point is greater than $\gamma^2\lambda$ or equal to the value , and the near wave zone, where the distance from the target to the observation point is less than or equal to the value $\gamma^2\lambda$ [38]. Sometimes the pre-wave zone is also distinguished [39]. Proximity and range in this case are relative concepts. Their approximate values depend, as follows from the expression $\gamma^2\lambda$, on whether radiation of what frequency is the object of observation. In the far wave zone, the radiation source is represented as a point, in the near one, its shape and size are taken into account. The choice of the target size in the experiment is also determined by the effective radius of the Coulomb field $\gamma\lambda$ of the incident particles. In the near wave zone, both the electron bunches themselves and the edge effects of radiation from the target can contribute to the observed signal. Nevertheless, in general, for each of the zones, we can say that the angular distribution of transition radiation is described by a cone, with a maximum of radiation in the angle of its opening equal to $1/\gamma$. It is convenient to calculate this parameter in terms of the average energy of electrons E_e in the beam as $\frac{1}{\gamma} = \frac{m_e c^2}{E_e}$, where $m_e c^2$ is the rest energy of the electron and m_e is the mass of the electron. This implies a different

interpretation of the Lorentz factor, as the ratio of the average energy of incident particles to their rest energy.

The presence of a cavity near the cone is explained by the radial symmetry of the incident beam, due to which the wave signal arriving at the observation point from two oscillating dipoles equidistant from the centre of the beam with the same phase, but polarized by the Coulomb field with mutually opposite intensity vectors, is detected at least intensity. Further, as you move away from the centre of symmetry, a phase difference appears, due to which the addition of pulses becomes more productive in the context of signal intensity.

The radiation of a selected frequency observed in the experiment can be coherent and incoherent. For the experimenter, the intensity of the coherent component will be quadratically greater than the intensity of the incoherent contribution of radiation. However, in order to understand what the fundamental difference between one and the other lies, it is necessary to dive into the details. As is known, coherence in the general sense is called a coordinated flow in time and space several oscillatory or wave processes. Thus, in order for the transition radiation to be coherent at a certain wavelength, it is necessary that the electrons that induce the radiation hit the target either simultaneously, or with a difference in time of incidence on the target equal to or less than the radiation wavelength preferred for observation. It turns out that the condition for observing a coherent signal , where is the root-mean-square deviation of the longitudinal size of the bunch (in this work, the direction of beam motion always coincides with the Z axis), assuming a Gaussian distribution of electrons inside the bunch, makes it possible to judge the beam length and determines the applicability of the method. Indeed, if the incoherent part of the radiation does not carry useful information, it makes no sense to observe it. Here we assume that the average speed of electrons is approximately equal to the speed of light, i.e.

As noted earlier, the coherent transition radiation signal observed in the detector contains information about the characteristics of the desired electron beam. The developed method of coherent transition radiation interferometry offers a way

to extract this information. Interferometry is the general name for a family of methods in which electromagnetic waves add up, causing the phenomenon interference, which is used to read the information embedded in the wave [40].Interferometry uses the principle of superposition to combine waves in such a way that the result will have some significant property that characterizes the initial state of the waves. This statement is true because when two waves of the same frequency are combined, the resulting intensity pattern is determined by the phase difference between the two original waves: waves that are in phase will interfere constructively, waves that are out of phase will exhibit destructive interference. . Waves that are not completely in phase or not in antiphase have an intermediate intensity from which their relative phase difference can be determined [40].

For a better understanding, consider an example of using interferometry in a real experiment conducted at LUCX in 2019 [53] (Figure 2).
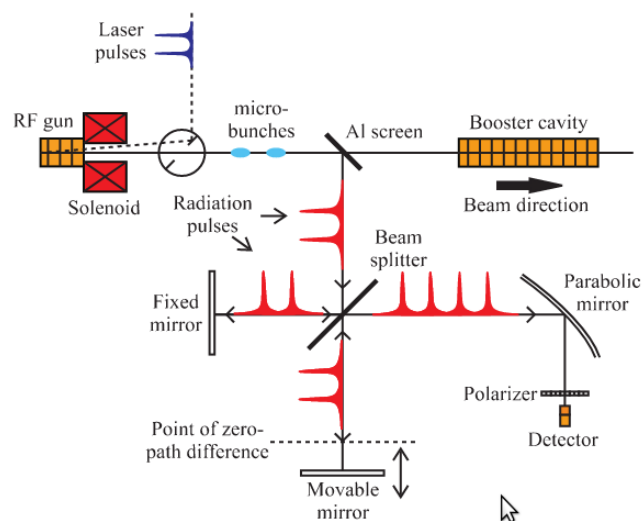
Figure 2 - Scheme of the LUCX experiment

In this example, interferometry was used as an intermediate step to restore the emission spectrum, through the Fourier Transform. We will give a diagram only in order to better understand how the signal is formed and how it is eventually converted into an interferogram. In the scheme presented, an electron beam consisting of two bunches crosses an aluminium target, the angle of inclination of which with respect to the direction of bunch motion is 45°. The transition radiation

resulting from the interaction of the beam and the target is directed to the Michelson interferometer, where, passing through a beam splitter, also inclined at an angle of 45° relative to the direction of radiation propagation, it is split into two components. One of the radiation components continues its path without changing its direction. The second component moves at a reflection angle to the beam splitter. Further, both components are reflected in mirrors installed perpendicular to the direction of their propagation, and again sent to the beam-splitting element. After that, the resulting signal enters the parabolic mirror, in the focus of which the radiation detector is located. (Also, in the above diagram, there is a polarizer in front of the detector to select one (vertical or horizontal) of the polarization components of the radiation, but its presence, when considering the principle of signal formation, is not significant in itself.) The detector converts the incoming signal into an electrical pulse. Further, by changing the position of one of the mirrors, one can obtain a certain sinusoidal dependence of the signal intensity on the mirror displacement distance. final schedule,

An analysis of the autocorrelation function, as will be shown below, allows one to make some judgments about the parameters describing the electron beam. In order to understand in more detail the connection "signal function - characteristics of the electron beam", it is necessary to consider and, in cases, supplement the mathematical formalism underlying the interferometry method, which will be the subject of the next part of the chapter. This is also the end of the work with the formation of the reader's conceptual apparatus of the proposed method.

1.2 Mathematical apparatus of the radiation interferometry method

Let us present a general mathematical expression for the radiation intensity depending on the pitch of the movable mirror of the Michelson interferometer. Recall that we are considering coherent transition radiation. So, a beam of charged particles crosses a flat rectangular metal target located at an angle of 45°. The interferometer is located at an angle of 90° to the beam trajectory. The generated radiation pulse propagates from the target to the input of the interferometer in some time. Further it is divided in the beam-splitting plate into two pulses and . After

reflection from the mirrors, they fold again and fall into the detector. Here, we neglect the influence of the exit window of the vacuum chamber and the properties of the beam splitter, however, we take into account the properties of the detector through the function - the sensitivity of the detector, within the frequency range . Thus

$$I(d) \sim \int_{v_1}^{v_2} cL^2 |E_1(t) + E_2(t)|^2 S(v)dv,$$

Where L is the distance traveled by one radiation component from the target to the detector, is the shift of the movable mirror. d Here

$$E_2(t) = E_1(t) \cdot e^{-i\Delta\varphi},$$

because the radiation pulse reflected from a movable mirror differs from the pulse reflected from a stationary mirror by a phase factor, where is the geometric difference in the radiation path in the interferometer (), is the speed of light in vacuum, is the radiation frequency. In our case, it is equal to the initial radiation pulse. Thus, we get: $\Delta\varphi = 2\pi\Delta lv/c \Delta l \Delta l = 2dcvE_1(t)E(t)$

$$cL^2 |E_1(t) + E_2(t)|^2 = cL^2 |E(t)|^2 \cdot \left|1 + e^{-\frac{i2\pi\Delta lv}{c}}\right|^2.$$

Note that , as a time-dependent function, after the Fourier transform, can be replaced by a function depending on the radiation frequency , and the expression for the total spectral-angular distribution of the radiation energy can be written in terms of $|E(t)||E(v)|$

$$\frac{d^2W}{d\omega d\Omega} = cL^2 |E(v)|^2.$$

Then

$$I(\Delta l) \sim \int_{v_1}^{v_2} \frac{d^2W}{d\omega d\Omega} M(v)S(v)dv,$$

where is the interference factor. $M(v) = \left|1 + e^{-\frac{i2\pi\Delta lv}{c}}\right|^2$

However, in order to show the connection between the radiation flying from the target and the beam of incident electrons, it is necessary to understand the derivation of the full spectral-angular distribution the energy of the initial radiation

from the standpoint that the basis of the radiation is the electrons incident on the target.

1.2.1 Derivation of the formula for the spectral-angular distribution of radiation

Let us show a consistent derivation of the general expression for the total intensity of polarization radiation from one bunch of charged particles presented in [41]. Let us write the expression in the approximation that the perturbing field does not depend on the change in the coordinates of individual particles inside the bunch.

The radiation field from all bunch electrons can be represented as the sum of the radiation fields of each individual electron in this bunch:

$$\vec{E}(\vec{r},\omega) = \sum_{j=1}^{N} \vec{E_j}(\vec{r_j},\omega),$$

where is the coordinate of the th electron in the bunch, in the coordinate system associated with the target, is the number of electrons in the bunch, is the circular frequency of the radiation under study, is the coordinate of the bunch center, in the coordinate system associated with the target, is the electric component of the field strength of the th electron in the bunch $.\vec{r_j} j N \omega \vec{r} \vec{E_j}(\vec{r_j},\omega) j$

In turn, the radiation field from the th electron in the bunch can be written as the product of the strength of the electric component in the far wave zone of the central electron and the exponential part, the degree of which includes the phase of the desired radiation:

$$\vec{E_j}(\vec{r_j},\omega) = \vec{E_0}(\vec{r},\omega) \cdot e^{i\varphi},$$

$$\varphi = \omega \left(\frac{\vec{s} \cdot \vec{r_j}}{c} \right),$$

here, is the speed of light in vacuum, is a vector that determines the type of radiation (it can be transition, diffraction or synchrotron radiation, etc.). Thus, the expression for the field from all bunch electrons can be written as:

$$\vec{E}(\vec{r},\omega) = \vec{E_0}(\vec{r},\omega) \cdot \sum_{j=1}^{N} e^{i\omega \left(\frac{\vec{s} \cdot \vec{r_j}}{c} \right)}.$$

Finally, we write the expression for the radiation intensity:

$$\frac{d^2 W}{d\omega d\Omega} = cL^2 \cdot \vec{E_0}(\vec{r},\omega) \cdot \vec{E_0}^{*}(\vec{r},\omega) \cdot \sum_{j=1}^{N} e^{i\omega \left(\frac{\vec{s} \cdot \vec{r_j}}{c} \right)} \cdot \sum_{p=1}^{N} e^{-i\omega \left(\frac{\vec{s} \cdot \vec{r_p}}{c} \right)},$$

where is the distance to the observation point. L

Let us denote the radiation intensity of a single electron, and write the previous expression in a more compact form: $\dfrac{d^2W_0}{d\omega d\Omega} = cL^2 \cdot \overrightarrow{E_0}(\vec{r}, \omega) \cdot \overrightarrow{E_0}^*(\vec{r}, \omega)$

$$\frac{d^2W}{d\omega d\Omega} = \frac{d^2W_0}{d\omega d\Omega} \cdot \sum_{j=1}^{N} \sum_{p=1}^{N} e^{i\frac{\omega \cdot \vec{s}}{c}(\overrightarrow{r_j} - \overrightarrow{r_p})}.$$

Let us break this expression into the sum of two terms, one of which will represent the sum of the diagonal elements of the matrix

$$\frac{d^2W_0}{d\omega d\Omega} \cdot \sum_{j=1}^{N} \sum_{p=1}^{N} e^{i\frac{\omega \cdot \vec{s}}{c}(\overrightarrow{r_j} - \overrightarrow{r_p})},$$

when , and the second is the sum of off-diagonal elements, when $:p = jp \neq j$

$$\frac{d^2W}{d\omega d\Omega} = \frac{d^2W_0}{d\omega d\Omega} \cdot \left(\sum_{\substack{p=1 \\ j \neq p}}^{N} \sum_{p=1}^{N} e^{i\frac{\omega \cdot \vec{s}}{c}(\overrightarrow{r_p} - \overrightarrow{r_p})} + \sum_{\substack{j=1 \\ p \neq j}}^{N} \sum_{p=1}^{N} e^{i\frac{\omega \cdot \vec{s}}{c}(\overrightarrow{r_j} - \overrightarrow{r_p})} \right).$$

Since the exponent in the first term is always zero, we can write:

$$\frac{d^2W_0}{d\omega d\Omega} \cdot \sum_{p=1}^{N} \sum_{p=1}^{N} e^{i\frac{\omega \cdot \vec{s}}{c}(\overrightarrow{r_p} - \overrightarrow{r_p})} = \frac{d^2W_0}{d\omega d\Omega} \cdot N.$$

This term corresponds to the usual incoherent radiation of electrons.N

The second term corresponds to coherent radiation. Let us perform some identical transformations using the properties of the Dirac -function [42]:δ

$$\sum_{\substack{j=1 \\ j \neq p}}^{N} \sum_{p=1}^{N} e^{i\frac{\omega \cdot \vec{s}}{c}(\overrightarrow{r_j} - \overrightarrow{r_p})} = \sum_{\substack{j=1 \\ j \neq p}}^{N} e^{i\omega\left(\frac{\vec{s} \cdot \overrightarrow{r_j}}{c}\right)} \cdot \sum_{\substack{p=1 \\ p \neq j}}^{N} e^{-i\omega\left(\frac{\vec{s} \cdot \overrightarrow{r_p}}{c}\right)} =$$

$$= \left[\sum_{\substack{j=1 \\ j \neq p}}^{N} \int e^{i\omega\left(\frac{\vec{s} \cdot \vec{r}}{c}\right)} \delta(\vec{r} - \overrightarrow{r_j}) dV \right] \cdot \left[\sum_{\substack{p=1 \\ p \neq j}}^{N} \int e^{-i\omega\left(\frac{\vec{s} \cdot \vec{r}'}{c}\right)} \delta(\vec{r}' - \overrightarrow{r_p}) dV' \right] =$$

$$= \left[\int e^{i\omega\left(\frac{\vec{s} \cdot \vec{r}}{c}\right)} \sum_{\substack{j=1 \\ j \neq p}}^{N} \delta(\vec{r} - \overrightarrow{r_j}) dV \right] \cdot \left[\int e^{-i\omega\left(\frac{\vec{s} \cdot \vec{r}'}{c}\right)} \sum_{\substack{p=1 \\ p \neq j}}^{N} \delta(\vec{r}' - \overrightarrow{r_p}) dV' \right].$$

Next, we introduce the notation

$$\sum_{\substack{j=1 \\ j \neq p}}^{N} \delta(\vec{r} - \overrightarrow{r_j}) = N\rho(\vec{r}),$$

$$\sum_{\substack{p=1 \\ p \neq j}}^{N} \delta(\vec{r}' - \overrightarrow{r_p}) = (N-1)\rho'(\vec{r}').$$

Obviously, is the exact expression for the normalized electron distribution density function in the bunch. In case when $,\rho(\vec{r})N \gg 1$

$$\rho(\vec{r}) \approx \rho'(\vec{r}').$$

When the distances between electrons in the bunch are much smaller than the wavelength of the radiation under study, the discrete function can be replaced by a continuous normalized function of the distribution density. Then: $\rho(\vec{r})$

$$\frac{d^2W_0}{d\omega d\Omega} \cdot \sum_{\substack{j=1 \\ j \neq p}}^{N} \sum_{\substack{p=1 \\ p \neq j}}^{N} e^{i\frac{\omega \cdot \vec{s}}{c}(\vec{r}_j - \vec{r}_p)} = \frac{d^2W_0}{d\omega d\Omega} \cdot N(N-1) \int e^{i\omega\left(\frac{\vec{s}\cdot\vec{r}}{c}\right)}\rho(\vec{r})dV \cdot \int e^{-i\omega\left(\frac{\vec{s}\cdot\vec{r}'}{c}\right)}\rho'(\vec{r}')dV' =$$

$$= \frac{d^2W_0}{d\omega d\Omega} \cdot N(N-1) \cdot F(\omega, \vec{s}),$$

$$F(\omega, \vec{s}) = \int e^{i\frac{\omega}{c}(\vec{s}\cdot\vec{r})}\rho(\vec{r})dV \cdot \int e^{-i\frac{\omega}{c}(\vec{s}\cdot\vec{r}')}\rho'(\vec{r}')dV' = \left|\int e^{i\frac{\omega}{c}(\vec{s}\cdot\vec{r})}\rho(\vec{r})dV\right|^2,$$

where is the bunch form factor.$F(\omega, \vec{s})$

Thus, we have obtained an expression for the total spectral-angular distribution of radiation:

$$\frac{d^2W}{d\omega d\Omega} = [N + N(N-1)F(\omega, \vec{s})] \cdot \frac{d^2W_0}{d\omega d\Omega}.$$

Note that this formula is valid for all types of polarization radiation. The difference between them will be determined by the final form factor of the charged particle beam.

1.2.2 Electron beam form factor

Let us now return to the signal intensity function. For the uniformity of writing the components of the expression, we will consider the form factor as a function depending on the frequency, keeping in mind the relationship between the cyclic (circular) frequency and the radiation frequency as . Let us also omit the phase vector , assuming that we know its form for transition radiation. Then, the expression for the signal intensity will look like:$\omega \nu \omega = 2\pi \nu \vec{s}$

$$I(\Delta l) \sim \int_{\nu_1}^{\nu_2} \frac{d^2W_0}{d\omega d\Omega} \cdot [N + N(N-1)F(\nu)] \cdot M(\nu) \cdot S(\nu)d\nu.$$

Assuming that the spectral-angular distribution of the radiation energy from one particle in the studied frequency range is equal to a constant and normalized, i.e. , we get the following expression:

$$I(\Delta l) \sim \int_{\nu_1}^{\nu_2} [N + N(N-1)F(\nu)] \cdot M(\nu) \cdot S(\nu)d\nu.$$

And although recently there have been works [43] that take into account the contribution of the incoherent component of radiation, and single out the so-called "incoherent" form factor into a separate component under certain observation conditions, in this work, the incoherent contribution of radiation is deprived of attention. Thus, we can neglect the small value N compared with and omitting the constants to get: $N(N-1)$

$$I(\Delta l) \sim \int_{\nu_1}^{\nu_2} F(\nu)M(\nu)S(\nu)d\nu.$$

The interference factor for different frequencies is a sinusoidal function (Figure 3). $M(\nu)$
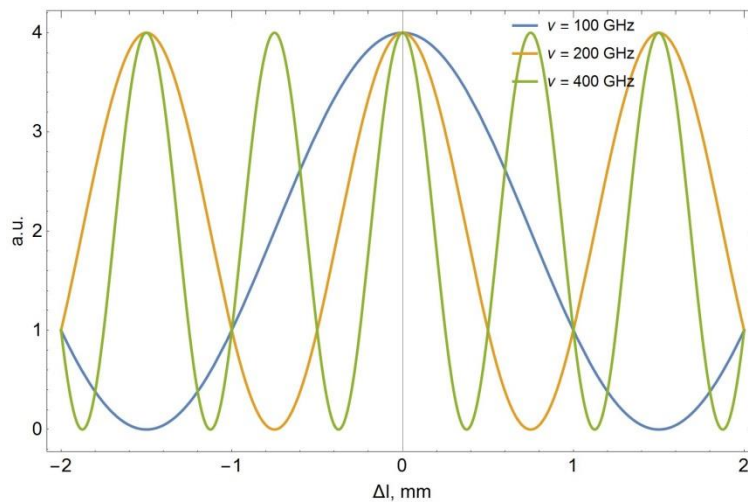
Figure 3 – View interference factor for different frequencies

Then, from the resulting expression, we can conclude that two factors will have a determining value on the type of interferogram: $F(\nu)$ And $.S(\nu)$ The detector can be either broadband or narrowband. In the first case, its sensitivity function is given by a uniform distribution, and in the second, it can be described by a Gaussian. Therefore, the decisive influence on the appearance $S(\nu)$ interferograms will render the form factor $F(\nu)$, and hence the structure of the beam (in other words, sequences of bunches), which can be complex. This is due to the fact that bunches in a beam can have different charges, longitudinal and transverse sizes, shape of particle distribution, distances between bunches, including the average energy from bunch

to bunch, and so on. Thus, it is critical for the method to develop the mathematical formalism of the form factor.

1.2.2.1 Calculation of the phase difference for transition and diffraction radiation

Knowing the formula for the complete spectral-angular distribution of radiation, we can specify the form factor for transition and diffraction radiation. As shown in 1.2.1, the form factor is determined by the radiation phase and the spatial distribution of electrons in the bunch:

$$F(\omega, \vec{s}) = \left| \int e^{i\frac{\omega}{c}(\vec{s}\cdot\vec{r})} \rho(\vec{r}) dV \right|^2.$$

Let us determine the vector components for the transition radiation. Consider the scheme for the formation of transition radiation in 2D (Figure 4): $\vec{s}$
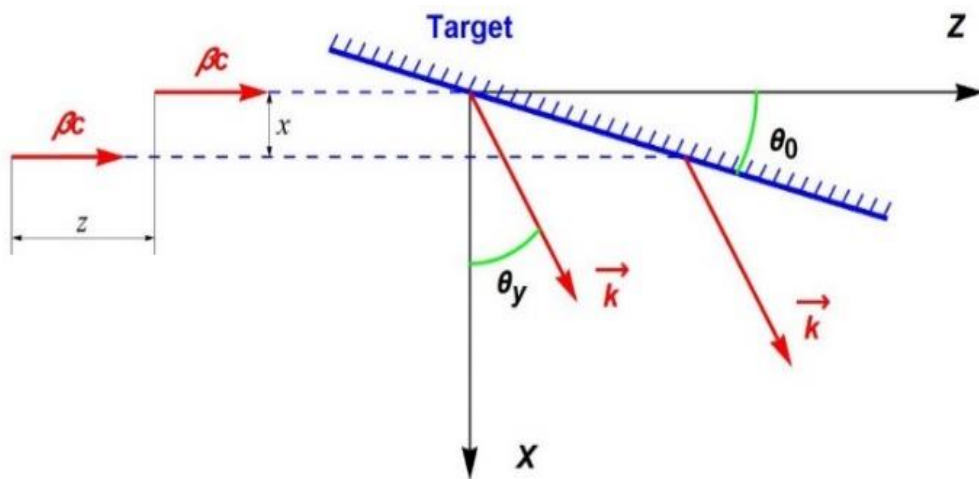
Figure 4 - Kinematics of transition radiation "backward" in the XOZ plane

We will consider as sources of transition radiation waves the points at which electrons cross a target inclined to the direction of the electron velocity at an angle. The electron located at the center of the bunch crosses the target at the origin of coordinates, and the electron with transverse coordinates at the point [37]. The radiation phase in this case is determined by the time interval from the moment the central electron crosses the target to the moment when the radiation induced by two electrons travels an equal distance to the detector located perpendicular to the

radiation propagation. In turn, this time interval can be divided into two parts (Figure 5) [41]:

$$\omega\left(\frac{\vec{s}\cdot\vec{r_j}}{c}\right) = \omega(t_1 - t_2).$$
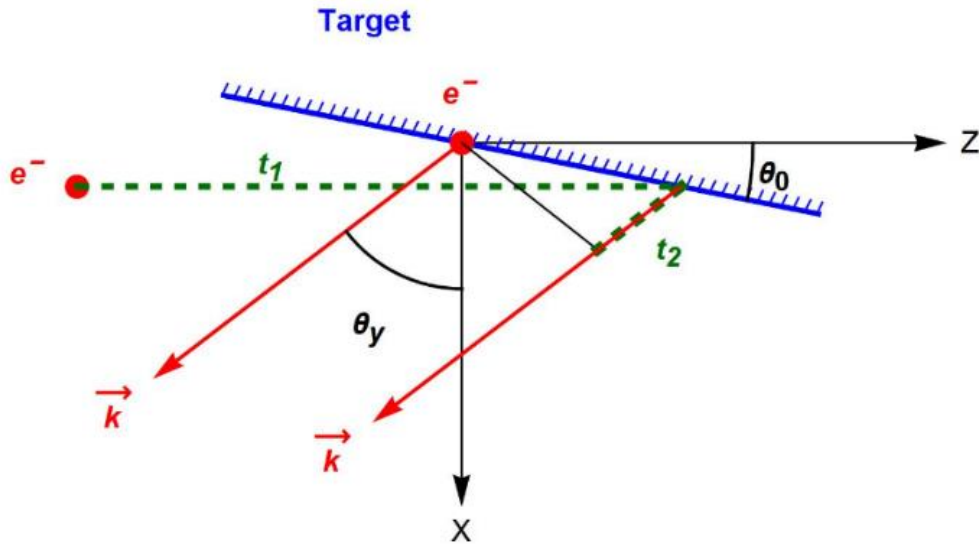
Figure 5 - To explain the formation of the radiation phase (projection onto the XOZ plane)

The first interval is the time taken by an electron with non-zero transverse coordinates to "fly" to the target, and it can be expressed as the ratio of the path traveled by this electron to the target to its velocity S v:

$$t_1 = \frac{S}{v} = \frac{x\cdot\cot\theta_0 - z}{\beta c},$$

Where $-\beta$ the ratio of the speed of electrons to the speed of light v $\beta = \frac{v}{c}$, also called the dimensionless velocity and expressed in terms of the Lorentz factor as

$\beta = \sqrt{1 - \frac{1}{\gamma^2}}$. Note that the minus sign in front of the - coordinate of the second electron levels out the sign of the - coordinate itself, that is, if the desired electron is ahead of the central electron, and does not lag behind it, then it travels a distance to the target less than , then the negative sign is preserved, and vice versa, if the electron lags behind the central one, as shown in figures 4 and 5, it travels a greater distance and the sign becomes positive

The second time interval is related to the distance that the radiation induced by the electron must travel to the point when the radiation from the first and second electrons will travel the same distance to the detector, and the radiation induced by the "non-central" electron must not always travel this path. Thus, radiation from the central electron can play the role of "catching up" radiation; as a rule, this depends on the angles that determine the direction of the radiation wave vector (which can also be interpreted as an observation vector, i.e., the position of the radiation detector in space), slope target with respect to the direction of electron propagation and the coordinates of the "non-central" electron.

To consider the geometry of the phase formation, this time we turn to three-dimensional schemes, since the exact analytical expression for the time interval, unlike as a rule, causes difficulties associated with working in space and the need for an extremely accurate analytical expression for the direction of the wave vector (Figure 6).$t_2 t_1$
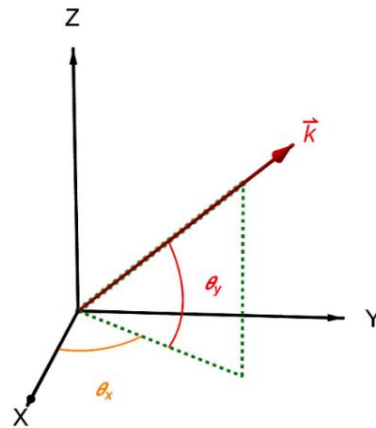
Figure 6 - On the expression of the direction of the wave vector in 3D

In this paper, the direction of the normalized wave vector in space is given by the angles

$$\hat{\vec{k}} = \frac{\vec{k}}{|\vec{k}|} = \{\cos \theta_y \cos \theta_x, \cos \theta_y \sin \theta_x, \sin \theta_y\},$$

and the time interval , is found as a projection of the vector onto the vector (Figure 7) divided by the radiation speed, that is, the speed of light:

$$t_2 = \frac{|\vec{r}| \cdot \cos\left(\hat{\vec{k}}, \vec{r}\right)}{c} = |\vec{r}| \frac{\vec{r} \cdot \hat{\vec{k}}}{|\vec{r}| \cdot |\hat{\vec{k}}| \cdot c} = \frac{\vec{r} \cdot \hat{\vec{k}}}{c}.$$
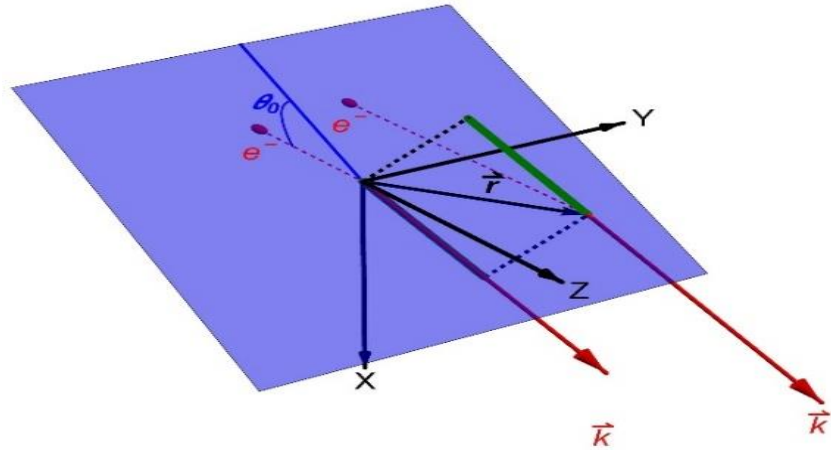
A)
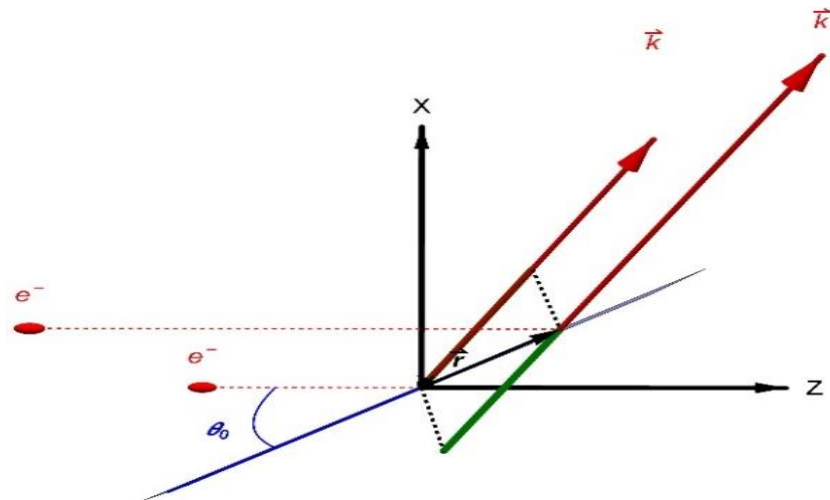
b)

Drawing7-Kinematics of transition radiation "back" in 3D (a), kinematics of transition radiation "back" side view (b)

Thus, the second time interval is determined by the expression:

$$t_2 = \frac{x \cdot \cos\theta_y \cos\theta_x + y \cdot \cos\theta_y \sin\theta_x + x \cdot \cot\theta_0 \sin\theta_y}{c}.$$

Let's check the obtained formula using the methods of analytical geometry, for this we will find the coordinates of the projection of the point

$$\vec{r} = \{x, y, x \cdot \cot\theta_0\} = \{x_1, y_1, z_1\}$$

34

on a straight line, with a direction vector

$$\hat{\vec{k}} = \{k_1, k_2, k_3\} = \{\cos\theta_y \cos\theta_x, \cos\theta_y \sin\theta_x, \sin\theta_y\},$$

and passing through the point. We write the canonical equation of this line:$\{0,0,0\}$

$$\frac{x}{k_1} = \frac{y}{k_2} = \frac{z}{k_3}.$$

Next, we find the form of the equation of a straight line perpendicular to the given one and passing through the point:$\vec{r}$

$$k_1(x - x_1) + k_2(y - y_1) + k_3(z - z_1) = 0.$$

We express the components and through the component :yzx

$$\frac{x}{k_1} = \frac{y}{k_2} \quad \Rightarrow \quad y = x\frac{k_2}{k_1},$$

$$\frac{x}{k_1} = \frac{z}{k_3} \quad \Rightarrow \quad z = x\frac{k_3}{k_1}.$$

And substitute in the formula for a line perpendicular to the given one:

$$k_1(x - x_1) + k_2\left(x\frac{k_2}{k_1} - y_1\right) + k_3\left(x\frac{k_3}{k_1} - z_1\right) = 0.$$

Let's express the component explicitly:x

$$x = k_1\left(\frac{x_1 k_1 + y_1 k_2 + z_1 k_3}{k_1^2 + k_2^2 + k_3^2}\right).$$

And substitute in the expression for the components and :yz

$$y = x\frac{k_2}{k_1} = k_2\left(\frac{x_1 k_1 + y_1 k_2 + z_1 k_3}{k_1^2 + k_2^2 + k_3^2}\right),$$

$$z = x\frac{k_3}{k_1} = k_3\left(\frac{x_1 k_1 + y_1 k_2 + z_1 k_3}{k_1^2 + k_2^2 + k_3^2}\right).$$

Thus, we have found the coordinates of the projection of the point onto the vector:$\vec{r}\hat{\vec{k}}$

$$\left\{k_1\left(\frac{x_1 k_1 + y_1 k_2 + z_1 k_3}{k_1^2 + k_2^2 + k_3^2}\right), k_2\left(\frac{x_1 k_1 + y_1 k_2 + z_1 k_3}{k_1^2 + k_2^2 + k_3^2}\right), k_3\left(\frac{x_1 k_1 + y_1 k_2 + z_1 k_3}{k_1^2 + k_2^2 + k_3^2}\right)\right\}.$$

Let's determine the length of the direction vector of this point:

$$\sqrt{\left[k_1\left(\frac{x_1 k_1 + y_1 k_2 + z_1 k_3}{k_1^2 + k_2^2 + k_3^2}\right)\right]^2 + \left[k_2\left(\frac{x_1 k_1 + y_1 k_2 + z_1 k_3}{k_1^2 + k_2^2 + k_3^2}\right)\right]^2 + \left[k_3\left(\frac{x_1 k_1 + y_1 k_2 + z_1 k_3}{k_1^2 + k_2^2 + k_3^2}\right)\right]^2} =$$

$$= \sqrt{\frac{(x_1 k_1 + y_1 k_2 + z_1 k_3)^2}{k_1^2 + k_2^2 + k_3^2}} = \sqrt{\frac{(x\cdot\cos\theta_y \cos\theta_x + y\cdot\cos\theta_y \sin\theta_x + x\cdot\cot\theta_0 \sin\theta_y)^2}{(\cos\theta_y \cos\theta_x)^2 + (\cos\theta_y \sin\theta_x)^2 + (\sin\theta_y)^2}} =$$

$$= x\cdot\cos\theta_y \cos\theta_x + y\cdot\cos\theta_y \sin\theta_x + x\cdot\cot\theta_0 \sin\theta_y.$$

This expression corresponds to the previously obtained expression for the numerator . In addition to analytical geometry methods, you can verify the correctness of the resulting expression using the created visualizer program (Appendix B) implemented in the Wolfram Mathematica package (version 11.3) [44]. Knowing the exact form of and for the presented geometry, we can write the complete expression for the radiation phase difference:$t_2 t_1 t_2$

$$\frac{\vec{s}\cdot\vec{r}}{c} = \frac{x\cdot\cot\theta_0 - z}{\beta c} - \frac{(x\cdot\cos\theta_y \cos\theta_x + y\cdot\cos\theta_y \sin\theta_x + x\cdot\cot\theta_0 \sin\theta_y)}{c} =$$

$$= \frac{-x\left[\cos\theta_y \cos\theta_x + \cot\theta_0\left(\sin\theta_y - \frac{1}{\beta}\right)\right] - y\cdot\cos\theta_y \sin\theta_x - z\cdot\frac{1}{\beta}}{c}.$$

We conclude that the vector components for the transition radiation in the presented geometry will have the following form:$\vec{s}$

$$\vec{s} = \begin{Bmatrix} s_x \\ s_y \\ s_z \end{Bmatrix} = \begin{Bmatrix} -\cos\theta_y \cos\theta_x - \cot\theta_0\left(\sin\theta_y - \frac{1}{\beta}\right) \\ -\cos\theta_y \sin\theta_x \\ -\frac{1}{\beta} \end{Bmatrix}.$$

These components differ from those obtained in [41] for the same geometry. The reason for this discrepancy is that it is not entirely clear how the wave vector is expressed in the above paper. Because of this, it is not possible to verify the validity of the expression obtained in [41] for the vector components.$\vec{s}$

Let us determine the vector components for the diffraction radiation by repeating the previous derivation step by step. First, let's consider the scheme for the formation of diffraction radiation in 2D (Figure 8):$\vec{s}$
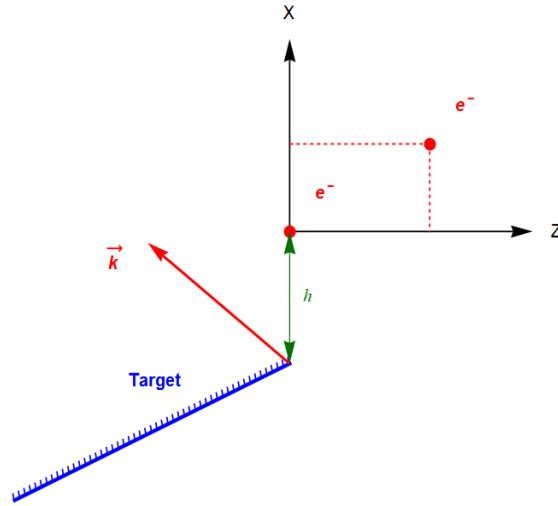
Figure 8-Kinematics of diffraction radiation "backward" in the XOZ plane

In Figure 8, the letter denotes the impact parameter - the shortest distance between the beam and the target, this parameter must be taken into account when calculating the diffraction radiation. Its main contribution to the radiation field strength $h \frac{d^2 W_0}{d\omega d\Omega}$ enters as $e^{-\frac{2\pi h}{\gamma\lambda}}$ [41].

In diffraction radiation, as in transition radiation, the source of radiation is currents in the target induced by flying relativistic electrons, the radiation phase in this case is determined by the moment of electron flight relative to some characteristic point of the target, and the phase differencethe time delay between the passage of the first and second particles over the characteristic point of the target.Δt

$$\omega\left(\frac{\vec{s}\cdot\vec{r}}{c}\right) = \omega \cdot \Delta t, \qquad\qquad .\Delta t = \frac{z}{\beta c}$$

In this case, the components of the vector for diffraction radiation in the presented geometry will have a simpler form than for the transition one, due to the absence of influence on the formation of the phase difference of the transverse coordinates of flying particles:$\vec{s}$

$$\vec{s} = \begin{Bmatrix} s_x \\ s_y \\ s_z \end{Bmatrix} = \begin{Bmatrix} 0 \\ 0 \\ \frac{1}{\beta} \end{Bmatrix}.$$

The desired type of form factor can be determined by substituting the vector for a specific case in the original formula.$\vec{s}$

37

1.2.2.2 Ultrarelativistic case

For ultrarelativistic particles, when the transition radiation will propagate in a narrow cone. Then, expanding the trigonometric components of the wave vector in the Maclaurin series, we can represent it in a simplified form. Let us present a consistent derivation of the mathematical expression of the wave vector for the ultrarelativistic approximation.$\gamma \gg 1$

Let's write:

$$\cos\theta_y \approx 1 - \frac{\theta_y^2}{2},$$

$$\cos\theta_x \approx 1 - \frac{\theta_x^2}{2},$$

$$\sin\theta_y \approx \theta_y,$$

$$\sin\theta_x \approx \theta_x.$$

In accordance with this, we transform the components of the wave vector

$$k_1 = \cos\theta_y \cos\theta_x \approx 1 - \frac{\theta_y^2 + \theta_x^2}{2},$$

$$k_2 = \cos\theta_y \sin\theta_x \approx \theta_x,$$

$$k_3 = \sin\theta_y \approx \theta_y.$$

Then

$$\hat{\vec{k}} = \{k_1, k_2, k_3\} = \left\{\cos\theta_y \cos\theta_x, \cos\theta_y \sin\theta_x, \sin\theta_y\right\} = \left\{1 - \frac{\theta_y^2 + \theta_x^2}{2}, \theta_x, \theta_y\right\}.$$

Let us calculate the vector components for the case of transition radiation from ultrarelativistic particles:$\vec{s}$

$$t_1 = \frac{x \cdot \cot\theta_0 - z}{\beta c},$$

$$t_2 = \frac{\vec{r} \cdot \hat{\vec{k}}}{c} = \frac{x \cdot \left(1 - \frac{\theta_y^2 + \theta_x^2}{2}\right) + y \cdot \theta_x + x \cdot \cot\theta_0 \cdot \theta_y}{c}.$$

$$\frac{\vec{s} \cdot \vec{r}}{c} = \frac{x \cdot \cot\theta_0 - z}{\beta c} - \frac{x \cdot \left(1 - \frac{\theta_y^2 + \theta_x^2}{2}\right) + y \cdot \theta_x + x \cdot \cot\theta_0 \cdot \theta_y}{c} =$$

$$= \frac{-x\left(1 - \cot\theta_0\left(\frac{1}{\beta} - \theta_y\right) - \frac{\theta_y^2 + \theta_x^2}{2}\right) - y \cdot \theta_x - \frac{z}{\beta}}{c}.$$

Then, the vector components for the case of transition radiation from ultrarelativistic particles have the form:$\vec{s}$

$$\vec{s} = \begin{Bmatrix} \vec{s}_x \\ \vec{s}_y \\ \vec{s}_z \end{Bmatrix} = -\begin{Bmatrix} 1 - \cot\theta_0\left(\frac{1}{\beta} - \theta_y\right) - \frac{\theta_y^2 + \theta_x^2}{2} \\ \theta_x \\ \frac{1}{\beta} \end{Bmatrix}.$$

1.2.2.3 Single bunch form factor

Let us proceed directly to the definition of the general form factor for various configurations of electron bunches in space.

For the definiteness of the form factor calculations, as well as for the possibility of an analytical solution, we will describe the normalized spatial distribution of electrons in the bunch by three independent Gaussians along the X, Y, and Z axes in the case of both transition and diffraction radiation:

$$\rho(\vec{r}) = \rho(x, y, z) = \frac{1}{\left(\sqrt{2\pi}\right)^3 \sigma_x \sigma_y \sigma_z} \exp\left[-\frac{1}{2}\left(\frac{x^2}{\sigma_x^2} + \frac{y^2}{\sigma_y^2} + \frac{z^2}{\sigma_z^2}\right)\right],$$

where , , are the characteristic bunch sizes along the axis$\sigma_x \sigma_y \sigma_z$X, Yand Z, respectively (Figure 9).Such a condition should be considered as an approximation due to the fact that the distribution of electrons in the bunch is subject to a limitation related to the conservation of the phase volume when the beam is converted in quadrupole lenses and other magnetic systems [41].

A)   b)
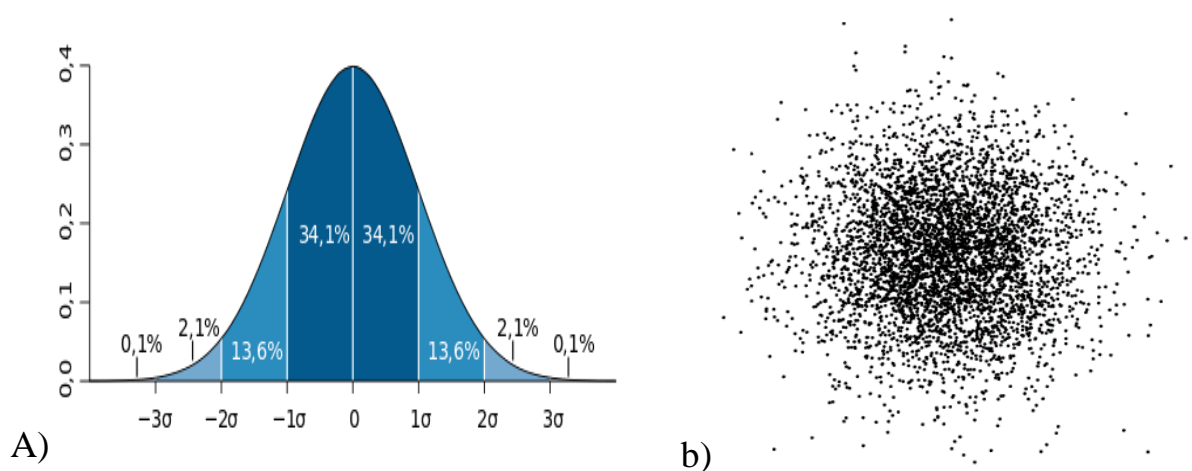
Figure 9 - Scheduleprobability density of the normal distribution (a), the form of the Gaussian distribution of electrons in the bunch in 2D (b)

In diffraction radiation, this approximation is valid if, in the geometry shown in Figure 8

$$\sigma_x \ll \frac{\gamma\lambda}{2\pi} e^{\frac{2\pi h}{\gamma\lambda}} \text{[41]}.$$

Thus, knowing the analytical expression for the distribution of electrons in the bunch and knowing the form of the phase difference for the case of transient and diffraction radiation, we proceed to the calculation of the form factor of one electron bunch. The scheme of the experiment is shown in Figure 10.
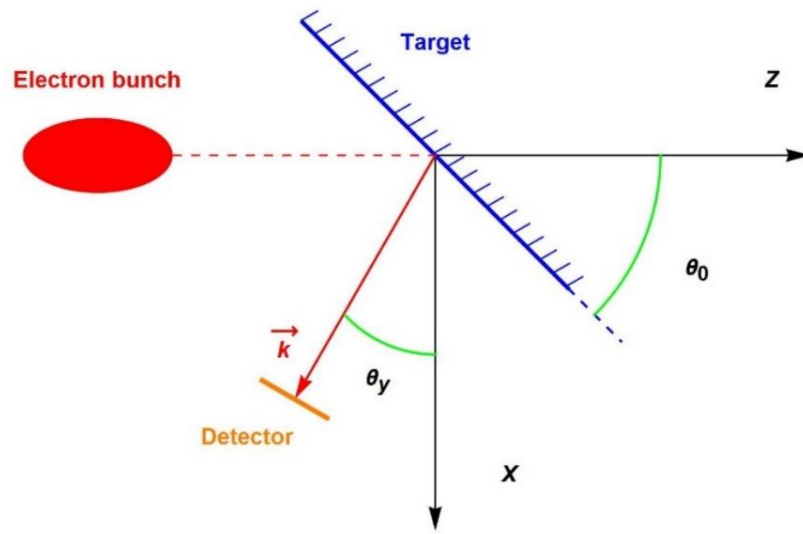
Figure 10 - Scheme of the experiment with one electron bunch

Let's write an expression for the form factor:

$$F(\omega, \vec{s}) = \left| \frac{1}{(\sqrt{2\pi})^3 \sigma_x \sigma_y \sigma_z} \iiint \exp\left[-\frac{1}{2}\left(\frac{x^2}{\sigma_x^2} + \frac{y^2}{\sigma_y^2} + \frac{z^2}{\sigma_z^2}\right)\right] \exp\left[i\frac{\omega}{c}(x \cdot s_x + y \cdot s_y + z \cdot s_z)\right] dxdydz \right|^2.$$

Let us split this expression into the product of three independent integrals

$$F(\omega, \vec{s}) = \left| \frac{1}{(\sqrt{2\pi})^3 \sigma_x \sigma_y \sigma_z} \left\{\int \exp\left[-\frac{1}{2}\frac{x^2}{\sigma_x^2} + i\frac{\omega}{c} x \cdot s_x\right] dx\right\} \left\{\int \exp\left[-\frac{1}{2}\frac{y^2}{\sigma_y^2} + i\frac{\omega}{c} y \cdot s_y\right] dy\right\} \left\{\int \exp\left[-\frac{1}{2}\frac{z^2}{\sigma_z^2} + i\frac{\omega}{c} z \cdot s_z\right] dz\right\} \right|^2$$

and calculate each of them separately.

According to the tables of integrals of exponential functions [45]:

$$\int_{-\infty}^{+\infty} \exp[-(ax^2 + 2bx + c)]dx = \sqrt{\frac{\pi}{2}} \exp\left[\frac{b^2 - ac}{a}\right].$$

For the integral: $\int_{-\infty}^{+\infty} \exp\left[-\frac{1}{2}\frac{x^2}{\sigma_x^2} + i\frac{\omega}{c} x \cdot s_x\right] dx$

$$a = \frac{1}{2\sigma_x^2}, \quad .b = -i\frac{1}{2}\frac{\omega}{c}s_x \quad c = 0$$

Then

$$\int_{-\infty}^{+\infty} \exp\left[-\frac{1}{2}\frac{x^2}{\sigma_x^2} + i\frac{\omega}{c}x \cdot s_x\right] dx = \sigma_x\sqrt{2\pi}\exp\left[-\frac{1}{2}\frac{\omega^2}{c^2}\sigma_x^2 s_x^2\right].$$

Similarly

$$\int_{-\infty}^{+\infty} \exp\left[-\frac{1}{2}\frac{y^2}{\sigma_y^2} + i\frac{\omega}{c}y \cdot s_y\right] dy = \sigma_y\sqrt{2\pi}\exp\left[-\frac{1}{2}\frac{\omega^2}{c^2}\sigma_y^2 s_y^2\right],$$

$$\int_{-\infty}^{+\infty} \exp\left[-\frac{1}{2}\frac{z^2}{\sigma_z^2} + i\frac{\omega}{c}z \cdot s_z\right] dz = \sigma_z\sqrt{2\pi}\exp\left[-\frac{1}{2}\frac{\omega^2}{c^2}\sigma_z^2 s_z^2\right].$$

Let's substitute the obtained values into the expression for the form factor:

$$F(\omega, \vec{s}) = \left|\frac{1}{(\sqrt{2\pi})^3 \sigma_x\sigma_y\sigma_z}\left\{\sigma_x\sqrt{2\pi}\exp\left[-\frac{1}{2}\frac{\omega^2}{c^2}\sigma_x^2 s_x^2\right]\right\}\left\{\sigma_y\sqrt{2\pi}\exp\left[-\frac{1}{2}\frac{\omega^2}{c^2}\sigma_y^2 s_y^2\right]\right\}\left\{\sigma_z\sqrt{2\pi}\exp\left[-\frac{1}{2}\frac{\omega^2}{c^2}\sigma_z^2 s_z^2\right]\right\}\right|^2,$$

and performing algebraic transformations, we obtain the form factor expression for one cluster:

$$F(\omega, \vec{s}) = \exp\left[-\frac{\omega^2}{c^2}\left(\sigma_x^2 s_x^2 + \sigma_y^2 s_y^2 + \sigma_z^2 s_z^2\right)\right].$$

The resulting formula is valid for both transition and diffraction radiation, its final form will be determined by the vector $\vec{s}$. For example, for diffraction radiation:

$$F(\omega, \vec{s}) = \exp\left[-\frac{\omega^2}{c^2}\left(\sigma_x^2 \cdot (0)^2 + \sigma_y^2 \cdot (0)^2 + \sigma_z^2 \cdot \left(\frac{1}{\beta}\right)^2\right)\right] =$$

$$= \exp\left[-\frac{\omega^2\sigma_z^2}{c^2}\left(\frac{1}{\beta}\right)^2\right].$$

For transition:

$$F(\omega, \vec{s}) = \exp\left[-\frac{\omega^2}{c^2}\left(\sigma_x^2 \cdot \left(-\cos\theta_y\cos\theta_x - \cot\theta_0\left(\sin\theta_y - \frac{1}{\beta}\right)\right)^2 + \sigma_y^2 \cdot \left(-\cos\theta_y\sin\theta_x\right)^2 + \sigma_z^2 \cdot \left(-\frac{1}{\beta}\right)^2\right)\right]$$

The following derivations of the form factor will not be accompanied by the substitution of specific components of the vector , i.e., they will be written in a general form (for the presented experimental geometries and the Gaussian distribution of electrons in the bunch) for compactness of the expressions obtained. $\vec{s}$

1.2.2.4 Form factor for a uniform cluster sequence

Let us consider a sequence of identical electron bunches, spaced at the same distance from each other, with a uniformly distributed space charge, assuming that

the centre of the first bunch is at the origin of the coordinate system associated with the target, and the bunches are counted against the direction of the bunches velocity, i.e. against the direction of the Z axis (Figure 11).ml

The normalized spatial distribution of electrons in a sequence of bunches in the geometry shown in Figure 11 will have the form:

$$\rho(x, y, z) = \frac{1}{m(\sqrt{2\pi})^3 \sigma_x \sigma_y \sigma_z} \exp\left[-\frac{1}{2}\left(\frac{x^2}{\sigma_x^2} + \frac{y^2}{\sigma_y^2}\right)\right] \sum_{p=1}^{m} \exp\left[-\frac{1}{2}\frac{(z+l\cdot(p-1))^2}{\sigma_z^2}\right].$$

Figure 11 - Scheme of a uniform sequence of electron bunches

Let's write the form factor of the following sequence:

$$F(\omega, \vec{s}) = \left| \frac{1}{m(\sqrt{2\pi})^3 \sigma_x \sigma_y \sigma_z} \left\{ \int \exp\left[-\frac{1}{2}\frac{x^2}{\sigma_x^2} + i\frac{\omega}{c}x \cdot s_x\right] dx \right\} \left\{ \int \exp\left[-\frac{1}{2}\frac{y^2}{\sigma_y^2} + i\frac{\omega}{c}y \cdot s_y\right] dy \right\} \left\{ \int \exp\left[-\frac{1}{2}\frac{(z+l\cdot(p-1))^2}{\sigma_z^2} + i\frac{\omega}{c}z \cdot s_z\right] dz \right\} \right|^2 $$

The solution for the first two integrals was discussed in the previous part of the chapter, so we will dwell on the solution of only the third integral in more detail.

The integral of the sum can be considered as the sum of integrals

$$\int_{-\infty}^{+\infty} \sum_{p=1}^{m} \exp\left[-\frac{1}{2}\frac{(z+l\cdot(p-1))^2}{\sigma_z^2} + i\frac{\omega}{c}z \cdot s_z\right] dz =$$

$$= \sum_{p=1}^{m} \int_{-\infty}^{+\infty} \exp\left[-\left(\frac{1}{2\sigma_z^2}z^2 + 2\left(\frac{l\cdot(p-1)}{2\sigma_z^2} - i\frac{\omega}{2c}s_z\right)z + \frac{l^2\cdot(p-1)^2}{2\sigma_z^2}\right)\right] dz,$$

and the coefficients , and , in this case have the following form:abc

$$a = \frac{1}{2\sigma_z^2}, \; , \; .b = \frac{l\cdot(p-1)}{2\sigma_z^2} - i\frac{\omega}{2c}s_z c = \frac{l^2\cdot(p-1)^2}{2\sigma_z^2}$$

In view of the foregoing, we write the solution for the third integral:

$$\sum_{p=1}^{m} \int_{-\infty}^{+\infty} \exp\left[-\left(\frac{1}{2\sigma_z^2}z^2 + 2\left(\frac{l\cdot(p-1)}{2\sigma_z^2} - i\frac{\omega}{2c}s_z\right)z + \frac{l^2\cdot(p-1)^2}{2\sigma_z^2}\right)\right] dz =$$

$$= \sigma_z\sqrt{2\pi}\exp\left[-\frac{1}{2}\frac{\omega^2}{c^2}\sigma_z^2 s_z^2\right]\sum_{p=1}^{m}\exp\left[-i\frac{\omega}{c}l\cdot(p-1)s_z\right],$$

and form factor:

$$F(\omega,\vec{s}) = \frac{1}{m^2}\exp\left[-\frac{\omega^2}{c^2}\left(\sigma_x^2 s_x^2 + \sigma_y^2 s_y^2 + \sigma_z^2 s_z^2\right)\right]\left|\sum_{p=1}^{m}\exp\left[-i\frac{\omega}{c}l\cdot(p-1)s_z\right]\right|^2.$$

1.2.2.5 Spatial distribution of charge in a sequence

We introduce a parameter that takes into account the distribution of the space charge in a sequence of bunches:

$$\mu_p = \frac{N_p}{\sum_{p=1}^{m} N_p}.$$

This parameter characterizes the fraction of the space charge in the -th bunch and is a normalized value:p

$$\sum_{p=1}^{m}\mu_p = \sum_{p=1}^{m}\frac{N_p}{\sum_{p=1}^{m} N_p} = 1.$$

The expression for the normalized spatial distribution of electrons in a sequence of identical bunches with the same distance between them, in the geometry presented in Figure 12, taking into account the parameter , looks as follows:$ml\mu_p$

$$\rho(x,y,z) = \frac{1}{(\sqrt{2\pi})^3\sigma_x\sigma_y\sigma_z}\exp\left[-\frac{1}{2}\left(\frac{x^2}{\sigma_x^2} + \frac{y^2}{\sigma_y^2}\right)\right]\sum_{p=1}^{m}\mu_p\exp\left[-\frac{1}{2}\frac{(z+l\cdot(p-1))^2}{\sigma_z^2}\right].$$
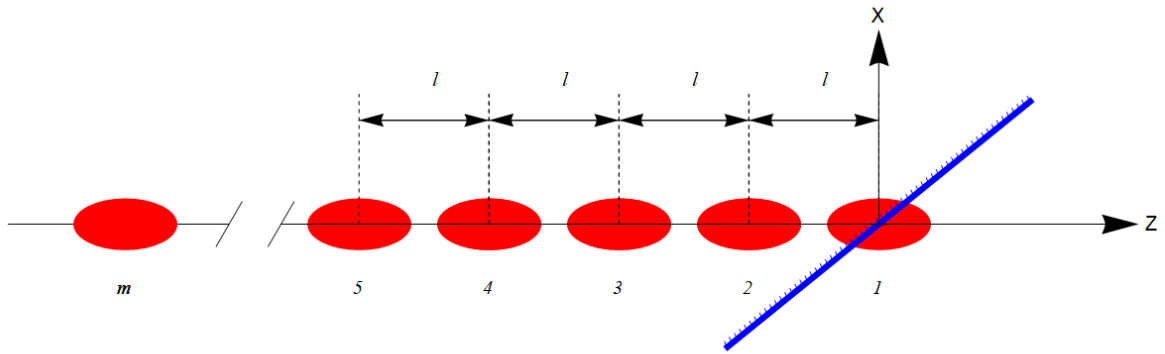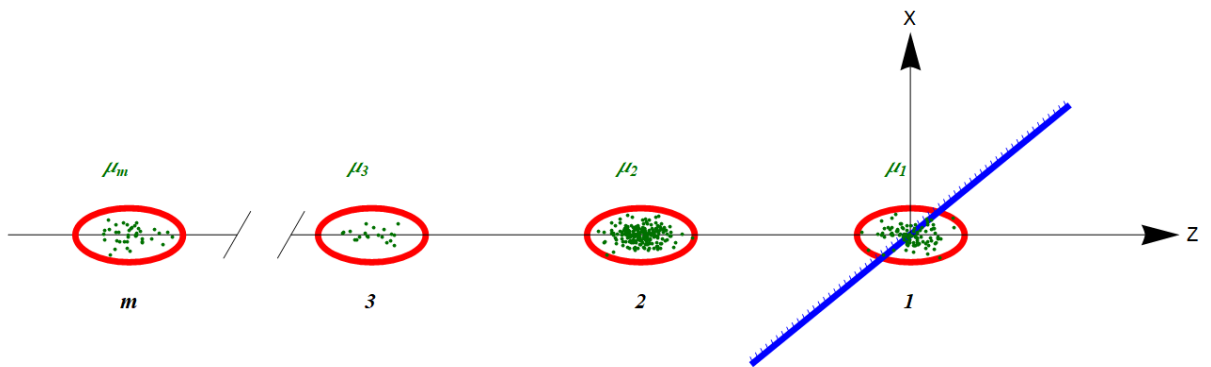

Figure 12 - Diagram of the sequence of electron bunches with a non-uniform charge distribution in the beam

It is easy to see that with a uniform charge distribution, when , the spatial distribution of electrons takes the form identical to the form of distribution from the previous part of the chapter. $\mu_1 = \mu_2 = \cdots = \mu_p$

Let us calculate the form factor of such a bunch distribution:

$$F(\omega, \vec{s}) = \left| \frac{1}{(\sqrt{2\pi})^3 \sigma_x \sigma_y \sigma_z} \left\{ \int \exp\left[-\frac{1}{2} \frac{x^2}{\sigma_x^2} + i \frac{\omega}{c} x \cdot s_x \right] dx \right\} \left\{ \int \exp\left[-\frac{1}{2} \frac{y^2}{\sigma_y^2} + i \frac{\omega}{c} y \cdot s_y \right] dy \right\} \left\{ \int \sum_{p=1}^{m} \mu_p \exp\left[-\frac{1}{2} \frac{(z+l\cdot(p-1))^2}{\sigma_z^2} + i \frac{\omega}{c} z \cdot s_z \right] dz \right\} \right|^2$$

The further course of reasoning is similar to that presented in the previous part of the chapter, with the only exception that we take the coefficient out of the integral sign, as a constant factor: μ_p

$$\int_{-\infty}^{+\infty} \sum_{p=1}^{m} \mu_p \exp\left[-\frac{1}{2} \frac{(z+l\cdot(p-1))^2}{\sigma_z^2} + i \frac{\omega}{c} z \cdot s_z \right] dz =$$

$$= \sum_{p=1}^{m} \mu_p \int_{-\infty}^{+\infty} \exp\left[-\left(\frac{1}{2\sigma_z^2} z^2 + 2 \left(\frac{l\cdot(p-1)}{2\sigma_z^2} - i \frac{\omega}{2c} s_z \right) z + \frac{l^2 \cdot (p-1)^2}{2\sigma_z^2} \right) \right] dz.$$

Then, the form factor, taking into account the distribution of the space charge in a sequence of identical (from the point of view of characteristic sizes , and) bunches spaced at the same distance from each other, will have the following form: $\sigma_x \, \sigma_y \sigma_z$

$$F(\omega, \vec{s}) = \exp\left[-\frac{\omega^2}{c^2} \left(\sigma_x^2 s_x^2 + \sigma_y^2 s_y^2 + \sigma_z^2 s_z^2 \right) \right] \left| \sum_{p=1}^{m} \mu_p \exp\left[-i \frac{\omega}{c} l \cdot (p-1) s_z \right] \right|^2.$$

1.2.2.6 Arbitrary distance between bunches

Consider the same sequence of electron bunches with an arbitrary space charge, the same size, but with different distances between them (Figure 13).

The distribution for this case can be written as:

$$\rho(x, y, z) = \frac{1}{(\sqrt{2\pi})^3 \sigma_x \sigma_y \sigma_z} \exp\left[-\frac{1}{2} \left(\frac{x^2}{\sigma_x^2} + \frac{y^2}{\sigma_y^2} \right) \right] \sum_{p=1}^{m} \mu_p \exp\left[-\frac{1}{2} \frac{(z-z_p)^2}{\sigma_z^2} \right],$$

where is the coordinate of the center of the -th bunch, counted from the origin of the coordinate system associated with the target. $z_p p$
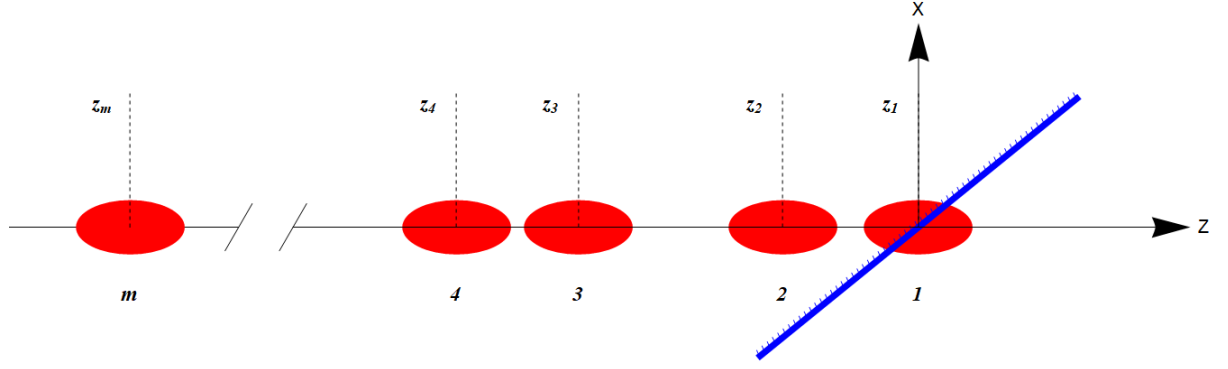
Figure 13 - Diagram of the sequence of electron bunches with a given longitudinal displacement

Let's calculate the form factor, as shown in the previous parts:

$$F(\omega, \vec{s}) = \left| \frac{1}{(\sqrt{2\pi})^3 \sigma_x \sigma_y \sigma_z} \left\{ \int \exp\left[-\frac{1}{2}\frac{x^2}{\sigma_x^2} + i\frac{\omega}{c}x \cdot s_x\right] dx \right\} \left\{ \int \exp\left[-\frac{1}{2}\frac{y^2}{\sigma_y^2} + i\frac{\omega}{c}y \cdot s_y\right] dy \right\} \left\{ \int \sum_{p=1}^{m} \mu_p \exp\left[-\frac{1}{2}\frac{(z-z_p)^2}{\sigma_z^2} + i\frac{\omega}{c}z \cdot s_z\right] dz \right\} \right|^2.$$

And already traditionally we will consider only the third integral:

$$\int_{-\infty}^{+\infty} \sum_{p=1}^{m} \mu_p \exp\left[-\frac{1}{2}\frac{(z-z_p)^2}{\sigma_z^2} + i\frac{\omega}{c}z \cdot s_z\right] dz = \sum_{p=1}^{m} \mu_p \int_{-\infty}^{+\infty} \exp\left[-\left(\frac{1}{2\sigma_z^2}z^2 + 2\left(-\frac{z_p}{2\sigma_z^2} - i\frac{\omega}{2c}s_z\right)z + \frac{z_p^2}{2\sigma_z^2}\right)\right] dz.$$

We select the coefficients a, b, c:

$$a = \frac{1}{2\sigma_z^2}, \quad b = -\frac{z_p}{2\sigma_z^2} - i\frac{\omega}{2c}s_z, \quad c = \frac{z_p^2}{2\sigma_z^2}$$

and write the solution for this integral:

$$\sum_{p=1}^{m} \mu_p \int_{-\infty}^{+\infty} \exp\left[-\left(\frac{1}{2\sigma_z^2}z^2 + 2\left(-\frac{z_p}{2\sigma_z^2} - i\frac{\omega}{2c}s_z\right)z + \frac{z_p^2}{2\sigma_z^2}\right)\right] dz =$$

$$\sigma_z\sqrt{2\pi}\exp\left[-\frac{1}{2}\frac{\omega^2}{c^2}\sigma_z^2 s_z^2\right]\sum_{p=1}^{m} \mu_p\exp\left[i\frac{\omega}{c}z_p s_z\right],$$

and form factor:

$$F(\omega, \vec{s}) = \exp\left[-\frac{\omega^2}{c^2}\left(\sigma_x^2 s_x^2 + \sigma_y^2 s_y^2 + \sigma_z^2 s_z^2\right)\right]\left|\sum_{p=1}^{m} \mu_p\exp\left[i\frac{\omega}{c}z_p s_z\right]\right|^2.$$

1.2.2.7 Lateral displacement of bunches in a sequence

The lateral displacement of bunches can also be described in terms of spatial distribution by introducing additional parameters and , which are the coordinates of the center of the -th bunch along the corresponding X and Y axes (Figure 14):$x_p y_p p$

$$\rho(x, y, z) = \frac{1}{(\sqrt{2\pi})^3 \sigma_x \sigma_y \sigma_z}\sum_{p=1}^{m} \mu_p\exp\left[-\frac{1}{2}\left\{\frac{(x-x_p)^2}{\sigma_x^2} + \frac{(y-y_p)^2}{\sigma_y^2} + \frac{(z-z_p)^2}{\sigma_z^2}\right\}\right]$$

Figure 14 - Diagram of the sequence of electron bunches with transverse biases

Let's calculate the form factor for this case:

$$F(\omega,\vec{s}) = \left| \frac{1}{(\sqrt{2\pi})^3 \sigma_x \sigma_y \sigma_z} \sum_{p=1}^m \mu_p \left\{ \int \exp\left[-\frac{1}{2}\frac{(x-x_p)^2}{\sigma_x^2} + i\frac{\omega}{c}x \cdot s_x\right] dx \right\} \left\{ \int \exp\left[-\frac{1}{2}\frac{(y-y_p)^2}{\sigma_y^2} + i\frac{\omega}{c}y \cdot s_y\right] dy \right\} \left\{ \int \exp\left[-\frac{1}{2}\frac{(z-z_p)^2}{\sigma_z^2} + i\frac{\omega}{c}z \cdot s_z\right] dz \right\} \right|^2.$$

Since an integral similar to those presented has already been considered above, we will omit the calculations and immediately present the resulting expression:

$$F(\omega,\vec{s}) = \exp\left[-\frac{\omega^2}{c^2}\left(\sigma_x^2 s_x^2 + \sigma_y^2 s_y^2 + \sigma_z^2 s_z^2\right)\right] \left| \sum_{p=1}^m \mu_p \exp\left[i\frac{\omega}{c}\left(x_p s_x + y_p s_y + z_p s_z\right)\right] \right|^2.$$

1.2.2.8 Cluster sizes in sequence

Let's move on to the sequence in which the bunches, in addition to the arbitrary parameters described above, also have sizes that vary from bunch to bunch (Figure 15).

It should be understood that the characteristic size is indicated conditionally in the diagram, and the actual size of the clot is found through the ratios presented in Figure 9.
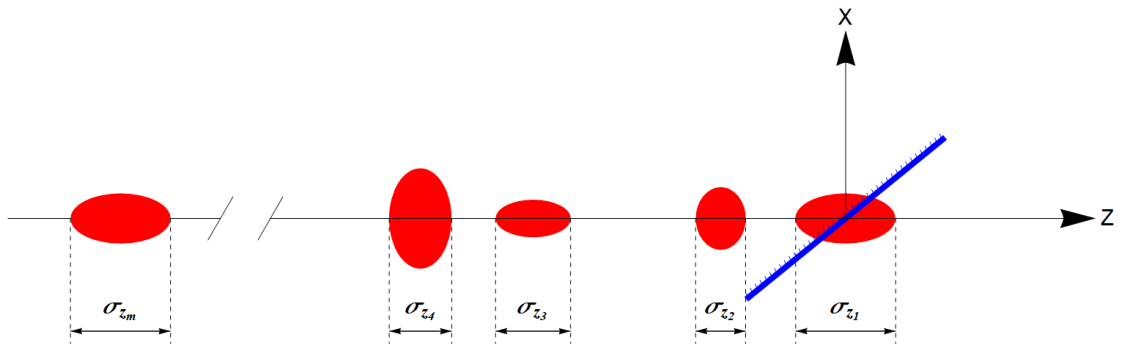
The size variability parameter can be taken into account using the expression for the normalized spatial distribution of electrons in a sequence of bunches:

$$\rho(x,y,z) = \sum_{p=1}^{m} \mu_p \frac{1}{\left(\sqrt{2\pi}\right)^3 \sigma_{x_p}\sigma_{y_p}\sigma_{z_p}} \exp\left[-\frac{1}{2}\left\{\frac{(x-x_p)^2}{\sigma_{x_p}^2} + \frac{(y-y_p)^2}{\sigma_{y_p}^2} + \frac{(z-z_p)^2}{\sigma_{z_p}^2}\right\}\right].$$
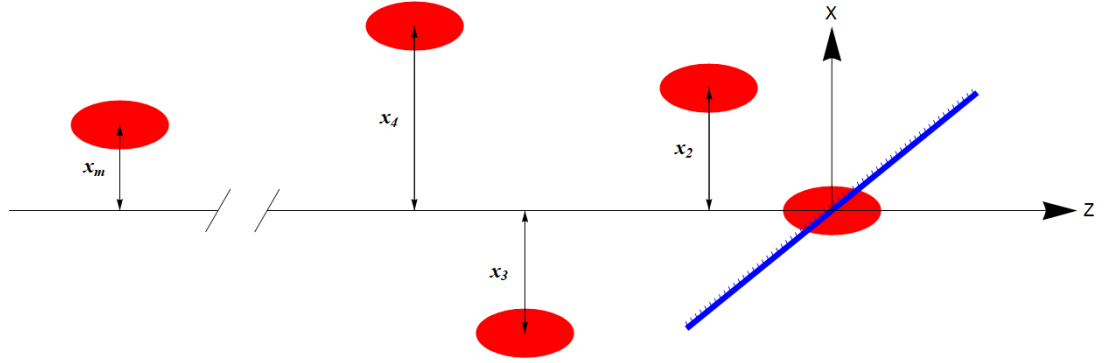
Let's write the form factor:

$$F(\omega,\vec{s}) = \left|\sum_{p=1}^{m} \mu_p \frac{1}{\left(\sqrt{2\pi}\right)^3 \sigma_{x_p}\sigma_{y_p}\sigma_{z_p}}\left\{\int \exp\left[-\frac{1}{2}\frac{(x-x_p)^2}{\sigma_{x_p}^2} + i\frac{\omega}{c}x\cdot s_x\right]dx\right\}\left\{\int \exp\left[-\frac{1}{2}\frac{(y-y_p)^2}{\sigma_{y_p}^2} + i\frac{\omega}{c}y\cdot s_y\right]dy\right\}\left\{\int \exp\left[-\frac{1}{2}\frac{(z-z_p)^2}{\sigma_{z_p}^2} + i\frac{\omega}{c}z\cdot s_z\right]dz\right\}\right|^2$$

We omit the calculations, since they will repeat the previous conclusions, and immediately write the final expression for the form factor

$$F(\omega,\vec{s}) = \left|\sum_{p=1}^{m} \mu_p \exp\left[-\frac{1}{2}\frac{\omega^2}{c^2}\left(\sigma_{x_p}^2 s_x^2 + \sigma_{y_p}^2 s_y^2 + \sigma_{z_p}^2 s_z^2\right)\right] \exp\left[i\frac{\omega}{c}\left(x_p s_x + y_p s_y + z_p s_z\right)\right]\right|^2.$$

1.2.2.9 Uniform distribution of electrons in bunches of different shapes

It is known that bunches of various shapes have an angular distribution of transition radiation different from the classical one [46]. In this case, it is interesting to consider the expression for the form factor for similar particle distributions. Here is a detailed derivation of the form factor expression for spherical, ellipsoidal and cylindrical single bunches with a uniform distribution of electrons in the cavity of the indicated shapes.

1.2.2.9.1 Spherical bunch

Let us first consider a simpler case for one spherical bunch with a uniform distribution of electrons in it (Figure 16).
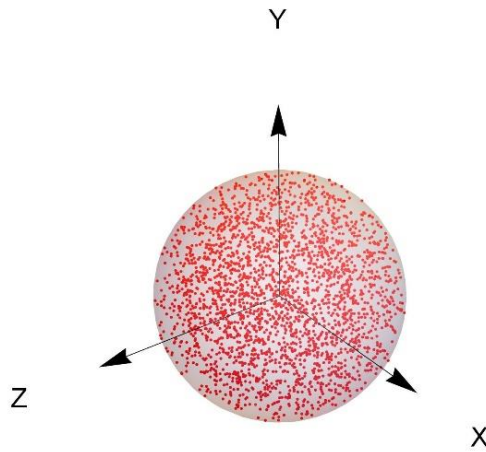
Figure 16 - Model of uniformly distributed electrons in the volume of a sphere

Recall the canonical equation of the sphere in Cartesian coordinates:

$$x^2 + y^2 + z^2 = R^2$$

Then, the distribution density of electrons in space will be described by the formula:

$$\rho(\vec{r}) = \begin{cases} Const & x^2 + y^2 + z^2 \leq R^2 \\ 0 & x^2 + y^2 + z^2 > R^2 \end{cases}$$

Now we need to find the normalization coefficient from the condition

$$\iiint_V \rho(\vec{r})dV = 1$$

To take the integral, let's move from Cartesian to spherical coordinates using the known relations:

$$\begin{cases} x = r\cos\varphi\sin\theta \\ y = r\sin\varphi\cos\theta \\ z = r\cos\theta \end{cases}$$

$$r \geq 0$$
$$0 \leq \varphi \leq 2\pi$$
$$0 \leq \theta \leq \pi$$

And also the Jacobian of the transition:

$$J(r,\theta,\varphi) = \det \begin{bmatrix} \dfrac{\partial x}{\partial r} & \dfrac{\partial x}{\partial \theta} & \dfrac{\partial x}{\partial \varphi} \\ \dfrac{\partial y}{\partial r} & \dfrac{\partial y}{\partial \theta} & \dfrac{\partial y}{\partial \varphi} \\ \dfrac{\partial z}{\partial r} & \dfrac{\partial z}{\partial \theta} & \dfrac{\partial z}{\partial \varphi} \end{bmatrix} =$$

$$= \det \begin{bmatrix} \sin\theta\cos\varphi & r\cos\theta\cos\varphi & -r\sin\theta\sin\varphi \\ \sin\theta\sin\varphi & r\cos\theta\sin\varphi & r\sin\theta\cos\varphi \\ \cos\theta & -r\sin\theta & 0 \end{bmatrix} =$$

$$= r^2 \sin\theta$$

$$\iiint_V \rho(\vec{r})dV = \int_0^R \int_0^\pi \int_0^{2\pi} (Const)\cdot r^2\sin\theta\, dr d\theta d\varphi + \int_R^{+\infty}\int_0^\pi\int_0^{2\pi} 0\cdot r^2\sin\theta\, dr d\theta d\varphi =$$

$$= Const\int_0^R r^2 dr \int_0^\pi \sin\theta\, d\theta \int_0^{2\pi} d\varphi = (Const)\cdot\frac{4}{3}\pi R^3$$

Let's find the normalization coefficient:

$$(Const)\cdot\frac{4}{3}\pi R^3 = 1,$$

$$Const = \frac{3}{4\pi R^3}.$$

Thus, the uniform normalized spatial distribution of electrons in a spherical bunch will have the form:

$$\rho(\vec{r}) = \begin{cases} \frac{3}{4\pi R^3} & r^2 \le R^2 \\ 0 & r^2 > R^2 \end{cases},$$

$$\vec{r} = \{r,\theta,\varphi\}.$$

Let's write the form factor in spherical coordinates:

$$F(\omega,\vec{s}) = \left| \int_0^R \int_0^\pi \int_0^{2\pi} e^{i\frac{\omega}{c}(\vec{s}\cdot\vec{r})}\rho(\vec{r})r^2\sin\theta\, dr d\theta d\varphi \right|^2 = \left| \frac{3}{4\pi R^3}\int_0^R \int_0^\pi \int_0^{2\pi} e^{i\frac{\omega}{c}(\vec{s}\cdot\vec{r})}r^2\sin\theta\, dr d\theta d\varphi \right|^2$$

1.2.2.9.2 Ellipsoidal bunch

Let us consider the case for one ellipsoidal bunch with a uniform distribution of electrons in it (Figure 17).
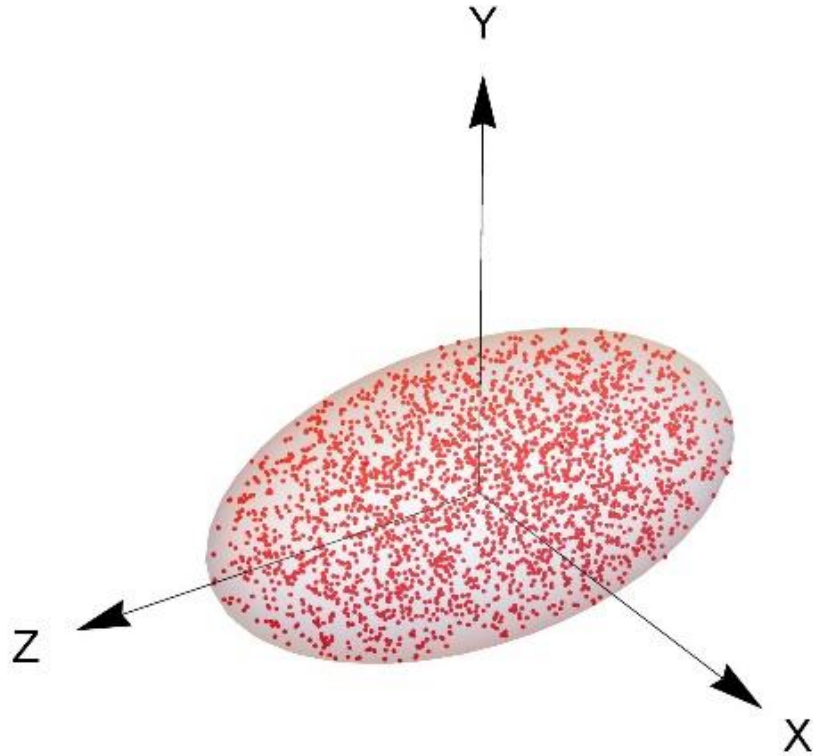
Figure 17 - Model of uniformly distributed electrons in the volume of an ellipsoid

Recall the canonical equation of an ellipsoid in Cartesian coordinates:

$$\frac{x^2}{a^2} + \frac{y^2}{b^2} + \frac{z^2}{c^2} = 1$$

Then, the distribution density of electrons in space will be described by the following formula:

$$\rho(\vec{r}) = \begin{cases} Const & \frac{x^2}{a^2} + \frac{y^2}{b^2} + \frac{z^2}{c^2} \leq 1 \\ 0 & \frac{x^2}{a^2} + \frac{y^2}{b^2} + \frac{z^2}{c^2} > 1 \end{cases}$$

Now we need to find the normalization coefficient from the condition

$$\iiint_V \rho(\vec{r})dV = 1$$

To take the integral, let's move from Cartesian coordinates to generalized spherical ones using the known relations:

$$\begin{cases} x = ar \cos \varphi \sin \theta \\ y = br \sin \varphi \sin \theta \\ z = cr \cos \theta \end{cases}$$

$$0 \leq r \leq 1$$
$$0 \leq \theta \leq \pi$$
$$0 \leq \varphi \leq 2\pi$$

And also the Jacobian of the transition:

$$J(r, \theta, \varphi) = \det \begin{bmatrix} \dfrac{\partial x}{\partial r} & \dfrac{\partial x}{\partial \theta} & \dfrac{\partial x}{\partial \varphi} \\ \dfrac{\partial y}{\partial r} & \dfrac{\partial y}{\partial \theta} & \dfrac{\partial y}{\partial \varphi} \\ \dfrac{\partial z}{\partial r} & \dfrac{\partial z}{\partial \theta} & \dfrac{\partial z}{\partial \varphi} \end{bmatrix} =$$

$$= \det \begin{bmatrix} a \cos \varphi \sin \theta & ar \cos \varphi \cos \theta & -ar \sin \varphi \sin \theta \\ b \sin \varphi \sin \theta & br \sin \varphi \cos \theta & br \cos \varphi \sin \theta \\ c \cos \theta & -cr \sin \theta & 0 \end{bmatrix} =$$

$$= abcr^2 \sin \theta.$$

$$\iiint_V \rho(\vec{r}) dV = \int_0^1 \int_0^\pi \int_0^{2\pi} (Const) \cdot abcr^2 \sin \theta \, dr d\theta d\varphi + \int_1^{+\infty} \int_0^\pi \int_0^{2\pi} 0 \cdot abcr^2 \sin \theta \, dr d\theta d\varphi =$$

$$= Const \frac{4\pi}{3} abc.$$

Let's find the normalization coefficient:

$$(Const) \cdot \frac{4\pi}{3} abc = 1,$$

$$Const = \frac{3}{4\pi abc}.$$

Thus, the uniform normalized spatial distribution of electrons in an ellipsoidal bunch will have the form:

$$\rho(\vec{r}) = \begin{cases} \dfrac{3}{4\pi abc} & r^2 \leq 1 \\ 0 & r^2 > 1 \end{cases}$$

$$\vec{r} = \{r, \theta, \varphi\}.$$

We write the form factor in generalized spherical coordinates:

$$F(\omega, \vec{s}) = \left| \int\limits_0^1 \int\limits_0^\pi \int\limits_0^{2\pi} \rho(\vec{r}) \cdot e^{i\frac{\omega}{c}(\vec{s}\cdot\vec{r})} \cdot abcr^2 \sin\theta \, dr d\theta d\varphi \right|^2 =$$

$$= \left| \frac{3}{4\pi} \int_0^1 \int_0^\pi \int_0^{2\pi} e^{i\frac{\omega}{c}(\vec{s}\cdot\vec{r})} \cdot r^2 \sin\theta \, dr d\theta d\varphi \right|^2.$$

1.2.2.9.3 Cylindrical bunch

Let us consider the case for one cylindrical bunch with a uniform distribution of electrons in it (Figure 18).
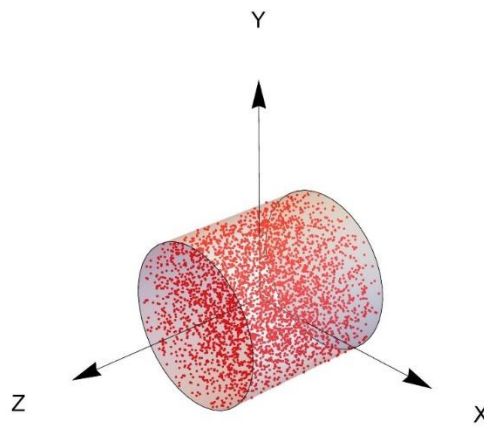
Figure 18 - Model of uniformly distributed electrons in the volume of a cylinder

Recall the canonical equation for a cylinder in Cartesian coordinates:

$$\frac{x^2}{a^2} + \frac{y^2}{b^2} = 1.$$

Then, the distribution density of electrons in space will be described by the following formula:

$$\rho(\vec{r}) = \begin{cases} Const & \dfrac{x^2}{a^2} + \dfrac{y^2}{b^2} \leq 1 \\ 0 & \dfrac{x^2}{a^2} + \dfrac{y^2}{b^2} > 1 \end{cases}$$

Now we need to find the normalization coefficient from the condition

$$\iiint\limits_V \rho(\vec{r}) dV = 1$$

To take the integral, let's move from Cartesian to cylindrical coordinates using the known relations:

$$\begin{cases} x = r \cos \varphi \\ y = r \sin \varphi \\ z = z \end{cases}$$

$0 \leq r \leq R$
$0 \leq \varphi \leq 2\pi$
$0 \leq z \leq h$

And also the Jacobian of the transition:

$$J(r, \varphi, z) = \det \begin{bmatrix} \dfrac{\partial x}{\partial r} & \dfrac{\partial x}{\partial \varphi} & \dfrac{\partial x}{\partial z} \\ \dfrac{\partial y}{\partial r} & \dfrac{\partial y}{\partial \varphi} & \dfrac{\partial y}{\partial z} \\ \dfrac{\partial z}{\partial r} & \dfrac{\partial z}{\partial \varphi} & \dfrac{\partial z}{\partial z} \end{bmatrix} = \det \begin{bmatrix} \cos \varphi & -r \sin \varphi & 0 \\ \sin \varphi & r \cos \varphi & 0 \\ 0 & 0 & 1 \end{bmatrix} = r$$

$$\iiint_V \rho(\vec{r})dV = \int_0^R \int_0^{2\pi} \int_0^h (Const) \cdot r dr d\varphi dz + \int_R^{+\infty} \int_0^{2\pi} \int_h^{+\infty} 0 \cdot r dr d\varphi dz =$$

$$= Const \cdot \pi R^2 h$$

Let's find the normalization coefficient:

$$(Const) \cdot \pi R^2 h = 1,$$

$$Const = \frac{1}{\pi R^2 h}.$$

Thus, the uniform normalized spatial distribution of electrons in a cylindrical bunch will have the form:

$$\rho(\vec{r}) = \begin{cases} \dfrac{1}{\pi R^2 h} & \dfrac{(r \cos \varphi)^2}{a^2} + \dfrac{(r \sin \varphi)^2}{b^2} \leq 1 \\ 0 & \dfrac{(r \cos \varphi)^2}{a^2} + \dfrac{(r \sin \varphi)^2}{b^2} > 1 \end{cases},$$

$$\vec{r} = \{r, \varphi, z\}.$$

Let's write the form factor in cylindrical coordinates:

$$F(\omega, \vec{s}) = \left| \int_0^R \int_0^{2\pi} \int_0^h \rho(\vec{r}) \cdot e^{i\frac{\omega}{c}(\vec{s}\cdot\vec{r})} \cdot r dr d\varphi dz \right|^2 = \left| \frac{1}{\pi R^2 h} \int_0^R \int_0^{2\pi} \int_0^h e^{i\frac{\omega}{c}(\vec{s}\cdot\vec{r})} r dr d\varphi dz \right|^2$$

1.2.2.10 Approximations, assumptions, limitations of the approach and plans for the development of the mathematical apparatus of the model

We list all the conventions of the proposed mathematical apparatus. Here both new and previously mentioned approximations and limitations will be given.

1.   The distribution of electrons in the bunch is given by three independent continuous distributions along three axes *X, Y* and Z.

2.   The field strength of an individual electron does not depend on the change in its position in the bunch.

3.   It is assumed that the number of electrons in the bunch is much greater than unity.

4.   In calculations of the coherent and incoherent components of the spectral-angular distribution formula, combinations of the interaction of two particles are taken into account, however, combinations of the interaction of three or more particles are not taken into account.

5.   It is assumed that the target has infinite dimensions and is made of a material with infinite conductivity, that is, it is an ideal conductor. Thus, the edge effects of the target, as well as the geometry of the experiment with targets of complex shapes, for example, spherical [47], are not taken into account.

6.   The incoherent form factor [43] was not taken into account in the formula for the total spectral-angular distribution of radiation.

7.   The influence of the Coulomb repulsion of charged particles in the beam is not taken into account.

8.   More complex geometrical parameters, such as the inclination of each bunch in space and the rotation of the target around two axes, are not taken into account (in the presented work, the target can be inclined only about one axis).

9.   An analytical expression for calculating the emission spectrum from a single electron is not given. More details about the possibility of calculation can be found in [48].

10.   The condition for observing a coherent signal at a chosen wavelength determines the applicability of the method for diagnosing an electron beam. $\lambda \geq \sigma_z$

11.   From the mathematical expression for the signal, it is impossible to judge the direction of bunch motion.

12.   The influence of the radiation propagation medium, as well as the throughput of the materials of the components of the interferometer and the accelerator branch pipe, are not taken into account.

It is necessary to carry out further work on the development of the mathematical formalism of the form factor, supplementing it, for example, with new parameters for bunch grouping, the spatial rotation of the target, and taking into account its edge effects; attention should also be paid to the incoherent radiation form factor. However, at this stage, we can talk about the sufficient fulfillment of the task of formulating a mathematical apparatus that describes the physical processes underlying the method. Let us return to the analysis of the dependence of the signal intensity on the motion of the interferometer mirror. In part 1.3. a description of the computer code created to analyze the influence of the bunch parameters on the form of the interferogram will be given.

1.3 Creation of modeling tools to analyze the relationship between the parameters of electron beams

Following the work plan, it is necessary to create tools for modeling interferograms that have a high (compared to human capabilities) speed of plotting, a simple interface, and also have the ability to vary each of the parameters of the desired mathematical expression in real time. In addition, the programs must have a high-quality three-dimensional visualization of the sequence of bunches and experimental geometries, since the resulting formulas abound in a variety of spatial parameters.

Recall that the mathematical expression describing the intensity of the signal depending on the step of the movable mirror of the interferometer has the form

$$I(\Delta l) = \int_{v_1}^{v_2} \frac{d^2 W_0}{d\omega d\Omega} \cdot [N + N(N-1)F(v)] \cdot \left| 1 + e^{-\frac{i2\pi \Delta l v}{c}} \right|^2 S(v) dv$$

This expression will underlie the code for simulation. The first version of the program is intended to demonstrate the dependence of the signal shape on a uniform sequence of electron bunches, thus using a simplified form factor expression.

$$F(\omega, \vec{s}) = \frac{1}{m^2} \exp\left[-\frac{\omega^2}{c^2}\left(\sigma_x^2 s_x^2 + \sigma_y^2 s_y^2 + \sigma_z^2 s_z^2\right)\right] \left|\sum_{p=1}^{m} \exp\left[-i\frac{\omega}{c} l \cdot (p-1)s_z\right]\right|^2$$

In the second version of the program, the form factor for an arbitrary sequence in the form is used.

$$F(\omega, \vec{s}) = \left|\sum_{p=1}^{m} \mu_p \exp\left[-\frac{1}{2}\frac{\omega^2}{c^2}\left(\sigma_{x_p}^2 s_x^2 + \sigma_{y_p}^2 s_y^2 + \sigma_{z_p}^2 s_z^2\right)\right] \exp\left[i\frac{\omega}{c}\left(x_p s_x + y_p s_y + z_p s_z\right)\right]\right|^2$$

In the model, we will assume that the detector sensitivity function has the form of a uniform distribution and is determined by the function:

$$S(\nu) = \begin{cases} 1, \ \nu_{Dmin} < \nu < \nu_{Dmax} \\ 0, \nu < \nu_{Dmin} \ \& \ \nu > \nu_{Dmax} \end{cases}$$

The problem was solved in the Wolfram Mathematica package. In the course of work, applications were created that meet the stated requirements (the listing is presented in Appendix C). Let's move on to a description of their purpose and functionality. Figure 19 shows the interface of the created application for the case of arbitrary sequences.
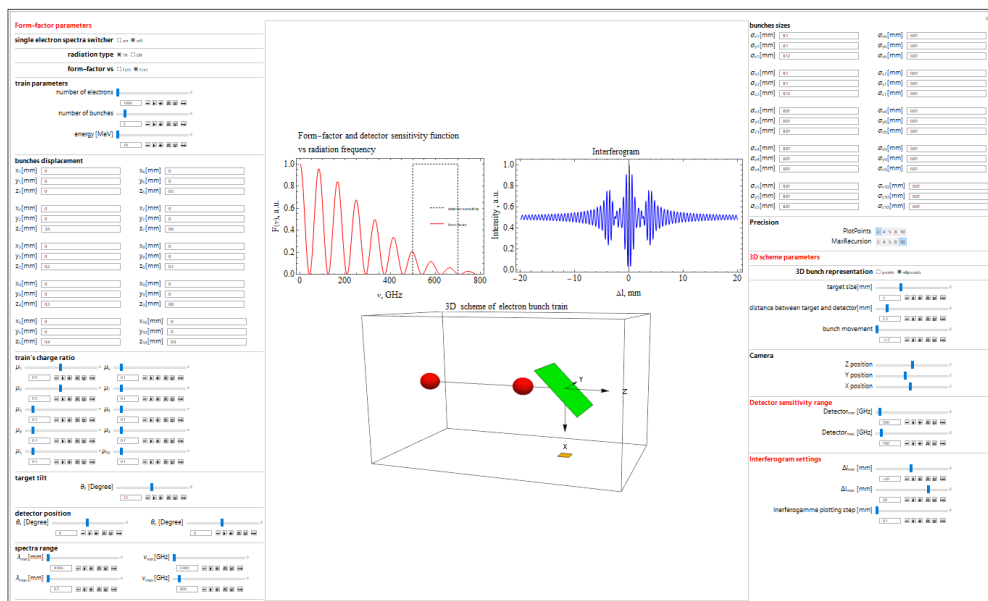
Figure 19 - Program interface for calculating the interferogram

In the central window of the program, 3 main elements are observed: a 3D diagram of the beam movement (the target is marked in green, the detector is marked in yellow, the color of the bunches changes depending on the energy), the form factor graph (solid red line) of the electron bunch sequence with the detector sensitivity function (black hatched line), and finally the interferogram itself (solid blue line). The control panel is divided into four blocks: "Form factor parameters", "3D scheme parameters", "Detector sensitivity range", "Interferogamma settings". Block names are highlighted in red font.

Let's list the functionality of the "Form factor parameters" block:

"Emission spectrum from one electron" allows you to connect a preloaded emission spectrum from one electron. Control via the radio button "on", "off". When connected, the name of the graph on the screen also changes from Form Factor to Emission Spectrum. Disabled by default.

"Switch of the type of radiation."This switcher allows the user to switch between two experiment geometries - transition and diffraction radiation, by changing the coordinates of the vector. $\vec{s}$

In the case of transition radiation

$$\vec{s} = \begin{Bmatrix} s_x \\ s_y \\ s_z \end{Bmatrix} = \begin{Bmatrix} -\cos\theta_y \cos\theta_x - \cot\theta_0 \left(\sin\theta_y - \frac{1}{\beta}\right) \\ -\cos\theta_y \sin\theta_x \\ -\frac{1}{\beta} \end{Bmatrix}.$$

In the case of diffraction radiation

$$\vec{s} = \begin{Bmatrix} s_x \\ s_y \\ s_z \end{Bmatrix} = \begin{Bmatrix} 0 \\ 0 \\ \frac{1}{\beta} \end{Bmatrix},$$

respectively. Control via the radio button "TR", "DR". On the 3D diagram, if the "DR" mode is selected, the target disappears. The transition radiation case "TR" is selected by default.

Form Factor View. Allows you to choose between displaying the graph of form factor versus emission frequency or form factor versus emission wavelength.

Control via the radio button "", "". By default, the representation of the form factor depending on the radiation frequency "" is selected.$F(\lambda)F(\nu)F(\nu)$

In the "Train parameters" the "number of electrons", "number of bunches", and "energy" are set. The "number of electrons" parameter allows you to set the number of all particles in the sequence. Slider control. Range from 100 to 50,000 particles. By default, 10000 particles are selected. The "number of clots" parameter allows you to set the number of clots in the sequence. Slider control. The parameter range is from 1 to 10 clusters, it is possible to add more, but this will make the manipulator visually loaded. The default value is 2. The "energy" parameter is responsible for the average energy of electrons in the bunch in units of MeV. On the 3D diagram, a change in the parameter is displayed as a change in the color of the bunches. Slider control. The parameter range is from 10 to 10000 MeV. The default value is 10 MeV.

"Cluster Offset" allows you to set the offset of each bunch relative to the X, Y, Z axes of the coordinate system associated with the target. Moreover, for the positive direction for the displacement along the Z axis and counting of the bunches, the direction opposite to the direction of the beam movement is taken. Dialog box control. Offset units - mm.

The "charge distribution" takes into account the fraction of the charge per bunch. Normalization is not automated. Slider control. The range of parameter change is from 0.01 to 1.

Target Tilt. Allows you to set the target inclination angle in degrees. Slider control. The parameter range is from 0 to 90 degrees. The target position in the ZOY plane is taken as the zero slope. For a tilt of 90 ° - a position in the XOY plane. The default value is set to 45° tilt.

"Detector position". The detector position is given by two angles, and . "" - sets the rotation around the Z axis, "" - around the Y axis. The control is carried out through the slider. The range of parameters is from -90 to 90 degrees. The position of the detector at {1,0,0}, in X, Y, Z coordinates, is taken as zero angles. The default value is 0° for each parameter.

"Spectral Range" is responsible for scaling the form factor graph by setting the minimum and maximum value of wavelengths or frequencies. For wavelengths, you can vary in the range from 0.01 to 100 mm, from 0.05 to 101 mm. The frequency can be varied in the range from 0.01 to 30000 GHz, from 0.05 to 30001 GHz. The parameters are controlled through the slider

The subblock "Bunch sizes" makes it possible to set the sizes of each bunch in the sequence, along the X, Y, Z axes, as the corresponding root-mean-square deviations of the distribution of particles in bunches „. The parameters are set via the dialog box in mm.

"Accuracy" allows you to increase or decrease the accuracy of plotting the form factor graph, thus balancing the calculation time when processing a large amount of data. The control is carried out through the built-in Mathematica functions MaxRecurcion and PlotPoints, changing their value to 2, 4, 5, 8 or 10.

The functionality of the "Parameters of the 3D scheme" block contains only those variators that are associated with the visualization of the beam and the geometry of the experiment. These include "bunch appearance", "target size", "target-to-detector distance", "bunch motion" and "camera position".

"Cluster View" allows the user to see clusters either as ellipsoids, or as a set of points in space, obeying a Gaussian distribution. Control via the radio button "points", "ellipsoids". By default, clusters are represented as ellipsoids "ellipsoids". "Target size" is given as half the size of the side of a square target in mm. Slider control. The size is selected based on the transverse dimensions of the clots.

"Target to detector distance" allows you to zoom in and out of the detector to the target. This parameter is intended to balance the appearance of the circuit when changing the parameters for thickening and target sizes, thus scaling the box described around the circuit. Set in mm. It is selected based on the size of the target. Slider control.

The "camera position" is given by three coordinates of the observation point, the Cartesian reference system associated with the target, with the gaze directed to the zero of the system, i.e. target center.

The "Detector sensitivity" block allows you to set the minimum and maximum boundaries of the detector sensitivity range in GHz. The boundary can be varied in the range from 0.01 to 30000 GHz, from 0.05 to 30001 GHz. The parameters are controlled through the slider. It is planned to implement a similar display of the detector sensitivity function for the case of dependence on the radiation wavelength, with the appropriate parameters.

The "Interferogram settings" block allows you to set the movement of the movable mirror by adjusting the parameters and - the boundaries of the displacement of the movable mirror of the interferometer relative to its zero position. Both parameters are given in mm. The range of possible values for - 40 to 0 mm. The range of possible values for 0 to 40 mm. The parameter "Step of building autocorrelation function" allows you to set the step by which the value in the calculation of the radiation intensity will change when passing through a series of values from to . The parameters are controlled through the sliders. The default parameters are -20 mm for accepted, 20 mm for accepted. The step of constructing the autocorrelation function is 0.1 mm.

It is necessary to add the ability to automatically calculate and display information about the characteristics of the autocorrelation curve, for example, about the number of oscillation packets on the interferogram, their width and distances between them. It will be fun to switch to the ultrarelativistic case and form factor for different particle distributions and bunch shapes. However, such a code is not of interest for the current study.

1.4 Numerical form factor calculation

After passing through a bunch in magnetic systems, its configuration can change in such a way that it becomes impossible or difficult to describe the distribution of electrons in a bunch or a sequence of bunches by an analytical formula, however, it is still necessary to express the form factor.

Let's imagine an algorithm for calculating the form factor for such a case. Let us return to the formulas for the full spectral-angular distribution of particles in a bunch before performing mathematical transformations:

$$\frac{d^2W}{d\omega d\Omega} = \frac{d^2W_0}{d\omega d\Omega} \cdot \sum_{j=1}^{N} \sum_{p=1}^{N} e^{i\frac{\omega \cdot \vec{s}}{c}(\vec{r_J} - \vec{r_p})},$$

and after:

$$\frac{d^2W}{d\omega d\Omega} = [N + N(N-1)F(\omega, \vec{s})] \cdot \frac{d^2W_0}{d\omega d\Omega}.$$

Equate the right sides:

$$N + N(N-1)F(\omega, \vec{s}) = \sum_{j=1}^{N} \sum_{p=1}^{N} e^{i\frac{\omega \cdot \vec{s}}{c}(\vec{r_J} - \vec{r_p})}.$$

And let's express the form factor:

$$F(\omega, \vec{s}) = \frac{\sum_{j=1}^{N} \sum_{p=1}^{N} e^{i\frac{\omega \cdot \vec{s}}{c}(\vec{r_J} - \vec{r_p})} - N}{N(N-1)}.$$

The calculation of the form factor "manually" in this case is not possible, because, in addition to the fact that the number of electrons in only one bunch can reach billionths, it is also necessary to know the coordinate of each electron in the bunch. However, if we are talking about electron bunch models, getting a list of the coordinates of each electron will not be a big deal. For example, using the ASTRA code [49], one can obtain the spatial distributions of electrons as close as possible to real ones (Figure 20).
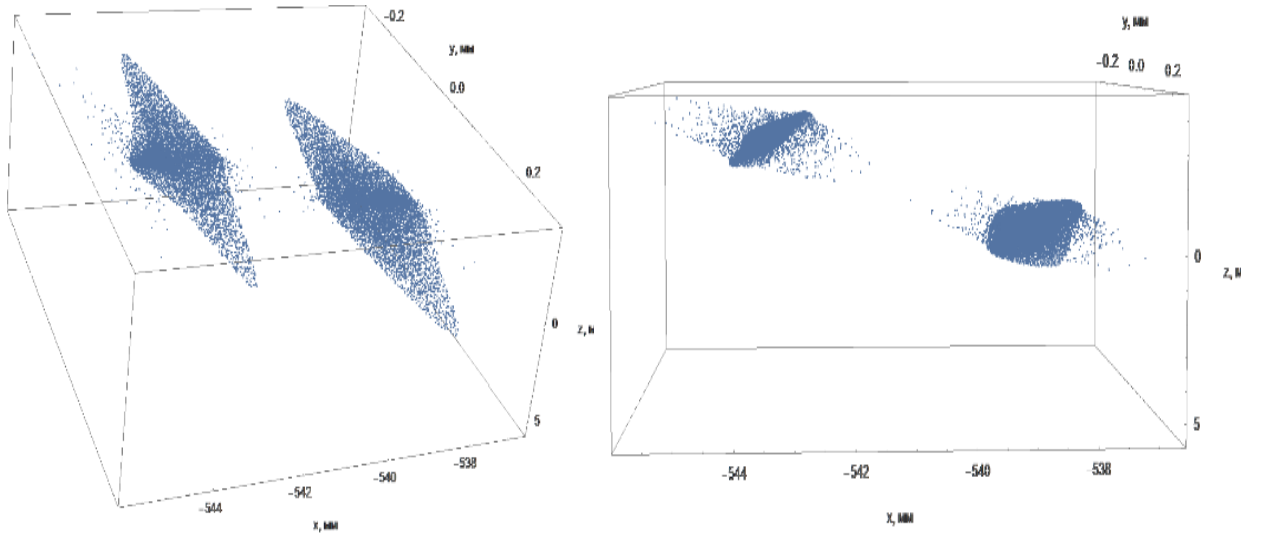
Figure 20 - Model of electron bunches after passing through a system of magnetic lenses, generated using the ASTRA code

The problem of processing large data arrays is solved using the computing capabilities of modern computers. Thus, for the numerical calculation of the form

factor in this way, it is necessary to have a list of coordinates of each electron in the bunch, set the components of the vector , and automate the calculation. That is, to determine the type of radiation, and create a special program for a computer (personal computer). Appendix D contains a code listing based on the above approach. The code is implemented in the Wolfram Mathematica package.$\vec{s}$

To test the method and code, we compared the results of form factor modeling by the proposed numerical and analytical approaches.Randomly generated 2 sets of point coordinates, which are one (Figure 21a) and two Gaussian clusters (Figure 21b) with the same transverse and longitudinal dimensions. Each bunch consisted of 1000 particles.

A)   b)
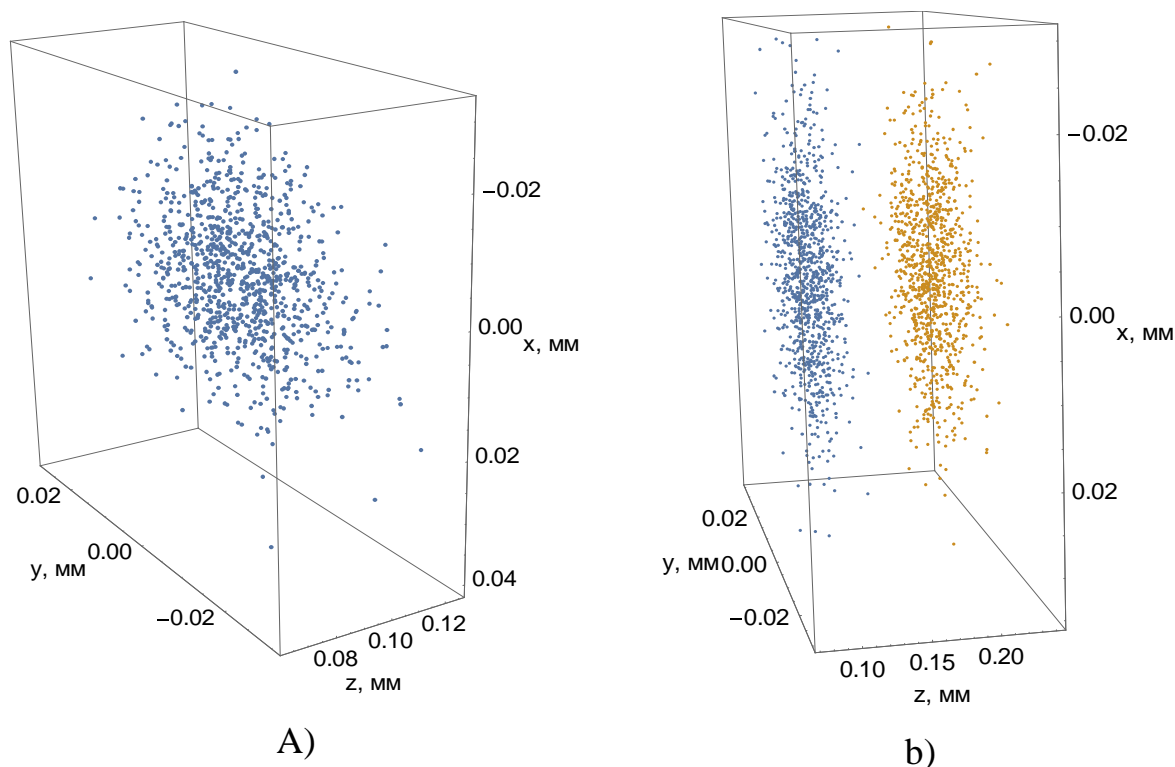
Figure 21 - View of one generated electron bunch (a), view of two generated electron bunches (b)

Figure 22 compares the form factors calculated based on the approaches described above for electrons with an energy of 10 MeV. The distance between two clusters is indicated by the letter L.
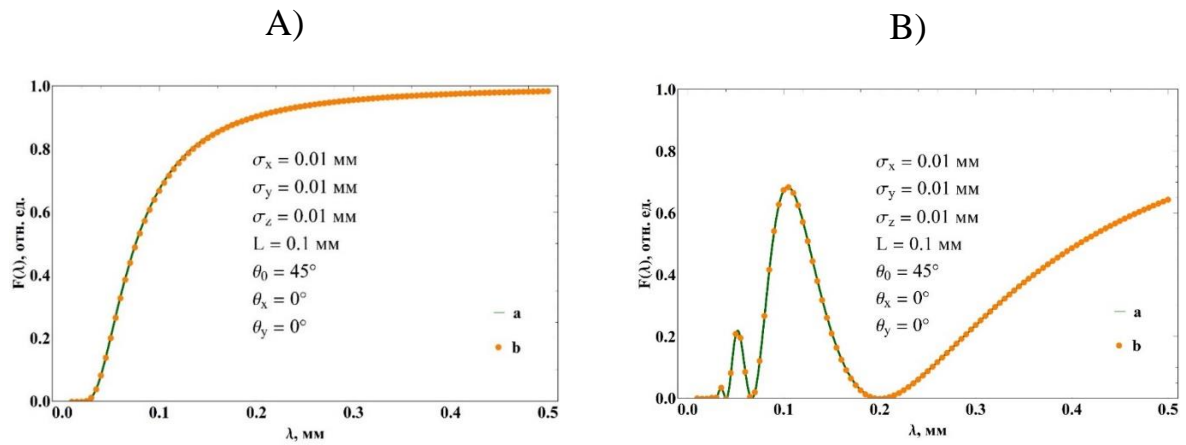
Figure 22 - Comparison of analytical (a) and numerical (b) approaches for the case of one (A)
and two electron bunches (B)

One can see good agreement between the two approaches for the case of the 1st and 2nd bunches. In the given wavelength range, the difference in values is mainly <2%, except for the intervals corresponding to the minima of the form factor. This is due to the calculations of small values at the limit of machine accuracy. Note that the comparison was made for specific values of the observation angle and the target tilt angle.

This method, however, has a significant drawback.– a sharp increase in the calculation time with an increase in the number of particles (Figure 23).
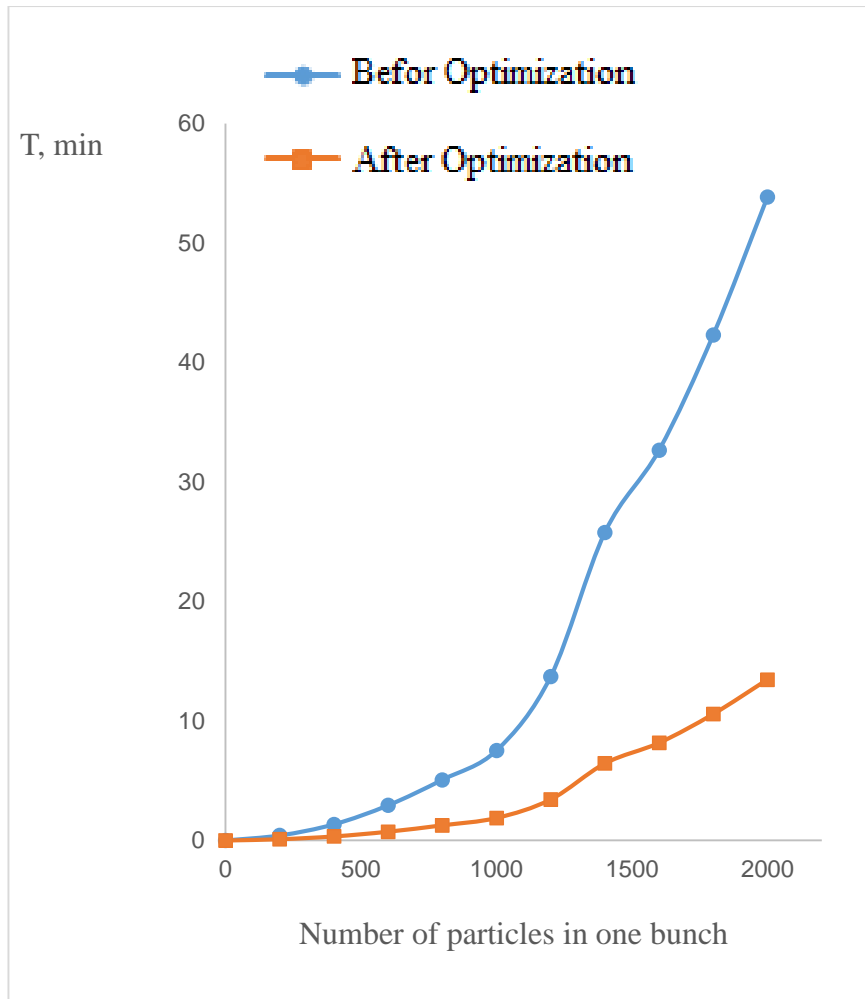
Figure 23 - Dependence of the form factor calculation time on the number of particles on a laptopAcer TravelMate P259-MG

Initially, the calculation of the form factor of real bunches (~108/1010 particles) on a computer of average performance required an enormous amount of time. Figure 23 shows the dependence of the calculation time on the Acer TravelMate P259-MG laptop on the number of particles in the cluster sequence before and after code optimization.As a result of optimization, it was possible to reduce the calculation time by approximately four times.

Below is a table comparing the two modeling methods.

Table 1 - Comparison of methods

	Analytical method	Numerical method
Pros	• High calculation speed • Spectrum construction accuracy	Allows you to calculate the form factor of bunch sequences of any configuration
Minuses	Only for distributions expressed analytically	• Need a list of all beam electron coordinates • Low calculation speed

It is necessary to continue to make attempts to optimize the presented code, since, as already mentioned, the number of particles in bunches can reach billions of values and, accordingly, the calculation of the form factor from such beams by the presented method will take too much time.

In order to use the obtained expression in the formula describing the interference signal, it is necessary either to interpolate the obtained discrete form factor function or go from integration to summation in the signal function itself. In the future, an attempt will be made to automate both approaches, to compare simulation results, as well as calculation speeds.

1.5 Section Conclusions

Thus, a detailed derivation of the mathematical expression for the autocorrelation function and its components - the full spectral-angular distribution of radiation and the form factor for the case of transient and diffraction radiation from uniform and non-uniform sequences of electron bunches is given. Carefully calculated are the components of the vector responsible for the formation of the phase difference for the case of transition and diffraction radiation in a given geometry, the determination of which, as a rule, causes difficulties in the transition from two-dimensional space to three-dimensional. In the expression for the form factor, in continuation of the bachelor's work, new parameters were introduced that take into account the expression for bunches of spherical, Gaussian, and cylindrical shapes with uniform distributions of electrons inside each bunch, and the transformation of the phase factor at ultrarelativistic particle velocity is also considered. The limitations and assumptions of the approach are given. $\vec{s}$

Based on the formulas obtained, manipulator applications have been created that allow dynamically setting the parameters of the sequence of electron bunches and experimental conditions to obtain an output interferogram, a spectrum of transition / diffraction radiation depending on the length or frequency of the output study, and a three-dimensional schematic visualization of the process of generation of transition radiation. These applications will be used further, in Section 2, to test

the constructed mathematical model on the data of experiments with the interferometry of radiation from real sequences of electron bunches, as well as to analyze the dependence of the behavior of the autocorrelation function on the plot on the parameters of the bunch sequences in Part 3 of this work.

In the future, it is planned to calculate the phase, that is, the vector $\vec{s}$ for all polarization radiations and use this expression to create new modeling tools, thus expanding the functionality of the already written code, the calculation capabilities of which are still limited only to transition and diffraction radiation. It is proposed to increase the speed of calculations of the created programs. To develop and refine the theory of polarization radiation, it is necessary to pay attention to the influence of the incoherent form factor and also introduce this parameter into the mathematical model. It is also worth considering the contribution to the spectral characteristics of radiation from the edge effects of the target, i.e. consider how the signal changes in the near and far wave zones, consider the emission spectra from cylindrical bunches with a Gaussian transverse distribution component. Besides, An important task will be to include in the model the influence of dynamic processes occurring inside the beam, for example, the influence of the Coulomb repulsion of particles. For working with experimental data, methodical work on the calculation of the emittance of an electron beam, and the algorithm for recalculating the temporal parameters of the beam into lengths of space and vice versa, are important. And it is also necessary to consider the units in which the characteristics of the beams in real diagnostics are represented. Those. to make a transition from the plane of abstract models and units of measurement to the space of real experiments. And it is also necessary to consider the units in which the characteristics of the beams in real diagnostics are represented. Those. to make a transition from the plane of abstract models and units of measurement to the space of real experiments. And it is also necessary to consider the units in which the characteristics of the beams in real diagnostics are represented. Those. to make a transition from the plane of abstract models and units of measurement to the space of real experiments.

2 Comparison of simulation results and data from real experiments

This chapter is dedicated toapprobation of the mathematical model and created applications.The simulation of interferograms based on the data of 3 real experiments is given. A comparison of the results of interferograms obtained in the simulation with real interferograms is given. Possible reasons for the appearance of discrepancies between the model and experiment are discussed.

Section 2.1 describes the simulation of the interferogram from two measurements of the transition radiation signal on the extracted electron beam of the TPU microtron, published in articles [50] and [51].

In Section 2.2, the modeling of interferograms is given, according to the data taken from the article [52] of the SDL laboratory, devoted to the creation of a THz radiation source. The simulation of this case is interesting because in the course of work it was necessary to take into account the influence of the materials of the interferometer, the window of the vacuum chamber, and the sensitivity range of the real detector.

Section 2.3 describes the modeling of experimental data obtained at the LUCX accelerator in which a group from Tomsk Polytechnic University took part. To date, the data has not been published. For the provision, please contact Dr. M. V. Shevelev [53], a direct participant in the experiment. The example of this simulation shows not only the performance of the mathematical model, but also a direct relationship between the beam parameters and the behavior of the autocorrelation function on the interferogram.

2.1 Comparison of the model with the experimental data of the TPU Microtron

First in the list of data for testing, we will present the interferograms obtained on the TPU microtron. This choice is due to the author's access to practically complete information about the experiment, the opportunity to obtain first-hand data and conduct a free discussion with people servicing the microtron. In addition, the tools that were used in the experiments, due to their throughput characteristics, did not require adjustment of the mathematical model, and hence any intervention in the already written code.An example of such measurements of the characteristics of

transition radiation, including the measurement scheme, is presented in sufficient detail in [50, 51]. In experimentsthe electron beam was exposed to air from the vacuum path of the accelerator through a beryllium window and passed through a copper rectangular screenlocated at an angle to the beam trajectory, at a distance of 320 mm from the window. The reverse transition radiation propagating along the direction of specular reflection was directed to a flat mirror, which reflected the radiation to the input to the interferometer. The interferometer consists of an input polarizer that passes the horizontal component, a fixed and movable mirror, a radiation splitter, and a parabolic mirror with a detector at its focus. The radiation splitter used, which is a periodic wire structure [50], has almost 100% transmission and reflection coefficients from almost zero to frequencies$\sim c/2\delta =$600 GHz, where is the gap between the wires.δA transcendental waveguide Ø15 mm was installed in front of the detector to suppress the long-wavelength emission spectrum from the high-frequency system of the accelerator. At the beginning of the experiment, the orientational dependence of the transition radiation (Figure 24) on the screen tilt angle was measured, at zero positionmovable interferometer mirrorwhen the distances from the divider to the mirrors are the same.
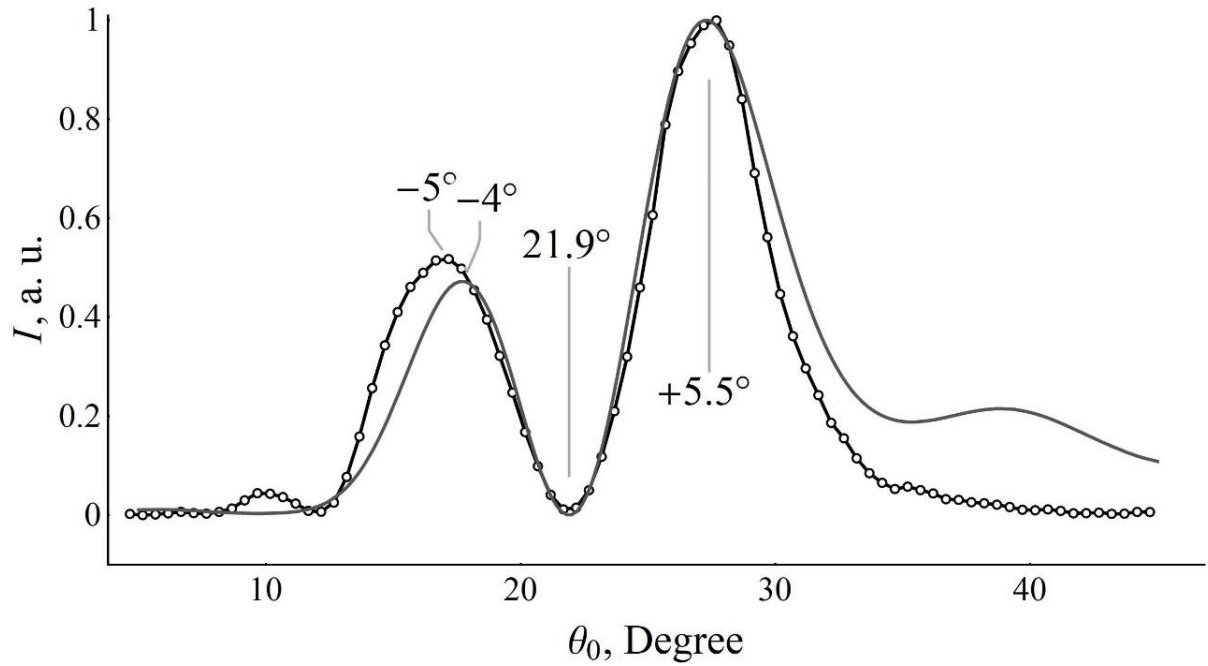
Figure 24 - Points united by a solid line - orientation dependences of the PR intensity normalized to the maximum, obtained in the experiment from an electron beam, the solid line - orientation dependences of the PR intensity normalized to the maximum, obtained in the simulation in a single-particle approximation for a frequency of 13.2 GHz

The target tilt angle was chosen as the angle between the beam direction and the target surface. Then, by setting the position of the transient radiation screen to the maximum radiation intensity, the interferogram (autocorrelation function) was measured. Each point in measurements-this is the averaging over 20 macropulses of the electron beam. The measured result was normalized to the beam current. The typical scatter of beam current values during measurements of interferograms varied within ±1% with several spikes up to 5% of the average value.

2.1.1 Description of the conditions for modeling an experiment carried out at the TPU Microtron

Let us give an example of how a mathematical expression is used when modeling an interferogram. In the following two examples, details will be omitted. Recall that the mathematical model that makes it possible to calculate the intensity of coherent transition radiation on the detector from the step of the moving mirror of the interferometer , where $d = \Delta l/2\Delta l$ is the optical path difference between the mirrors in the interferometer:

$$I(\Delta l) = \int_{v_1}^{v_2} \frac{d^2 W_0}{dv d\Omega} [N + N(N - 1)F(v)]S(v)M(v)dv,$$

69

$$F(\nu) = \frac{1}{m^2} exp\left[-\frac{4\pi^2\nu^2}{c^2}\left(\sigma_x^2 s_x^2 + \sigma_y^2 s_y^2 + \sigma_z^2 s_z^2\right)\right]\left|\sum_{p=1}^m exp\left[-i\frac{2\pi\nu}{c}l\cdot(p-1)s_z\right]\right|^2,$$

$$\vec{s} = \begin{Bmatrix} s_x \\ s_y \\ s_z \end{Bmatrix} = \begin{Bmatrix} -\cos\theta_y\cos\theta_x - \cot\theta_0\left(\sin\theta_y - \frac{1}{\beta}\right) \\ -\cos\theta_y\sin\theta_x \\ -\frac{1}{\beta} \end{Bmatrix},$$

$$M(\nu) = \left|1 + e^{-\frac{i2\pi\Delta l\nu}{c}}\right|^2,$$

$$S(\nu) = \begin{cases} 1 & \nu \in \{\nu_{Dmin}, \nu_{Dmax}\} \\ 0 & \nu \notin \{\nu_{Dmin}, \nu_{Dmax}\} \end{cases}.$$

Here the multiplier$\frac{d^2W_0}{d\nu d\Omega}$- emission spectrum from one electron (Figure 25),

which takes into account the finite size of the target.
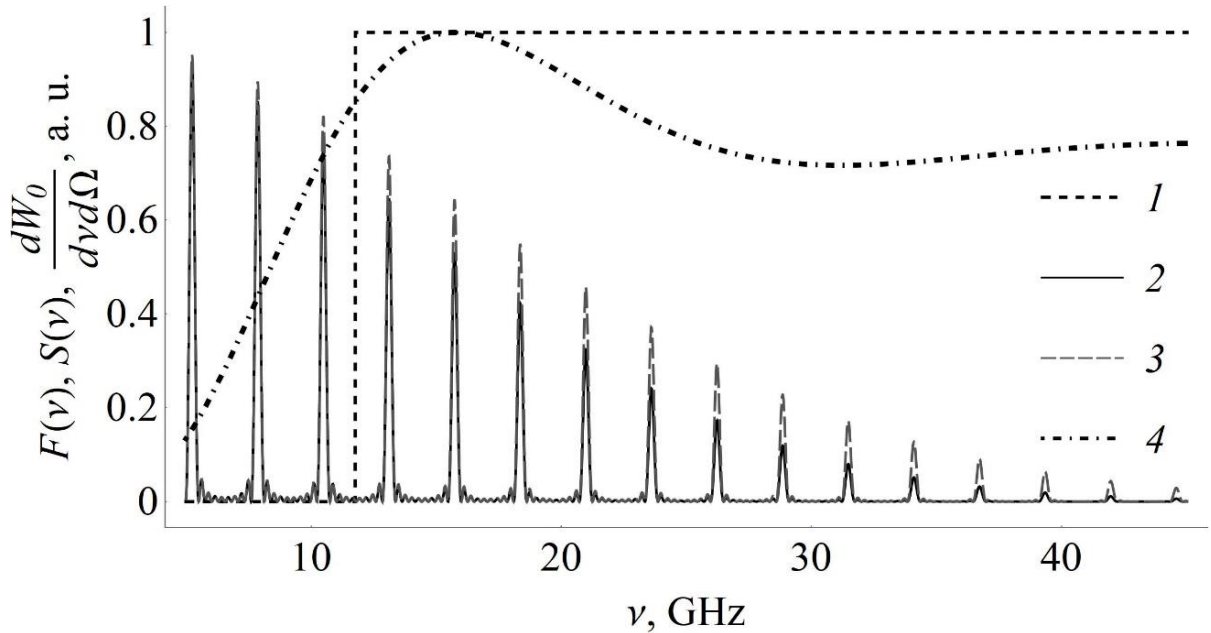
Figure 25 - Dotted line - detector sensitivity range , solid line - form factor of a sequence of 10 bunches for a distance between bunches of 114 mm at$S(\nu)F(\nu)$ σ_z =2.4mm, the dashed line is the form factor of the sequence$F(\nu)$ of 10 bunches for a distance between bunches of 114 mm at σ_z =2 mm, dash-dotted line – normalized TR spectrum from one electron for a target of finite size

In this paper, this factor and the orientational dependence of the transition radiation (Figure 24) were calculated by numerical simulation methods [48] based on the generalized method of surface currents [54]. Further, is the number of electrons in the entire beam,$NF(\nu)$– form factor (Figure 25), – interference factor

(Figure 26), – detector sensitivity function (Figure 25), where – frequency range of detector sensitivity. $M(\nu) S(\nu) \{\nu_{Dmin}, \nu_{Dmax}\}$
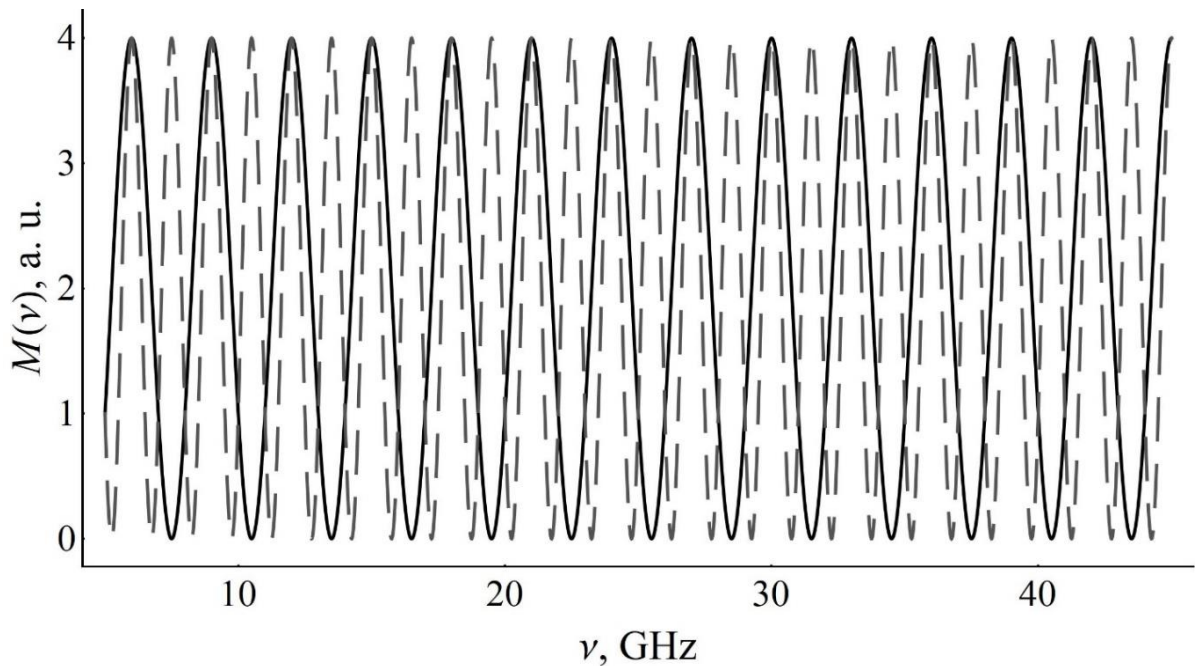
Figure 26 - Examples of interference factors for different values of the radiation path difference: solid line - path difference 100 mm, dashed line - path difference 200 mm

Here is the radiation frequency, νc is the speed of light in vacuum; is the number of bunches in the beam; observation angles counted from the X axis (– in the direction of the Y axis, – in the direction of the Z axis), is the tilt of the target, is the relative velocity of electrons in units of the speed of light. Vector for selected parameters (table 2) equals $\{- 0.135, 0, - 1.004\}$. This means that the transverse dimensions of the bunches do not significantly affect the transition radiation spectrum. An additional description of each of the factors in the model is also given in [55]. In the simulation, the distance from the center of the target coinciding with the origin of the coordinate system (right-handed) to the point of observation of the transition radiation spectrum was 10 m, i.e. the detector is located in the far wave zone, which corresponds to the measured characteristics (for more details, see [38]). The detector aperture was not taken into account; the detector is assumed to be a point detector. The detector sensitivity was taken equal to unity in the range from 11.76 GHz to 60 GHz (Figure 25), where the minimum value is determined by the

diameter of the transcendental waveguide, and the maximum value is the passport value. In the model, the target is assumed to be absolutely conductive and has the shape of a rectangular screen. Since the target is located symmetrically relative to the horizontal plane in which the measurements are made, the transition radiation contains only the horizontal polarization component, respectively, the calculation of the spectrum was carried out only for this component. In order to speed up the calculations, it was assumed that the number of bunches in the beam is 10. When modeling, the sequence of electron bunches in the beam is considered to be uniform in terms of the charge distribution within the sequence, all bunches are the same in size. The distribution of electrons in bunches is assumed to be Gaussian. The distance between two neighboring bunches in the beam corresponds to the frequency of the field of the high-frequency system of the accelerator. In the simulation, the observation point was located at an angle = 45° from the electron beam trajectory, where the mirror was located in the experiment. As shown in Figure 24, the maximum radiation in the orientational dependence in this observation geometry was for a target tilt angle of 27.4°. This dependence was calculated for a radiation frequency of 13.2 GHz. This frequency for the microtron beam is dominant when using transcendent waveguide Ø15 mm, which acts as a low-pass filter, and which is confirmed by earlier measurements [51]. We add that this frequency corresponds to the 5th order in terms of the fundamental frequency $\nu_k = k \times \nu_{RF} (k = 1, 2, ...)$. To compare the dependences in Figure 24, the experimental curve was shifted along the abscissa axis until the minima coincided, and the pedestal was subtracted from it along the ordinate axis. The mirror step in the interferometer in the calculations was 0.05 mm (step Δl =0.1 mm). The modeling range of the autocorrelation function is chosen in accordance with the range of experimental data. For comparison with the simulation, the experimental autocorrelation functions were shifted along the vertical axis by zero by the mean value of the points along the y-axis. For convenience, the parameters of experiments and simulations are presented in the table below.

Table 2 - Parameters of experiments and simulation of data obtained on the TPU microtron

Parameter name	Meaning
Electron energy	6.1 MeV
Macro pulse frequency	8 Hz
Number of bunches in a macropulse	~104
bunch population	~108
The frequency of the high-frequency field,ν_{RF}	2.63 GHz
The length of the electron bunch, σ_z	2.4mm
Target size (horizontal × vertical)	300×200 mm2
target slope,θ_0	27.4°
Observation angle, ,$\theta_y \theta_x$	45°, 0°
The distance between the clots in the bundle, l	114 mm; 111.5 mm
Horizontal \ vertical size of the clot,$\sigma_x \backslash \sigma_y$	1.7mm \ 0.85mm
Detector sensitivity function	Uniform distribution
Detector sensitivity range,$\{\nu_{Dmin}, \nu_{Dmax}\}$	{11.76GHz, 60GHz}
The range of modeling the autocorrelation function byΔl	-100 ÷ 500 mm
Integration range,$\nu_1 \div \nu_2$	0 ÷ 65 GHz

2.1.2 Results and discussions of the simulation of the experiment carried out at the TPU Microtron

As shown in Figure 25, changing the clot length results ina change in the relative intensity of the peaks in the transition radiation spectrum and a shift in the coherence threshold. Figure 27 shows the final spectra of coherent transition radiation obtained in calculations for different distances between bunches, the length of each bunch$\sigma_z = 2.4$ mm.
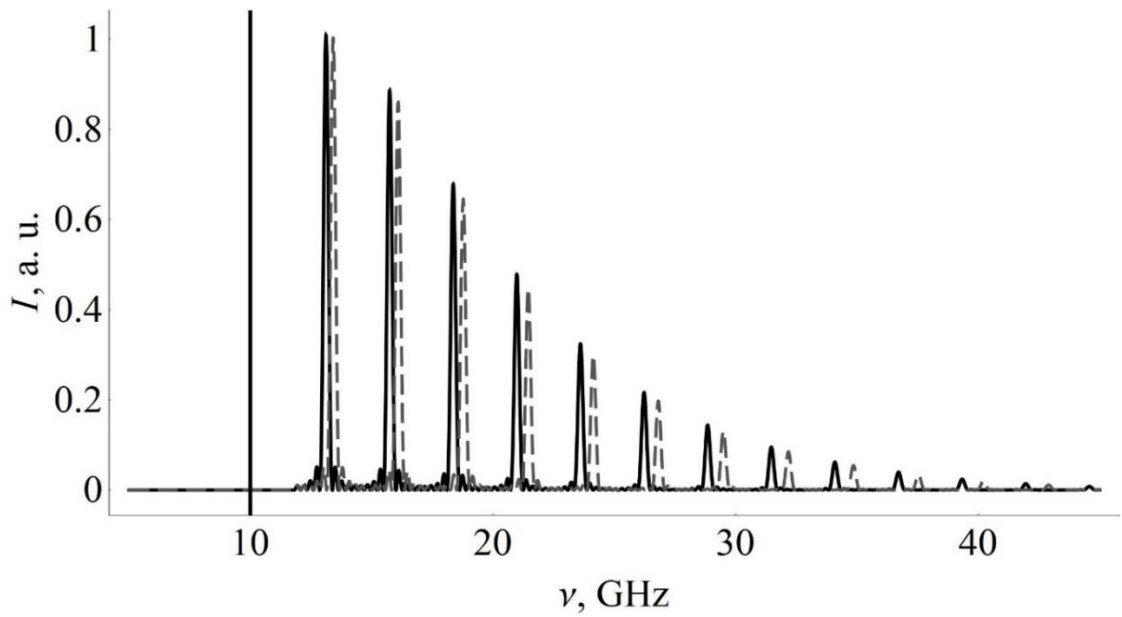
Figure 27 - The final calculated spectrum of TR from the beam (σ_z =2.4mm) seen by a detector with a given frequency range for different distances between the bunches: the solid line is the distance between the bunches of 114 mm, the dashed line is the distance between the bunches of 111.5 mm.

It is clearly seen that the transition radiation spectrum is a set of narrow lines, the relative intensities of which for the given experimental conditions mainly depend on the single-particle spectrum (i.e., the target size) and the coherence threshold (i.e., the length of the bunches). In this case, taking into account the target size in the simulation does not significantly affect the interferogram, since under experimental conditions the target size is larger than the effective radius of the Coulomb field of electrons. Figure 28 compares the simulated autocorrelation functions and the experimental one taken from [50]. It can be seen from the figure that the shift of the movable mirror by 150 mm (travel difference 300 mm) is not sufficient for a correct comparison, and hence a more accurate determination of the distance between the bunches.
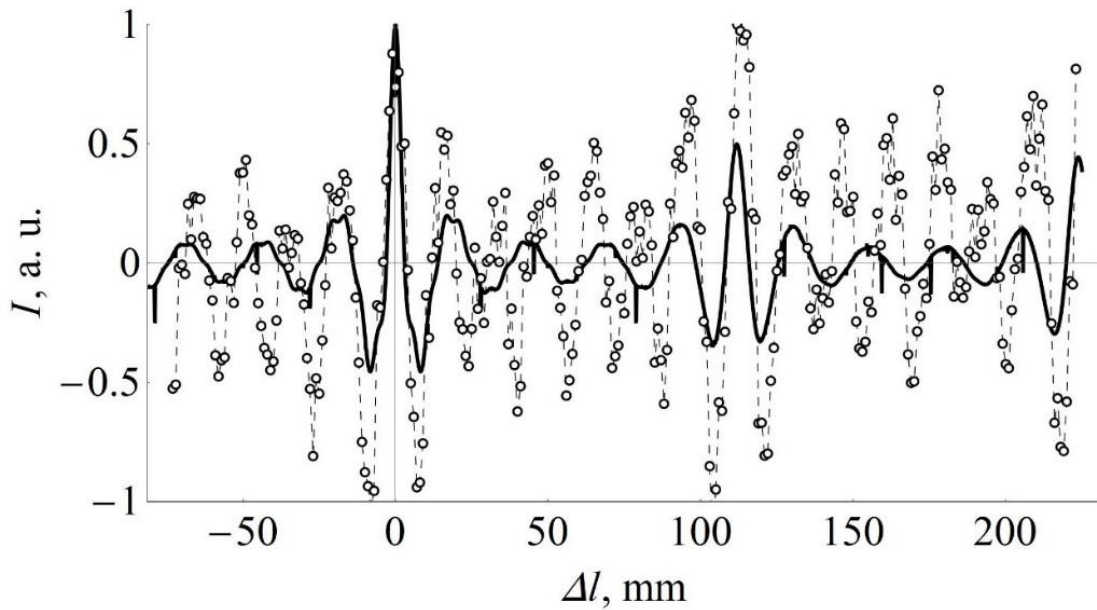
Figure 28 - TR autocorrelation functions: points united by a dotted line – obtained in the experiment [50], solid line – obtained by modeling in an interferometer at = 114 mm, dashed line – obtained by modeling in an interferometer at = 111.5 mm.l l

Later, measurements were taken with a shift of 300 mm.A comparison of the new measured autocorrelation function and the simulated functions is shown in Figure 29.
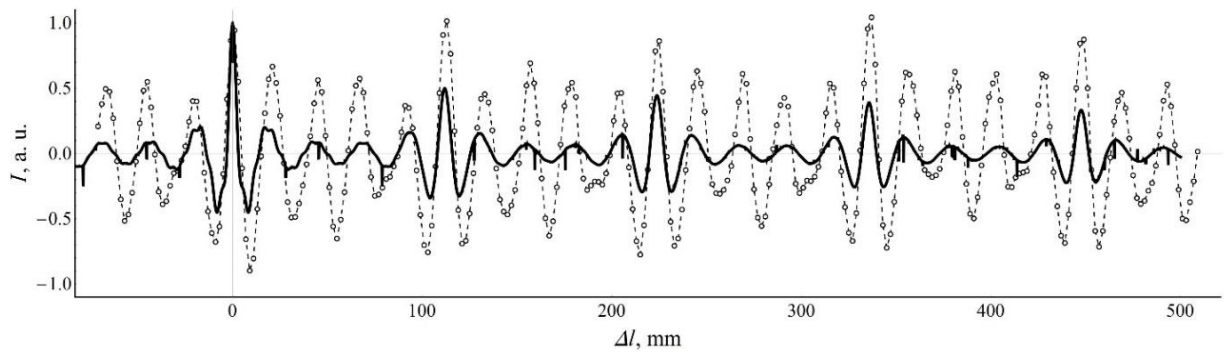
Figure 29 - Autocorrelation functions of PI: points united by a dotted line - obtained in the experiment, a solid line - obtained by modeling in an interferometer at = 111.5 mm, a dashed line - obtained by modeling in an interferometer at = 114 mm.ll

The comparison shows an exact match in the number of both main, as in Figure 28, and intermediate peaks in the autocorrelation function for a given modeling range. The reason for the discrepancy in the number of intermediate peaks in Figure 28 needs to be investigated. However, in the case when the distance between the electron bunches = 114 mm, there is a shift of the main peaks to the right side relative to the

75

experimental data. At the same time, the position of the main peaks of the simulated autocorrelation function more accurately matches the measurement data when the distance between bunches = 111.5 mm. It should be noted that before these measurements, on the TPU microtron it was assumed that the distance between the bunches, or otherwise the frequency of the high-frequency field of the accelerator, does not change and is equal to 114 mm and 2.63 GHz, respectively. This change from previous measurements, as it turned out, it is connected with the fact that after the replacement of the cathode unit and the resonator, which was made after and before the measurements presented in Figures 28 and 29, respectively, it becomes necessary to re-tune the new resonator of the microtron high-frequency system. This led to a change in the frequency of the high-frequency field. Another discrepancy between the measurement and simulation results, the small amplitude of the peaks in the autocorrelation function compared to the experiment, also requires additional research. Thus, the distance between bunches = 114 mm corresponds to the frequency

This led to a change in the frequency of the high-frequency field. Another discrepancy between the measurement and simulation results, the small amplitude of the peaks in the autocorrelation function compared to the experiment, also requires additional research. Thus, the distance between bunches = 114 mm corresponds to the frequency

This led to a change in the frequency of the high-frequency field. Another discrepancy between the measurement and simulation results, the small amplitude of the peaks in the autocorrelation function compared to the experiment, also requires additional research. Thus, the distance between bunches = 114 mm corresponds to the frequency v_{RF}= 2.63 GHz, l=111.5 mm - = 2.69 GHz. Then, for the 5th order of radiation, this frequency shift of the high-frequency field leads to a shift of the peak position by $5v_{RF}' \times (-) = 0.3$ GHz. Since the resolution of the interferometer is estimated on the order of $\sim c/2\delta = 0.5$ GHz, then this shift of the peak position can hardly be detected experimentally. This requires replacing the stepper lineengine.

2.2 Comparison of the model with the experimental data of the SDL laboratory

Let us describe the modeling of interferons in the article [52]. This article aims to obtain a THz radiation source based on the transition radiation generation method, with the possibility of frequency tuning by modulating the parent electron beam. The scheme for obtaining a transition radiation pulse is as follows: an electron beam with an average electron energy of 120 MeV, after passing through two sections of a linear accelerator, is brought into the air through the window of a vacuum chamber, consisting of a z-cut quartz crystal 2.5 inches in diameter, and then crosses 2 centimeters in diameter an aluminum screen directed at an angle of 45° to the direction of beam motion. The generated pulse of reverse transition radiation is directed to a parabolic mirror, from where it is redirected to a Michelson interferometer with a Mylar beam splitter 25 μm thick. After the interferometer has passed, the signal enters a helium-cooled silicon bolometer that serves as a detector. In total, the article presents interferograms from 4 sequences, the number of bunches in which is 2, 3, 8, and 18. The distance between the bunches is formed by the delay of laser pulses applied to the photocathode. The value of this delay for sequences is 0.4, 0.7, 1.8, and 3.6 ps, respectively. Longitudinal profile of a sequence of electron bunches, i.e. its longitudinal distribution is determined using a scintillation screen. The electron beam is then deployed by a dipole magnet located behind the last section of the accelerator. Different time slices of the electron bunch are projected onto the scintillation screen in different horizontal positions, and so, the longitudinal profile of the electron bunch turns into a transverse profile. Thus, interferograms are particularly interesting for modeling, in terms of what is obtained from sequences of electron bunches of uneven size. As well as sequences with different numbers of clots. Among other things, the solution of the modeling problem is complicated by the emergence of new parameters of the mathematical expression for the signal intensity. These additions are related to the throughput of the materials used in the experiment. Among other things, the solution of the modeling problem is complicated by the emergence of new parameters of the mathematical expression for the signal intensity. These additions are related to the throughput of the materials

used in the experiment. Among other things, the solution of the modeling problem is complicated by the emergence of new parameters of the mathematical expression for the signal intensity. These additions are related to the throughput of the materials used in the experiment.

2.2.1 Description of the conditions for modeling an experiment conducted in the SDL laboratory

Thus, the influence of the materials of the window of the vacuum chamber and the beam splitter used in the experiment of the original article was taken into account. The mathematical expression for the new code was

$$I(\Delta l) = \int_{v_1}^{v_2} \frac{d^2 W_0}{dv d\Omega} [N + N(N - 1)F(v)]S(v)M(v)V(v)T(v)dv,$$

Where $V(v)$ is a multiplier responsible for the spectral transmission capacity of the window material of the vacuum chamber, and is the beam-splitting plate. $T(v)$

Recall that in this case the form factor expression for non-uniform sequences is used. Characteristics and are passport data. The graph of the throughput of the window of the vacuum chamber [56] is shown in Figure 30.
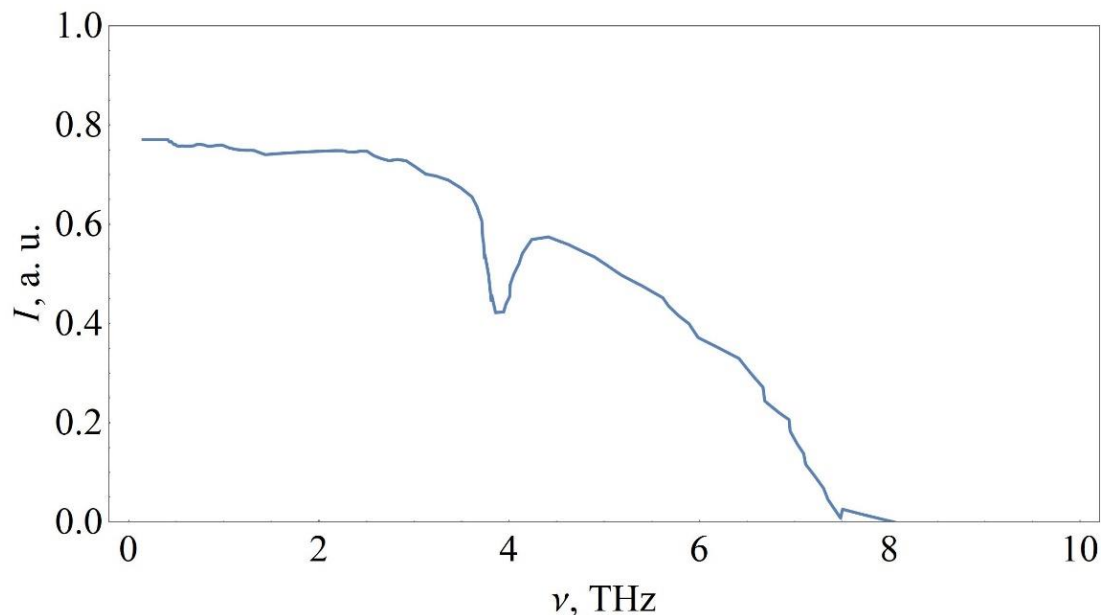
Figure 30 - The throughput of the material of the window of the vacuum chamber

The graph of the throughput of the Mylar beam-splitting plate of the interferometer [57] with a thickness of 25 μm has the form (Figure 31):
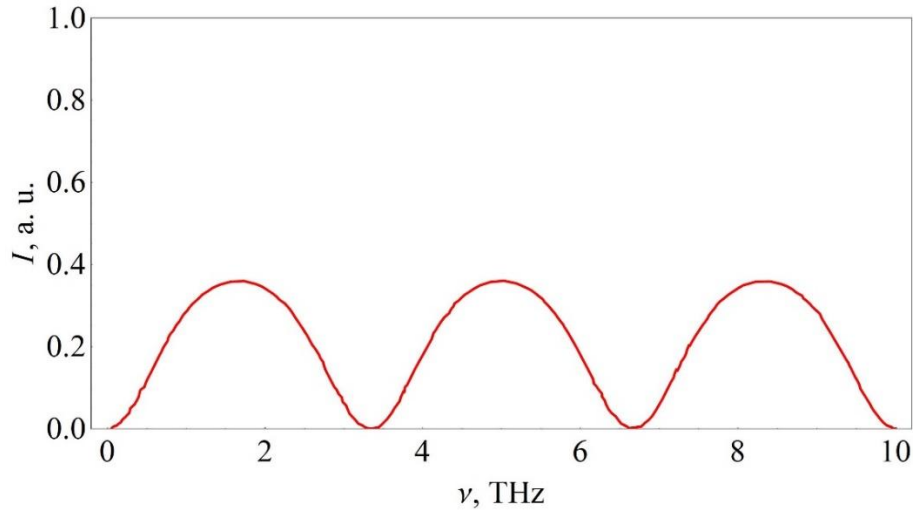
Figure 31 - Bandwidth of the Mylar beam splitter

The extraction of experimental data from graphs of the density of electron distributions in a sequence of electron bunches was carried out in the program [58]. The data on the transverse sizes of the bunches were calculated from the plots of the electron density distributions from the original article, obtained using a scintillation screen, assuming a Gaussian distribution. A 4.2 K General Purpose Bolometer [59] was supposed to be used as a detector (Figure 32).

Figure 32 - Sensitivity range of the simulated bolometer

The simulation was carried out taking into account the emission spectrum, as from the final target(Figure 33), and from an endless target, i.e. for case $.\frac{d^2W_0}{d\nu d\Omega} = 1$
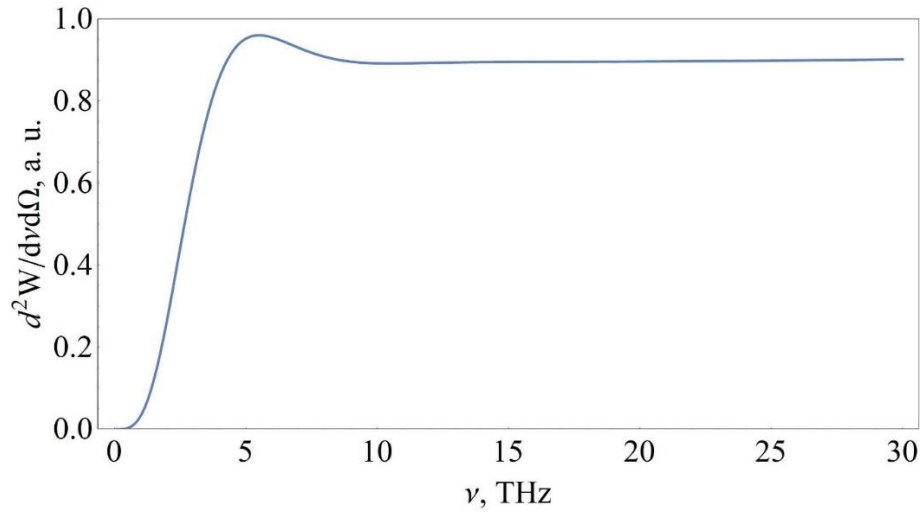
Figure 33 - The emission spectrum from one electron at finite values of the target size

The parameters of the sequence of electron bunches and the experimental conditions are given in Table 3.

Table 3 - Parameters of experiments and data modeling of the SDL laboratory

Parameter name	Meaning
Electron energy	120 MeV
The number of bunches in the sequence, m	2, 3, 8, 18
Electron bunch length, σ_z	From article [52]
Target diameter	2 cm
Vacuum chamber window diameter	2.5 inches
target slope, θ_0	45°
The thickness of the Mylar beam splitter in the interferometer	25 μm
observation angle, θ_y, θ_x	0.24°, 0°
Distance between clots in a bundle, l	From article [52]
Horizontal \ vertical size of the clot, $\sigma_x \backslash \sigma_y$	From article [52]
Detector sensitivity function	Uniform distribution
Detector sensitivity range, $\{\nu_{Dmin}, \nu_{Dmax}\}$	{0.15 THz, 20 THz }
The range of modeling the autocorrelation function by Δl	-9 ÷ 9 ps
Integration range, $\nu_1 \div \nu_2$	0.15 ÷ 20 THz

2.2.2 Results and discussions of the simulation of the experiment conducted in the SDL laboratory

Figures 34 and 35 show the spectra of transition radiation from four sequences of electron bunches and their corresponding autocorrelation functions. For comparison, the experimental autocorrelation functions from the article [52] are given.
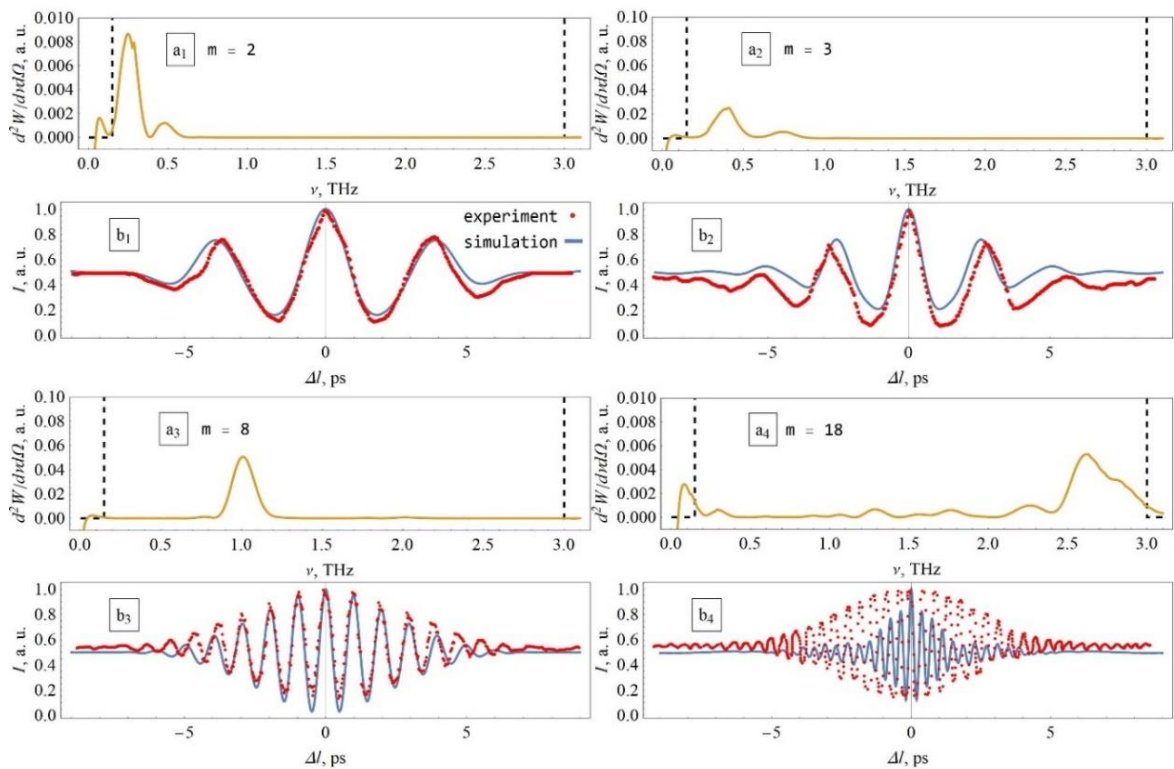
Figure 34 - Transition radiation spectra from an infinite target, dotted line - detector sensitivity function (a), normalized autocorrelation functions obtained by modeling and from experimental data (b)
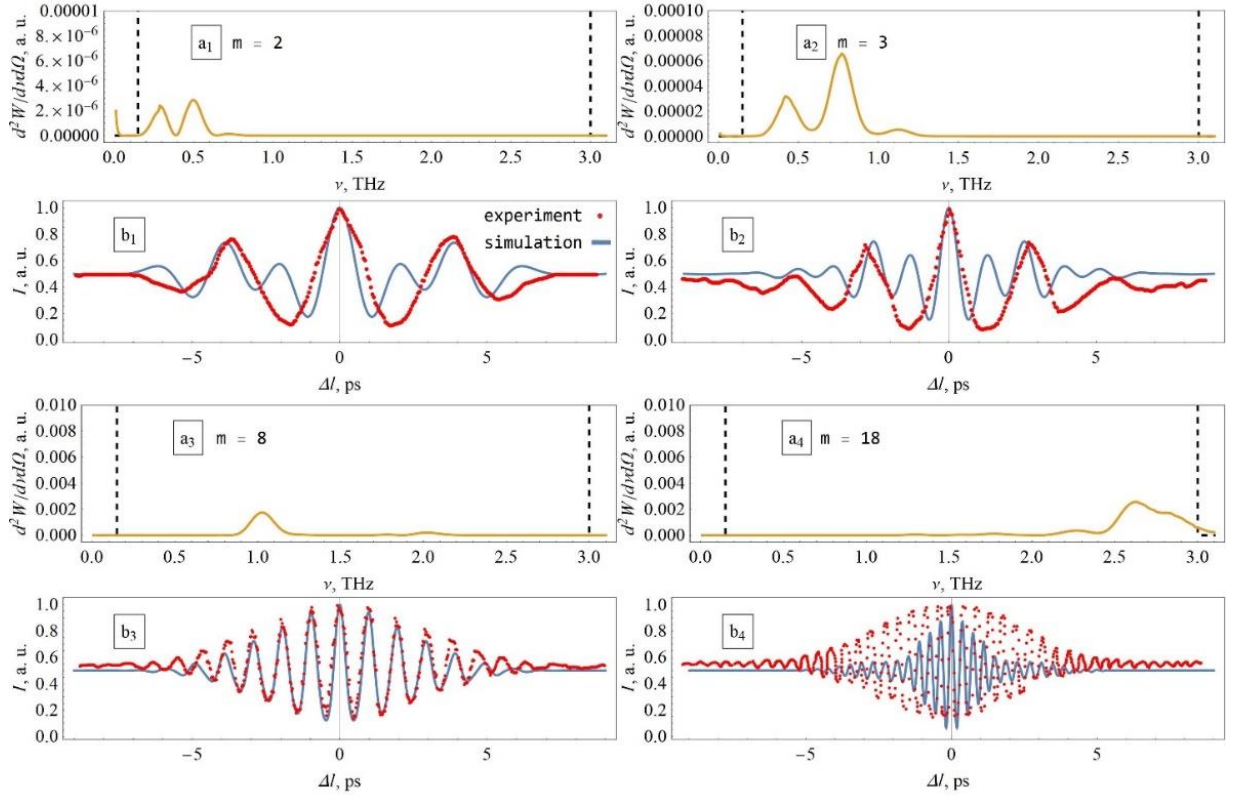
Figure 35 - Transition radiation spectra from a target of finite size, dotted line - detector sensitivity function (a), normalized autocorrelation functions obtained by modeling and from experimental data (b)

Comparison of experimental and simulated interferons for 2, 3, 8 shows good agreement in the behavior of functions with a slight difference in the position of the peaks. The behavior of the autocorrelation function for case 18 is very different. As can be seen from the spectrum for 18, the main emission peak is not monochromatic. In addition, an additional peak is observed in the low frequency region. All this leads to the appearance of modulations in the interferogram. There are several assumptions explaining the nature of the discrepancy between experimental data and simulations. This is either a possible error in the calculation of the throughput of the interferometer beam splitter or an insufficient description of the experimental conditions in the article [52]. Note that taking into account the spectrum of transition radiation, assuming the use of a target of finite dimensions.

2.3 Comparison of the Model with Experimental Data Obtained at the LUCX Facility

The article on which the following data is taken to test the model for June 2023 is not published. Interferogram measurements were carried out at the LUCX setup in 2019 [53]. Two electron bunches were generated on a photocathode and then accelerated in a high-frequency gun up to 7.8 MeV. The charge of each bunch in this case was 50 pC. After the high-frequency gun, a magnetic solenoid was installed that controls the transverse size and beam divergence. Transition radiation was generated from a 60 x 30 mm2 aluminum screen oriented at an angle of 48° with respect to the electron beam trajectory and was recorded by a detector located at a distance of 1.3 m from the photocathode inside the vacuum chamber. The radiation pulses propagated through a vacuum window made of a z-cut quartz crystal 90 mm in diameter, and the spectral characteristics of the radiation were measured with a Michelson interferometer installed in front of the vacuum window of the chamber. To register the radiation, a detector with a Schottky diode with a sensitivity range of 320–460 GHz was used. The detector was located at the focus of a parabolic mirror, and a wire polarizer with a pitch of 75 mm and a grid diameter of 15 mm was placed in front of the detector inlet. Thus, the interferograms of transition radiation for horizontal polarization were measured. As mentioned earlier, it was these data that served as the starting point for the idea of developing the method. and a wire polarizer with a pitch of 75 mm and a grid diameter of 15 mm was installed in front of the detector inlet. Thus, the interferograms of transition radiation for horizontal polarization were measured. As mentioned earlier, it was these data that served as the starting point for the idea of developing the method. and a wire polarizer with a pitch of 75 mm and a grid diameter of 15 mm was installed in front of the detector inlet. Thus, the interferograms of transition radiation for horizontal polarization were measured. As mentioned earlier, it was these data that served as the starting point for the idea of developing the method.

2.3.1 Description of experiment simulation conditions

For comparison, numerical simulation of the experimental conditions was also carried out using the ASTRA tracking program to estimate the distribution of particles in a sequence of electron bunches at the moment of interaction with an aluminum screen. The results are listed in table 4.

Table 4 - The value of the distances between the bunches obtained through the ASTRA simulation and the corresponding delays of laser pulses applied to the photocathode in the experiment

Delay of laser pulses [experimental data], ps	2.0	6.0	10.0	12.0	15.0	17.0	18.0	19.0
Distance between bunches [ASTRA simulation], ps	2.659	6.73	10.012	11.597	13.696	17.412	18.179	20.7

We use these data to model interferograms and compare them with experimental data. In this case, a variant of the form factor expression for a uniform sequence will do. We will consider the radiation spectrum from one electron as a constant value, i.e. in the approximation of an infinite target size. The number of clusters in the sequence, we take equal to two. The electron energy is assumed to be 8 MeV. The length of the electron bunches was taken to be 0.4 ps. Integration limits from 50 to 2000 GHz. The detector sensitivity function was determined using a Gaussian distribution with a maximum position at a frequency of 360 GHz and a window width at half maximum of 70.8 GHz. For convenience, the simulation parameters are given in Table 5.

Table 5 - Parameters of experiments and modeling data obtained at the LUCX accelerator

Parameter name	Meaning
Electron energy	8 MeV
The number of bunches in the sequence, m	2
The length of the electron bunch, σ_z	0.4 ps
Target size	60×20 mm2

target slope, θ_0	48°
observation angle, θ_y, θ_x	0.64°, 0°
Distance between clots in a bundle	From Table 4
Horizontal \ vertical size of the clot, $\sigma_x \backslash \sigma_y$	0.4 ps
Detector sensitivity function	Gauss
FWHM window width of the detector sensitivity function	70.8 GHz
The position of the maximum of the detector sensitivity function	360 GHz
The range of modeling the autocorrelation function by Δl	-30 ÷ 30 ps
Integration range, $\nu_1 \div \nu_2$	50 ÷ 2000 GHz

2.3.2 Results and discussions of the simulation of the experiment carried out at the LUCX accelerator

Below are the simulation results (dynamics of interferogram changes) for different distances between two bunches, corresponding to the delays of laser pulses from Table 4.
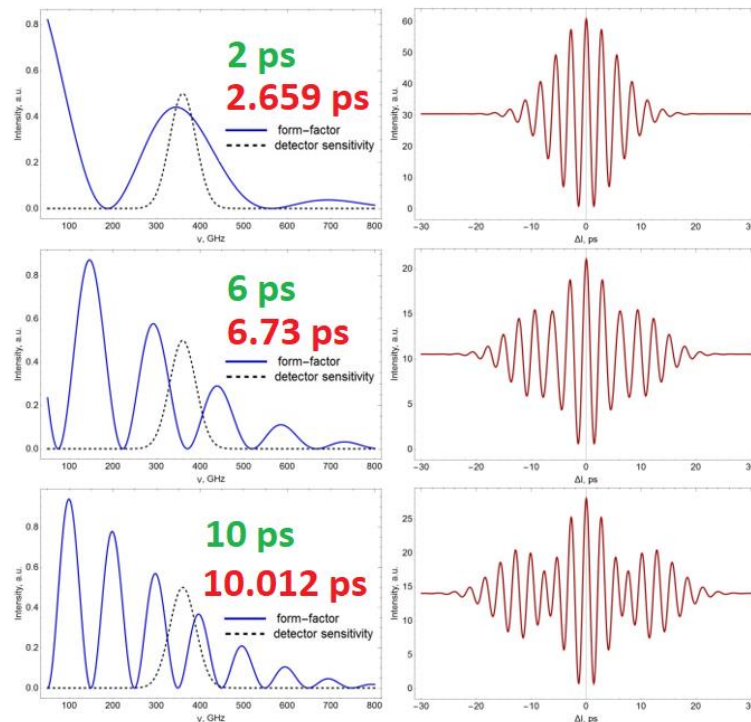
Figure 36.1 - On the left is a graph of the form factor and sensitivity function of the detector at the appropriate distances between the bunches (red), with an increasing top-down delay of laser pulses with values of 2, 6 and 10 ps (green), on the left is an interferogram
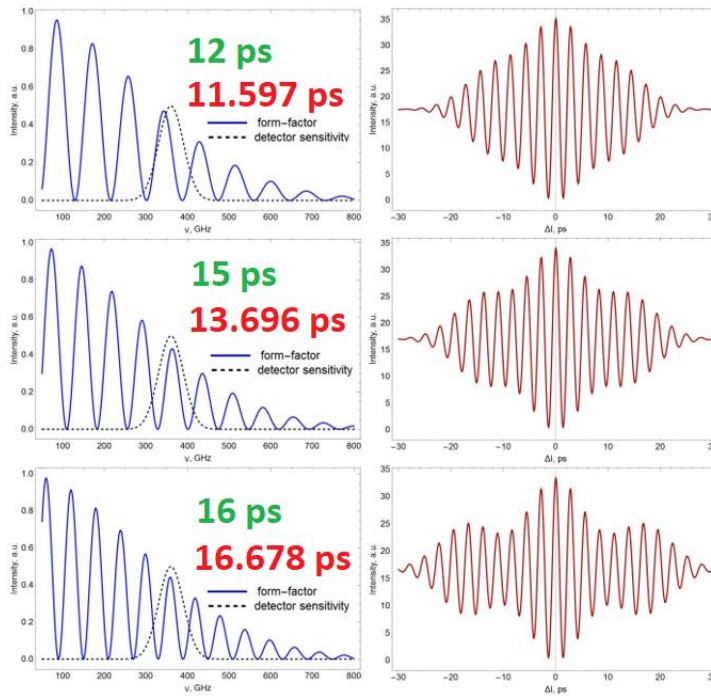
Figure 36.2 - On the left is a graph of the form factor and sensitivity function of the detector at the appropriate distances between bunches (red), with an increasing top-down delay of laser pulses with values of 12, 15 and 16 ps (green), on the left is an interferogram
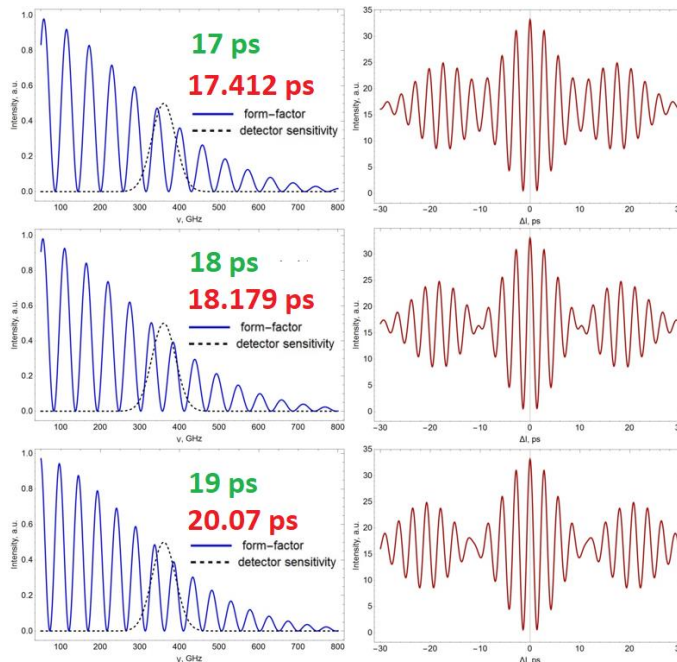
Figure 36.3 - On the left is a graph of the form factor and sensitivity function of the detector at the appropriate distances between bunches (red), with an increasing top-down delay of laser pulses with values of 17, 18 and 19 ps (green), on the left is an interferogram

The values of the distances between the maxima of the oscillation packets, simulated and experimentally obtained interferograms (Figure 37, Figure 38) show a coincidence, which once again demonstrates the efficiency of the model.
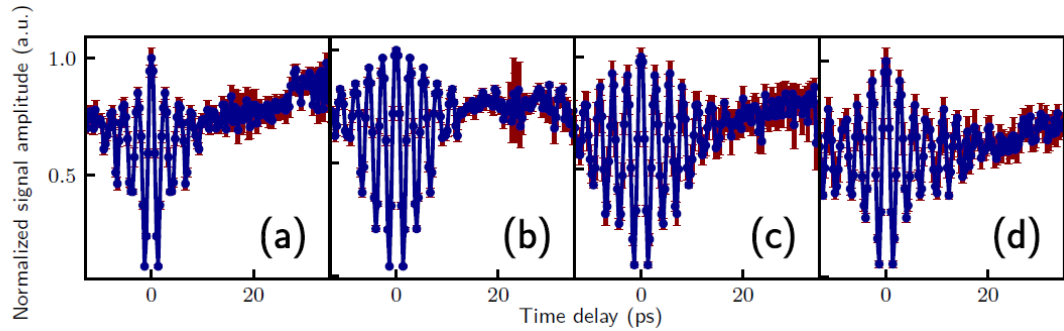
Figure 37 - The first set of experimental interferograms obtained at LUCX for the delay between laser pulses of 2 ps (a), 6 ps (b), 10 ps (c) and 12 ps (d)
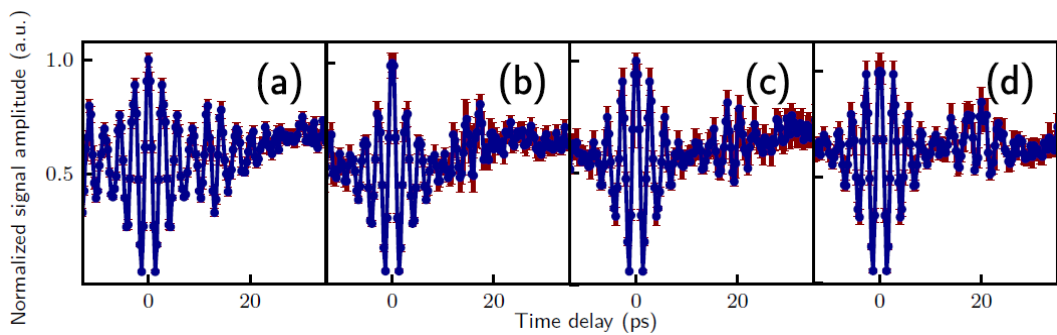
Figure 38 - The second set of experimental interferograms obtained on LUCX for the delay between laser pulses of 15 ps (a), 16 ps (b), 18 ps (c) and 19 ps (d)

On the experimental data one can see a slight horizontal asymmetry of the pattern. It is assumed that this was influenced by the alignment of the interferometer.

As can be seen from the graph (Figure 39) of comparing the distance between the electron bunches modeled in the ASTRA program and the distances between the intensity maxima of the oscillation packets obtained in the experiment, a high correlation is observed. It was the observation of this dependence that ultimately led to the idea of searching for other manifestations of the relationship between the beam-by-beam characteristics and the interference pattern. The next section describes the results of the analysis carried out.
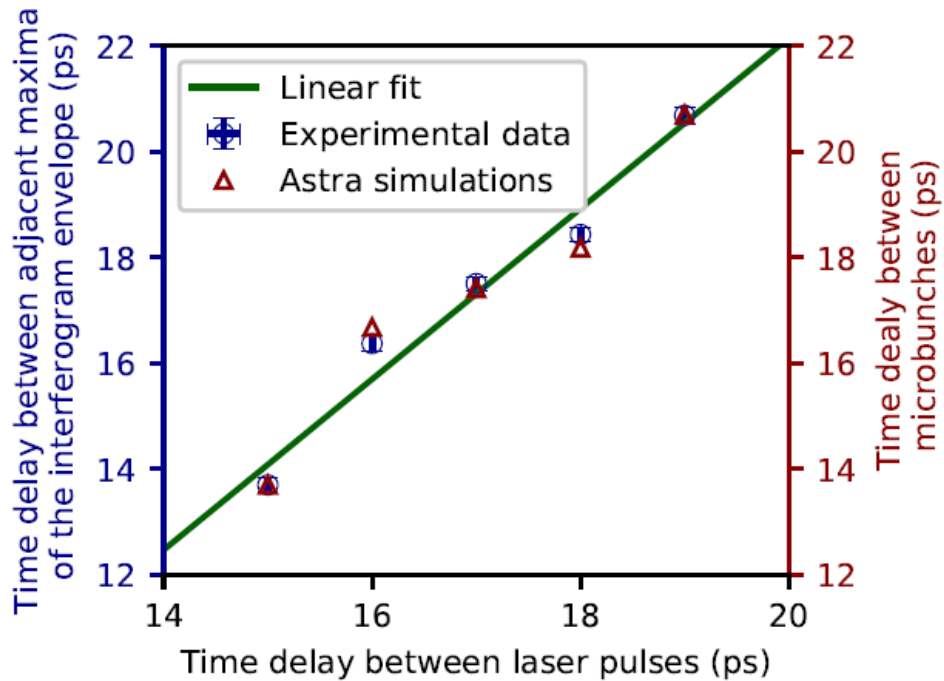
Figure 39 - Measured distance between the maxima of the envelope curves of the autocorrelation function (blue dots) and simulation of the distance between bunches depending on the time delay between laser pulses using the linear fitting function (green line). The red triangular dots correspond to the simulation done with ASTRA

2.4 Section Conclusions

Thus, a certain agreement between the mathematical model and experimental data was demonstrated. The operability of the created code for modeling has been confirmed. There are a number of small discrepancies. We briefly list them in the order in which they appear in the text of the chapter:

The results of modeling the autocorrelation function based on the mathematical model presented in the article show good agreement with the experimental data. Using the TPU microtron as an example, the possibility of using the developed method for diagnosing the temporal structure of charged particle beams was confirmed. The small discrepancies found between the model and experimental data are explained by the lack of knowledge about the exact characteristics of instruments and equipment after scheduled repairs, as well as the accelerator parameters in each specific experiment.

The discrepancy between the model and the experimental interferogram in the SDL experiment shown in Figures 34 and 35 may be due to the use of an inaccurate

spectral response of the Mylar beam splitter material. Thus, it is assumed that the slope of 45°, under which the beam splitter stood in the experiment, introduces distortions into the form of the radiation distribution, and, as a result, affects the interferogram. The order of size of the target diameter indicated in the original paper also raises questions, because, as a rule, a larger target is used to observe the declared THz frequencies. This question remains open for discussion. In general, for sequences of 10 or less clusters, a good predictive power of the model is demonstrated.

The smallest discrepancy was achieved when modeling LUCX interferograms. It is assumed that a small horizontal asymmetry of the experimental interferograms is a consequence of the interferometer tuning, and therefore is not significant for the development of the method.

Although LUCX was chronologically the first experiment on which the mathematical model was tested, the author considered it appropriate to place this case at the end of the chapter. Since it is these experimental data that are a vivid example of the manifestation of certain patterns in the behavior of the autocorrelation function with a change in the repetition rate of electron bunches and serve as a logical forerunner of the next chapter of this work.

3 Analysis of the influence of some parameters of the electron beam on the form of the interferogram

The chapter is devoted to the fifth and final stage of the development of the problem method for this stage - the analysis of how the parameters of the bunch sequence and the characteristics of the detector are related to the patterns observed on the interferogram. The chapter considers the parameters of only uniform sequences, and presents the detector sensitivity function as a constant normalized value, uniformly distributed within the specified sensitivity.

3.1 Description of simulation conditions for analysis

The model shown uses the form factor expression for a uniform sequence. Particles in bunches follow a Gaussian distribution. The target is represented by an infinite thin metal plate inclined at an angle of 45° to the beam direction. Thus, the emission spectrum from one electron is assumed to be equal to unity. The average electron energy is 8 MeV. The detector is located at an angle of 3.6° relative to the direction of specular reflection to the direction of beam incidence on the target, at the maximum of the angular distribution. The detector sensitivity function is described by a uniform distribution. Let us consider some general cases and visually analyze the influence of changes in the parameters of a uniform sequence of electron bunches on the shape of the interferogram. Let us take a uniform sequence of bunches of the same length with a different number of bunches in it, the distance between the bunches and their lengths, and a detector with a relatively narrow and wide sensitivity band in the low-frequency and high-frequency ranges. For clarity, illustrations are provided with explanations. The structure of the figures is as follows: the bunch sequence form factor and the detector sensitivity band are shown on the left, and the interferogram is shown on the right. The legend on the left shows the calculations of the characteristic frequencies and times. Changing parameters are marked with a red ellipse. Some spikes in interferograms are associated with errors in numerical calculations. Clarifying explanations are made in the figure captions under each series of graphs. For definiteness, the parameters chosen are close to those in a series of experiments at the LUCX accelerator.

Table 6 - Parameters of experiments and modeling data obtained at the LUCX accelerator

Parameter name	Meaning
Electron energy	8 MeV
Target size	∞
target slope, θ_0	45°
observation angle, θ_y, θ_x	3.64°, 0°
Horizontal \ vertical size of the clot, $\sigma_x \setminus \sigma_y$	0.4 ps
Detector sensitivity function	Uniform distribution
The range of modeling the autocorrelation function by Δl	-30 ÷ 30 ps
Integration range, $\nu_1 \div \nu_2$	50 ÷ 2000 GHz

3.2 Results of the analysis of the influence of the parameters of electron bunch sequences on the form of the interferogram

Let us begin the description of the results of the analysis of parameters related to the detector sensitivity function.
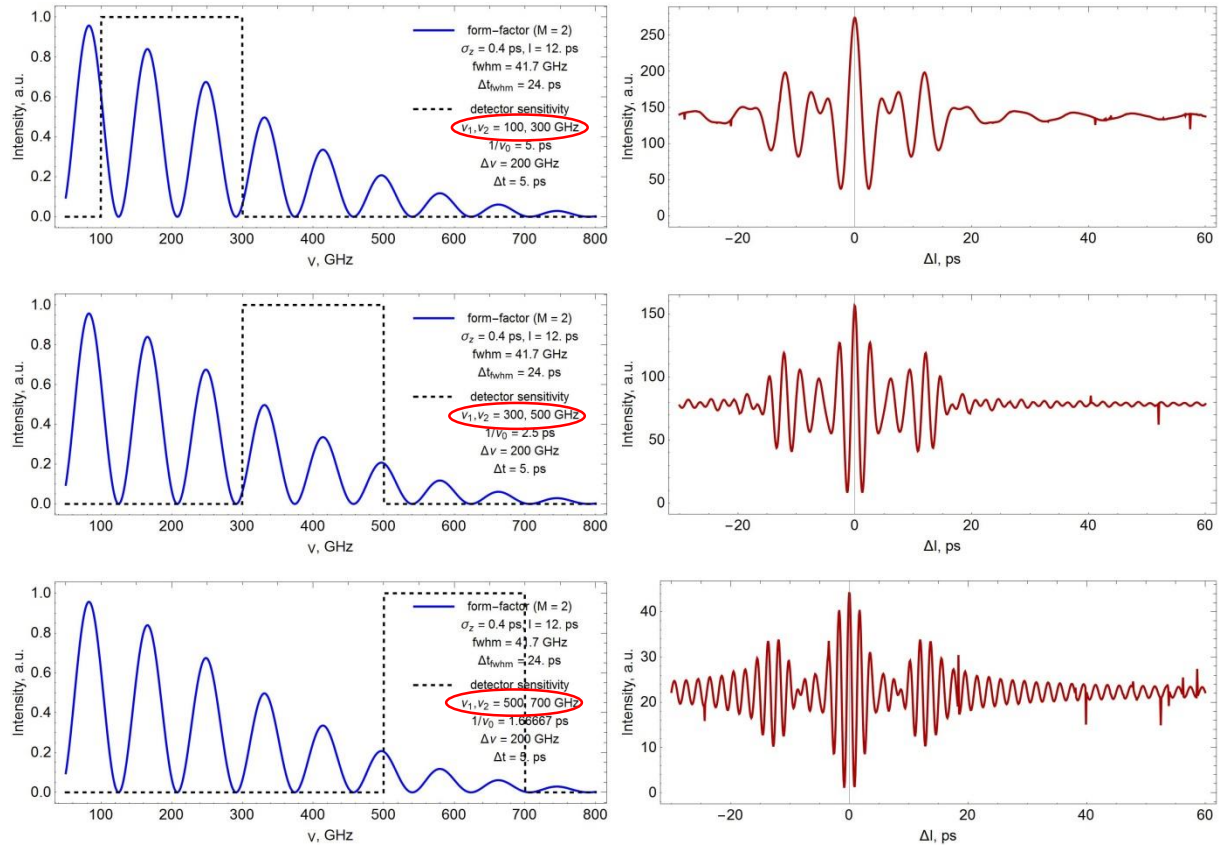
Figure 40 - Dynamics of changes when the detector range is shifted from low-frequency to high-frequency

According to Figure 40, we can conclude that the more the detector sensitivity band is in the high-frequency range, the more high-frequency oscillations are present in the interferogram.
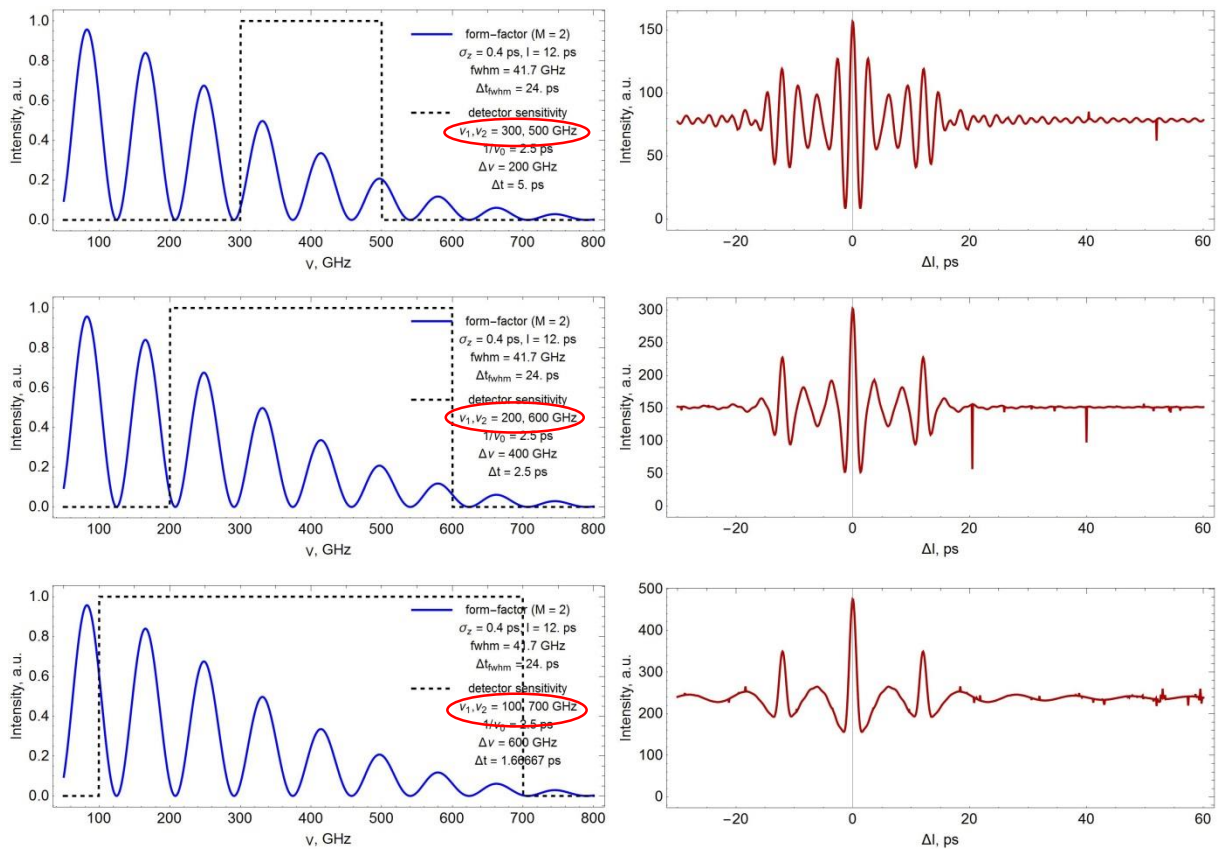
Figure 41 - Dynamics of changes with broadening of the detector sensitivity band

From Figure 41, we can conclude that the wider the sensitivity band of the detector, the narrower the duration of the oscillation packets.
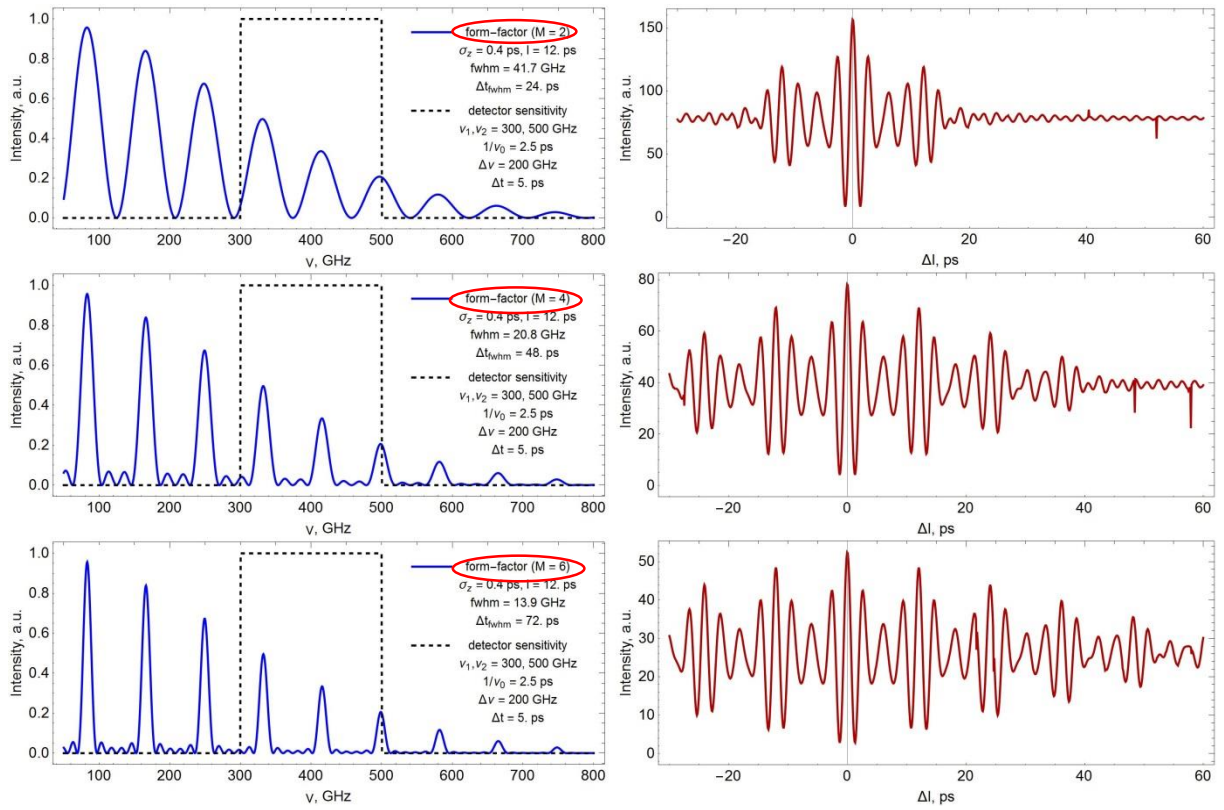
Figure 42 - Dynamics of changes with an increase in the number of clots

In the simulation series shown in Figure 42, the following relationship is traced: the greater the number of clots m in sequence, the wider the total duration of the oscillation packets, where the number of oscillations is equal to $2m - 1$.
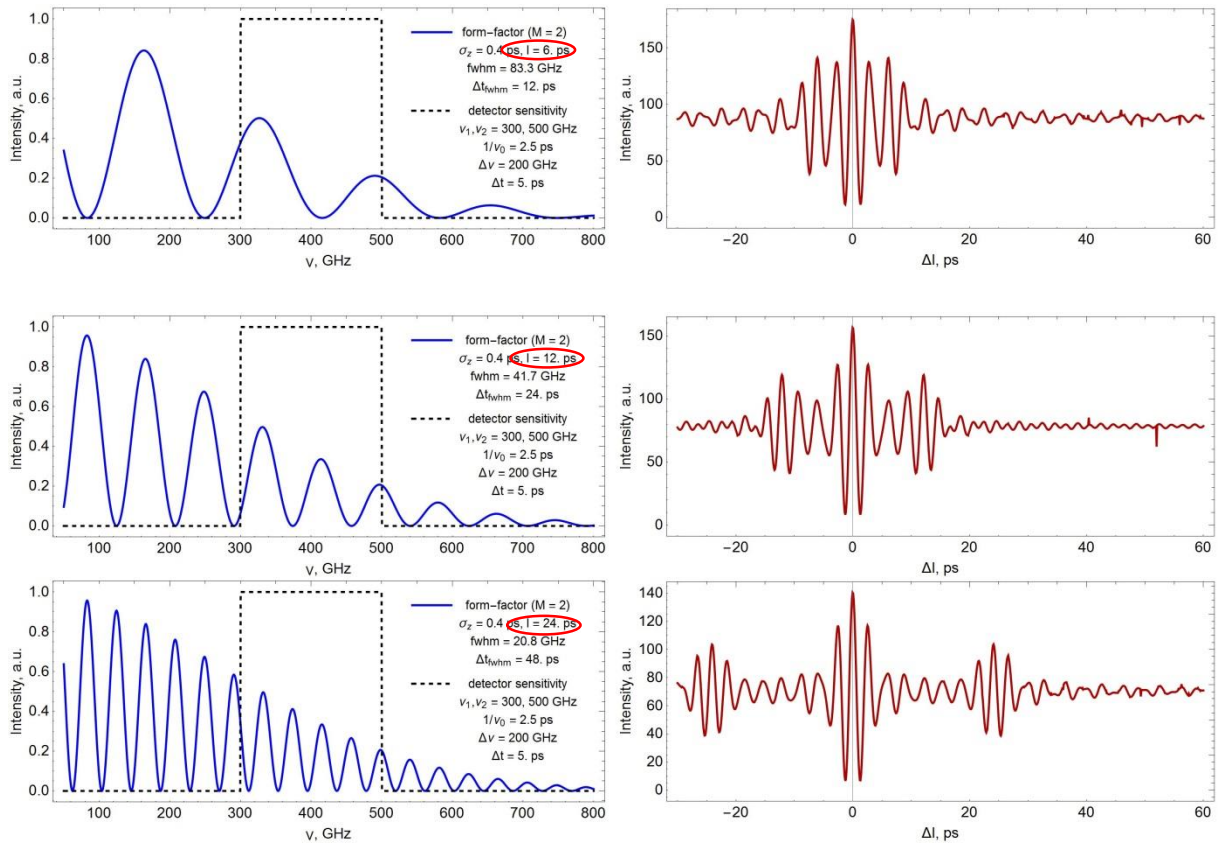
Figure 43 - Dynamics of changes with increasing distance between clots

As follows from Figure 43, the greater the distance between bunches in a sequence, the greater the distance between oscillation packets. Moreover, the distance between bunches corresponds to the distance between symmetrical packets.
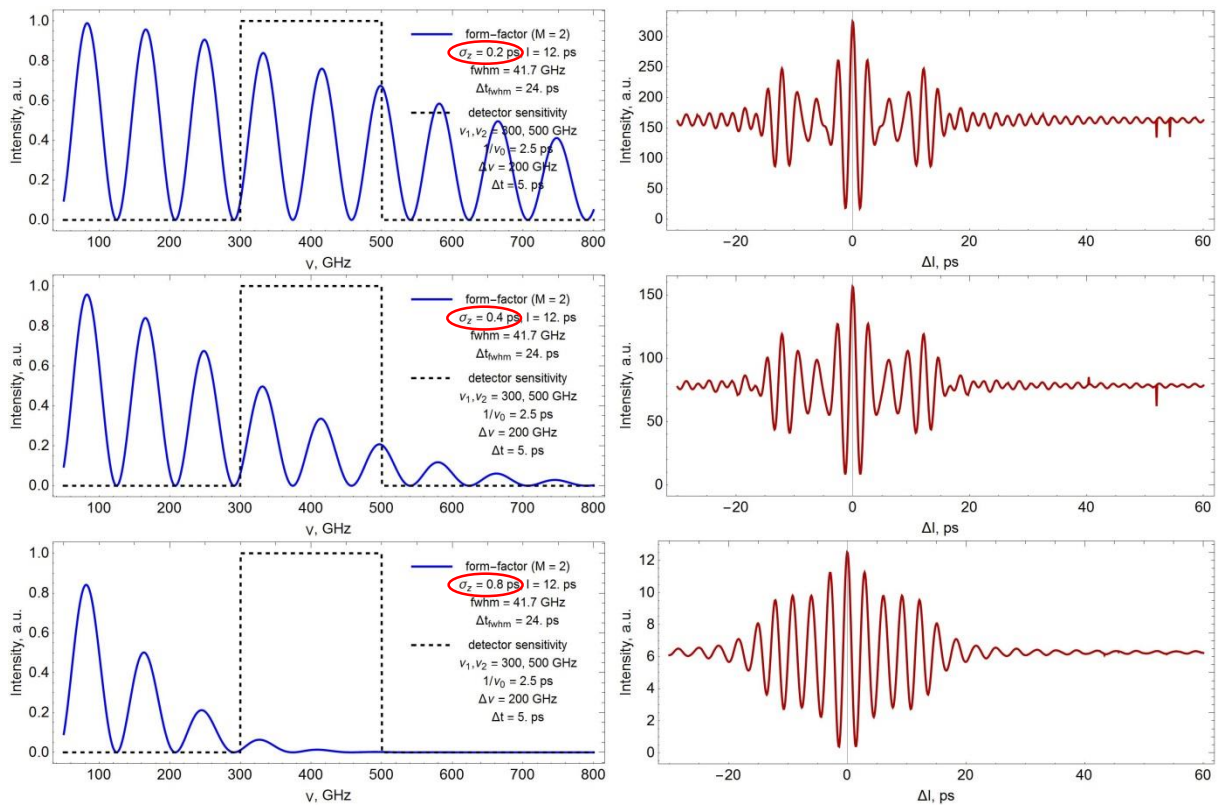
Figure 44 - Dynamics of changes with an increase in the length of clots

From Figure 44, we can conclude that the longer the bunches, the greater the amplitude of oscillations in each packet of oscillations. Because of this, when a certain ratio of the length of the bunches to the distance between them is reached, it becomes difficult to distinguish oscillation packets in the interferogram.

Table 7 summarizes the results of this analysis.

Table 7 - Description of the influence of bunch sequence parameters on the type of interferogram

Designation	Electron beam parameter	Interferogram behavior	Influence
σ_z	Clot length	Oscillation amplitude in oscillation packets	An increase in the relative amplitude of oscillation packets with an increase in the distance between bunches
l	Distance between bunches	Distance between oscillation packets	An increase in the distance between oscillation packets with an increase in the distance between bunches, the correspondence of these parameters to each other
m	Number of clots	Total width of all oscillation packages	An increase in the number of oscillation packets on an interferogram with an increase in the number of bunches in a sequence. $$m$$ The number of oscillation packets is determined by the formula $$2m-1$$
$\Delta \nu$	Sensitivity bandwidth	Oscillation Packet Width	With an increase in the width of the spectral sensitivity window of the detector, the oscillation packets become narrower.
ν_{Dmin}, ν_{Dmax}	Frequency range	Oscillation frequency in the interferogram	With a shift in the detector sensitivity limits to the high frequency range, the frequency of oscillations in the interferogram increases

An analysis of the influence of the number of bunches and distances between bunches on the appearance of the interferogram was presented at the RuPAC conference in 2021 [55]. The development of the method will be followed by the search for ways to obtain information about non-uniform sequences of electron bunches by interference methods. Uneven in terms of charge distribution, bunch sizes, distances between bunches, etc. From the analysis of uniform sequences, it would also be interesting to analyze the influence of the energy and transverse

dimensions of bunches on the appearance of the interferogram, as well as bunches of different shapes.

3.3 Section Conclusions

In the presented chapter, the regularities of changes in the interferogram with varying detector parameters, namely the width of the sensitive band and the frequency range, as well as the parameters of the sequence of electron bunches, including the length of bunches in a sequence, the number of bunches in a sequence, and the distance between bunches, are revealed. When the detector sensitivity is shifted towards high frequencies, the amount ofhigh-frequency oscillations in the interferogram. The larger the sensitivity band of the detector, the fewer intermediate oscillations on the interferogram and the more the main peaks stand out. It is shown that the number of bunches in the sequence m correlates with the number of oscillation packets in the interferogram as . The longer the bunches, the greater the relative amplitude of oscillations in each packet of oscillations. The greater the distance between bunches, the greater the distance between oscillation packets.$nn = 2m - 1$

To develop the method, it is necessary to continue analyzing the "beam-interferogram" relationship and consider the parameters of non-uniform sequential electron bunches. In addition, the influence of the detector sensitivity function on the final spectrum should be taken into account and appropriate mathematical models should be prepared, for example, for the case when the detector sensitivity band is given by a Gaussian function.

4 Financial management, resource efficiency and resource conservation

The objective of this section is to calculate the cost of developing a method for diagnosing beams of electron bunch sequences based on coherent radiation interferometry, namely, developing software for analyzing the interferogram-electron beam relationship.

Today, more than half of all existing particle accelerators are used in medicine. These areas include diagnostics, treatment, as well as fundamental research in the field of biophysics and pharmaceuticals. In the last two areas, sequences of electron bunches of ultrashort duration and spatial modulation find wide practical application. To date, there are a limited number of methods for diagnosing such sequences. This work presents a new method for diagnosing charged particle beams based on transition radiation interferometry. As part of the project, a number of programs have been written that allowto simulate interferograms from transition radiation, allowing to calculate the parameters of real experiments,in a shorter time and with fewer resources.

4.1 Analysis of competitive technical solutions

In this section, the competitiveness of the research is considered, using the example of considering two approaches to modeling coherent radiation interferograms - traditional numerical modeling and the proposed analytical one.

Option 1 is a program that conducts simulation using an analytical approach, when the calculation of interferograms is performed in the approximation of an independent distribution of particles in a bunch, expressed by a continuous analytical function.

Option 2 is a code for calculating the interferogram by numerical simulation methods, when the position of each electron in the sequence of electron bunches is taken into account. This option will be the main competitive solution to the proposed software.

The scorecard compares the strengths and weaknesses of competing technical solutions. Comparative analysis is carried out on the most important indicators using an expert assessment on a five-point scale, where 1 is the worst assessment, and 5 is

the best assessment of the compliance of the technical solution with the indicator. The total weight of all indicators in the sum should be 1. The analysis of competitive technical solutions is determined by the formula $C = \sum W_i \cdot P_i$. Here $C-$ competitiveness of research or competitor; W_i- criterion weight; P_i- score i-th criteria. The scorecard analysis presented in Table 8 will be used to assess the competitiveness of a study, where C_1 And C_2- competitiveness of code variant 1 and 2.

Table 8 - Scorecard for comparing competitive technical solutions

Criteria for evaluation	Criteria weight Wi	Points		Competitiveness	
		$P_{\text{вар.1}}$	$P_{\text{вар.2}}$	C_1	C_2
1	2	3	4	5	6
Technical criteria for evaluating resource efficiency					
Compliance of simulation results with the results of a real experiment	0.14	4	5	0.56	0.7
Calculation speed	0.13	5	1	0.65	0.13
Possibility to set exotic spatial distributions of electrons	0.12	2	5	0.24	0.6
Ability to conduct parallel calculations	0.11	5	1	0.55	0.11
Visualization	0.1	5	1	0.5	0.1
Technical Skill Requirements	0.09	5	3	0.45	0.27
Code Flexibility	0.08	5	5	0.4	0.4
Economic criteria for evaluating efficiency					
Resource costs	0.14	5	4	0.7	0.56
Estimated service life	0.09	5	4	0.45	0.36
Total	**1**	**41**	**29**	4.5	3.23

The results of the analysis presented in Table 8 allow us to conclude that the competitiveness of the analytical modeling method is higher than the numerical one for the most part, especially in cases where high accuracy of calculations can be neglected in favor of speed. However, these indicators may change if we wrap the code of option 2 in a more intuitive interface and create a full-fledged program like option 1, but at this stage this possibility is not implemented, moreover, numerical methods will always be inferior in speed to analytical ones, and this Definitely one of the biggest cons of option 2.

4.2 SWOT analysis

SWOT Analysis – Strengths, Weaknesses, Opportunities and Threats – is a comprehensive analysis of a research project.

SWOT analysis consists in describing the strengths and weaknesses of the project, in identifying opportunities and threats for the implementation of the project that have manifested or may appear in its external environment.

Strengths are factors that characterize the competitive side of a research project. Strengths indicate that the project has a distinctive advantage or special resources that are special in terms of competition. In other words, strengths are the resources or capabilities that project management has that can be used effectively to achieve goals.

Weaknesses are shortcomings, omissions, or limitations in a research project that hinder the achievement of its objectives. This is something that does not work well within the project or has insufficient capabilities or resources compared to competitors.

Opportunities include any preferred present or future situation that occurs in the project environment, such as a trend, change, or perceived need, that maintains demand for project results and allows project management to improve its competitive position.

Threat is any undesirable situation, trend or change in a project's environmental conditions that undermines or threatens its present or future competitiveness. A threat can be a barrier, a constraint, or anything else that can cause problems, disruptions, harm, or damage to the project.

The first stage consists in describing the strengths and weaknesses of the project, identifying opportunities and threats.

The second stage is to identify the compliance of the strengths and weaknesses of the research project with the conditions of the external environment. This overlap or mismatch should help determine the extent to which strategic change is needed. As part of the second stage, the final matrix of the SWOT analysis was compiled (Table 9).

Table 9 - SWOT analysis

	Strengths (strengths) S1. Allows you to take into account any spatial distribution of bunches in the sequence; S2. Allows you to calculate the interferogram on any computer at any time; S3. Ability to improve the code; S4. Intuitive program interface, allows you to do without programming skills; S5. The ability to dynamically change the parameters of bunches and the geometry of the experiment in real time; S6. High speed of calculation of interferograms; S7. Visualization of the experiment.	Weaknesses (weaknesses) W1. The given formulas are valid only for an infinite plane-parallel target with infinite conductivity; W3. Suitable only for distributions of electrons in bunches described by an analytical formula.
Opportunities (opportunities) O1. Carrying out simulation before setting up the experiment; O2. Diagnosis of bunch sizes using real interferograms; O3. Creation of new installations based on predictive models; O4. Using the program for educational purposes;	O1O2S1S4S5S6S7 - evaluate the quality of the program on a real experiment and make the program available to the public; O3S1S5S6S7 – to simulate radiation interferograms with the desired characteristics and present the parameters of the bunches for reconstruction on real installations; O4S1S2S4S5S6S7 - use the program as a visual demonstration of the interaction of ionizing radiation with matter in the relevant courses, for a better understanding of the physics of the process by students and simulation of the experiment in the absence or high cost of operating real installations.	O1O2W1 - enter additional target geometries and set them in the program, if necessary in the experiment; O1O2W2 - combine with the code for calculating the interferogram from each particle in the bunch, in the case when the distribution cannot be specified analytically.
Threats T1. On existing installations, there are well-established systems for calculating values;	T1S1S3S4S6S7 - the simplicity of the interface, the visualization of the experiment and the high speed of calculations and the flexibility of the code are the decisive factors in popularizing the program among research institutes, moreover, the newly introduced bunch parameters taken into account in the program are innovative and increase the predictive ability of the model.	T1W1 - supplement the program with various target geometries or generalize the method by specifying the target shape with an analytical formula; T1W2 - integrate into the program the code based on numerical simulation and use this approach in the case of exotic distributions of electrons in bunches.

4.3 Project initiation

The purpose of the project work is to develop a method for diagnosing the parameters of electron bunch sequences using the method of coherent radiation interferometry.

With a high repetition density of bunches in a sequence and their short length, it is possible to achieve a higher temporal resolution of the study of the processes occurring in the irradiated sample, i.e. object of chemical or biophysical research than when irradiating more from simpler sequences of electron bunches. Research of this kind is carried out with free electron lasers and synchrotron sources.

At the moment, there are a limited number of methods for diagnosing such sequences, so diagnostic specialists are trying to increase their methodological arsenal, and also welcome all sorts of ideas and innovations.

Thus, the target market for this development will be the scientific, educational industry and the industry connected with accelerator technology, namely, beam diagnostics. The teams that ensure the quality of beams at synchrotrons and free electron lasers are selected as the main consumers (Table 10).

Table 10 - Stakeholders of the project

Parties concerned	expectations
Commands that ensure the quality of electron beams at synchrotrons	Improving the quality of diagnostics of electron beam characteristics
Educational institutions	Using the created software to simulate the work on the accelerator

Table 11 provides information on the purpose and results of the project, as well as information on the criteria for achieving the goals.

Table 11 - Objectives and results of the project

Project goals:	Development of a method for diagnosing electron beams by coherent radiation interferometry
Expected results of the project:	Created description of the methodology for measuring the characteristics of beams and ready-made software for simulating the experiment
Criteria for acceptance of the project result:	Coincidence of experimental data and computer simulation results
Requirements for the project result:	Ease of use of created programs
	High predictive ability of the model

To carry out this scientific research, it is necessary to form a working group, which includes a leader and an engineer. Based on the type of planned work, the position of the performer of this work is determined. The developed list of tasks and work performed within the framework of the study, as well as the distribution of performers by type of work performed, is presented in the form of table 12.

Table 12 - Project structure

No. p / p	FULL NAME, main place of work job title	Role in the project	Functions	Labor costs, hour.
1	Shkitov Dmitry Andreevich, PhD, researcher, TPU	Supervisor	Project coordination; Assistance in the process of processing the results of experiments. Control of the study.	128
2	Toktaganova Marzhan Meyramkhanovna, Master student of IATSH TPU,	Engineer	Selection and study of materials on the topic; Creation of a theoretical base Writing computer programs Modeling of interfeograms and comparison with the results of real experiments Analysis of the regularities of the influence of beam parameters on the characteristics of interferograms	576
Total				704

Project constraints are all factors that can serve as a limitation on the degree of freedom of project team members (Table 13).

Table 13 - Project Constraints

Factors	Limitations / Assumptions
Project budget	216011.36rub.
Source of financing	TPU within the framework of the development program No. "Priority"-2030-NIP/IZ-005-0000-2022.
Project timeline:	02/01/2023 - 04/29/2023
Project management plan approval date	02/01/2023
Project Completion Date	04/29/2023

As part of the planning of a scientific project, a project schedule and a Gantt chart were built. The Gantt chart, or harmonica, is a bar chart illustrating the project schedule (Figure 45).

Table 14 - Project Schedule

Title of works	Duration, days	Work start date	Work completion date	Executor
Drafting and approval of terms of reference	4	1.02.2023	4.02.2023	Supervisor
Choice of research direction	2	5.02.2023	6.02.2023	Supervisor
	2	7.02.2023	8.02.2023	Engineer
Selection and study of materials on the topic	12	9.02.2023	02/20/2023	Engineer
Scheduling of research work	3	21.02.2023	22.02.2023	Supervisor
Formation of the theoretical base	13	02/23/2023	8.03.2023	Engineer
Creation of a program code for calculating an interferogram by an analytical method	13	9.03.2023	03/21/2023	Engineer
Creation of a program code for calculating interferograms by a numerical method	13	03/22/2023	3.04.2023	Engineer
Control of created programs	2	04/04/2023	5.04.2023	Supervisor
	2	6.04.20223	04/07/2023	Engineer
Simulation of interferograms from real bunches	6	8.04.2023	04/13/2023	Engineer
Comparison of the obtained results	1	04/14/2023	04/14/2023	Supervisor
	1	04/15/2023	04/15/2023	Engineer
Analysis of regularities in the influence of bunch parameters on radiation characteristics	4	04/16/2023	04/19/2023	Engineer
Quality control of work performance and consulting the contractor	4	20.04.2023	04/23/2023	Supervisor
Drawing up an explanatory note to the program code	6	04/24/2023	04/29/2023	Engineer

№		Исп.	T_{ki}, Кол.дн.	Продолжительность работ											
				Февраль			Март			Апрель			Май		
				1	2	3	1	2	3	1	2	3	1	2	3
1	Составление и утверждение технического задания	Исп.1	4	▨											
2	Выбор направления исследований	Исп.1 Исп.2	4	█											
3	Подбор и изучение материалов по теме	Исп.2	12		█										
4	Календарное планирование работ по проведению исследования	Исп.1	3			▨									
5	Формирования теоретической базы	Исп.2	13				█								
6	Создание программного кода для расчета интерферограмм аналитическим методом	Исп.2	13					█							
7	Создание программного кода для расчета интерферограмм численным методом	Исп.2	13						█	█					
8	Контроль созданных программ	Исп.1 Исп.2	4							▨█					
9	Моделирование интерферограмм от реальных сгустков	Исп.2	6								█				
10	Сравнение полученных результатов	Исп.2	4								█				
11	Анализ закономерностей влияния параметров сгустков на характеристики излучения	Исп.1 Исп.2	2									▨			
12	Контроль качества выполнения работ и консультирование исполнителя	Исп.1	4									▨			
13	Составление пояснительной записки к программному коду	Исп.2	6									█	█		

Примечание:

▨ – Исп. 1 (научный руководитель), █ – Исп. 2 (инженер)

Figure 45 - Gantt Chart

This chart lists the tasks that need to be completed on the vertical axis and time slots on the horizontal axis. The width of the horizontal bars on the graph shows the duration of each activity.

4.4 Research budget

The amount of costs associated with the implementation of this work is the basis for the formation of the project budget. This budget will be presented as the lower limit of the project cost at the conclusion of the contract with the customer.

To form the final cost, all calculated costs for individual items related to the head and the student are summed up.

In the budgeting process, the following grouping of costs by items is used:

- material costs for scientific and technical research;

- depreciation of equipment used for scientific work;

- basic salary;

- additional salary;

- labor tax;

- overhead costs.

Material costs for scientific research

This article includes the cost of purchasing all types of materials, components and semi-finished products necessary to perform work on this topic. The amount of material assets required is determined by consumption rates.

The calculation of the cost of material costs is made according to the current price lists or contractual prices. The cost of material costs includes transport and procurement costs (3-5% of the price). This article also includes the costs of paperwork (stationery, replication of materials). The results for this article are recorded in table 15.

Table 15 - Material costs

Name	Unit	Quantity	Price per unit, rub.	Costs, rub.
Office paper A4	pack.	1	350	350
Stationery	pack.	1	200	200
Notebook Acer TravelMate P259	PC.	1	38500	38500
Total for materials				39050
Transport and procurement costs (5%)				1952.5
Total				41002.5

Basic salary

This score includes the base salary of participants directly involved in the implementation of the work for this study. The amount of labor costs is determined based on the complexity of the work performed and the current system of remuneration.

Basic salaryis calculated using the following formula:

$$З_{осн} = З_{дн} \cdot T_{раб}$$

where Zosn is the basic salary of one employee; Tr is the duration of work performed by a scientific and technical worker, slave. days; Zdn - the average daily wage of an employee, rub.

The average daily wage is calculated by the formula:

$$З_{дн} = \frac{З_{м} \cdot M}{F_{д}},$$

where Zm is the monthly official salary of the employee, rub.; M - the number of months of work without vacation during the year: with a vacation of 48 slaves. days M=10.4 months, 6-day week; Fd - the actual annual fund of working time of scientific and technical personnel, slave. days (251).

Table 16-Working time balance

Working time indicators	
Calendar number of days	365
Number of non-working days - weekend - holidays	 52 14
Loss of working time - vacation - period of isolation - absenteeism due to illness	 48
Valid annual fund of working time	251

Employee's monthly salary:

$$З_{м} = З_{б} \cdot (k_{пр} + k_{д}) \cdot k_{р}$$

where Zb - base salary, rub.; kpr – premium coefficient; kd - coefficient of additional payments and allowances; kp – district coefficient.

The calculation of the basic salary is given in table 17.

Table 17-Basic salary calculation

Performers	Zb, rub.	k_{etc}	k_d	k_R	Zm, rub	Zdn, rub.	Tr, slave. days	Zosn, rub.
Scientific director Shkitov D.A., Researcher	27154	-	-	1.3	35300.2	1462.6	16	23401.6
Master student Toktaganova M.T. Engineer	20064				26083.2	1080.7	72	77810.4
Total								**101212**

Additional salary

This item includes a number of payments provided for by labor legislation, for example, payment for regular and additional holidays; payment of time associated with the performance of state and public duties; pay for work experience, etc.

Additional salarycalculated on the basis of 10-15% of the basic salary, employees directly involved in the implementation of the topic:

$$З_{доп} = k_{доп} \cdot З_{осн},$$

where Zdop - additional wages, rub.; kdop – coefficient of additional salary (10%); Zosn - basic salary, rub.

Table 19-Additional salary calculation

	Supervisor	Engineer
Salary, rub.	23401.6	77810.4
Add. salary, rub.	2340.16	7781.04
Total:	**10121.2**	

Deductions to off-budget funds

Tax to extra-budgetary funds is obligatory according to the norms established by the legislation of the Russian Federation, to state social insurance, pension fund and medical insurance from the expenses of employees.

Deductions to off-budget funds are determined from the equation:

$$C_{внеб} = k_{внеб} \cdot (З_{осн} + З_{доп})$$

where kvneb is the coefficient of deductions for payment to off-budget funds.

In accordance with the Federal Law of July 24, 2009 No. 212-FZ, the amount of insurance premiums is set at 30%. Institutions carrying out educational and scientific activities have an indicator of 27.1%.

Table 20- Calculationtax to off-budget funds

	Supervisor	Engineer
Contribution ratio	0.271	
Salary (basic and additional), rub.	25741.76	85591.44
Tax to off-budget funds, rub.	6976.02	23195.28
Total:	**30171.3**	

Overheads

Overhead costs include other management and maintenance costs that can be charged directly to the project. In addition, this includes expenses for the maintenance, operation and repair of equipment, production tools and equipment, buildings, structures, etc.

Overhead costs range from 30% to 90% of the base and additional wages of employees.

Overhead costs are calculated according to the equation:

$$C_{\text{накл}} = k_{\text{накл}} \cdot (3_{\text{осн}} + 3_{\text{доп}})$$

,

where knakl is the coefficient of overhead costs.

Table 21- Calculationoverhead

	Supervisor	Engineer
overhead ratio	0.3	
Salary, rub.	25741.76	85591.44
Overhead costs, rub.	7722.53	25677.43
Total:	**33399.96**	

Other direct expenses

Energy costs for equipment are calculated according to the equation:

$$C = P_{el} \cdot P \cdot F_{eq},$$

110

where - electricity tariffs (5.8 rubles per 1 kWh);P_{el}

$P-$ equipment power, kW;

$F_{eq}-$ time of equipment use, hours.

Estimated energy costs are shown in Table 22.

Table 22 - Calculationenergy costs

Names	Work time, hour.	Electricity	Electricity tariffs, rub	The price of energy rub
Laptop	400	0.045 kWh	5.8	104.4
Total:				104.4

Formation of estimated costs

The calculated cost of the studies is the basis for the cost estimate for the project.

The definition of the research budget is given in Table 23.

Table 23 - Grouping of expenses by items

Article	Expenses, rub.
1. Material costs	41002.5
2. Base salary	101212
3. Additional salary	10121.2
4. Extrabudgetary funds	30171.3
5. Overheads	33399.96
6. Electricity	104.4
Total Planned Costs	**216011.36**

4.5 Determining the resource efficiency of a study

The definition of effectiveness is based on the calculation of the integral indicator of the effectiveness of scientific research. Its finding is associated with the definition of two weighted averages: financial efficiency and resource efficiency.

An integral indicator of the financial efficiency of scientific research is obtained in the course of assessing the budget for the costs of three (or more) options for carrying out scientific research. To do this, the largest integral indicator of the implementation of the technical task is taken as the calculation base (as a denominator), with which the financial values for all options are correlated.

The integral financial indicator of development is defined as:

$$I_f^d = \frac{C_i}{C_{max}},$$

where is the integral financial indicator of development; I_f^d

C_i is the cost of the i-th version;

C_{max} – the maximum cost of a research project (including analogues).

The resulting value of the integral financial development indicator reflects the corresponding numerical increase in the development cost budget by several times (the value is greater than one), or the corresponding numerical decrease in the development cost by several times (the value is less than one). one but greater than zero).

Since the development has one execution, then $= 1$. I_f^d

The integral indicator of the resource efficiency of the variants of the object of study can be determined as follows:

$$I_f^d = \sum_{i=1}^{n} a_i b_i^a,$$
$$I_m^p = \sum_{i=1}^{n} a_i b_i^p,$$

where is the integral indicator of resource efficiency for the i-th development option; I_m^p

a_i - weight coefficient of the i-th development option;

b_i^a, b_i^p - scoring of the i-th development option, is set by the expert according to the selected rating scale;

n – number of comparison parameters.

The calculation of the integral indicator of resource efficiency is presented in the form of table 24.

Table 24 - Evaluation of the characteristics of the options for the execution of the study for the performer

Criteria	Weight coefficient	Option 1 (Current project)	Option 2	Option 3
1. Code quality control	0.1	2	5	5
2. Ease of use	0.2	5	4	5
3. The speed of introducing updates to the program	0.3	5	4	4

4. Computer resource consumption	0.2	5	3	3
5. Accessibility for the average user	0.1	5	2	2
6. Version control system	0.1	2	5	5
Total:	**1**	**4**	**3.8**	**4**

Integral indicator of resource efficiency of the current project:

$$I_{p1} = 0.1 * 2 + 0.2 * 3 + 0.3 * 5 + 0.2 * 5 + 0.1 * 5 + 0.1 * 2 = 4 ;$$

The integral indicator of development efficiency (is determined on the basis of the integral indicator of the efficiency of the use of resources and the integral financial indicator according to the formula:I_e^p)

$$I_e^p = \frac{I_m^p}{I_f^a}, I_e^a = \frac{I_m^a}{I_f^a} \text{ and etc.}$$

$$I_e^p = \frac{4}{1} = 4$$

Comparison of the integral indicator of the effectiveness of the current project and analogues will determine the comparative efficiency. Comparative efficiency of the project:

$$E_c = \frac{I_e^p}{I_e^a}$$

Thus, the development efficiency is presented in Table 25.

Table 25 - Development efficiency

No.	Indicator	Points of the current project
1	Integral financial indicator of development	1
2	Integral indicator of resource efficiency of development	4
3	Integral efficiency indicator	4

Comparison of the values of integral performance indicators makes it possible to understand and choose a more effective solution to a technical problem in terms of financial and resource efficiency.

4.6 Section Conclusions

Thus, in this section, the stages of designing and creating competitive developments that meet the requirements in the field of resource efficiency and resource saving have been developed.

These steps include:

- development of the general economic idea of the project, formation of the concept of the project;

- organization of work on a research project;

- identification of possible research alternatives;

- study planning;

- assessment of the commercial potential and prospects for scientific research from the standpoint of resource efficiency and resource saving;

- determination of resource (resource-saving), financial, budgetary, social and economic efficiency of the project.

5 Social responsibility

Currently, there is a desire to improve all aspects of human life, including the rules of labor protection and safety. This is achievable by introducing an integrated system of actions at all stages and levels of the production process.

Occupational health and safety regulations are necessary to prevent accidents, ensure safety in the workplace and are binding on everyone.

The work is devoted to the development of a method for diagnosing the parameters of charged particle beams based on coherent radiation interferometry. Scope of the method cover the areas of high energy physics, and accelerator technology, in particular, diagnostics of charged particle beams. The results of the work can also be used as additional educational material in the above-mentioned disciplines. The main work on the development of the theory of the method and computer simulation was carried out in room 243 of building 11Tomsk Polytechnic University on a laptopAcer TravelMate P259. The relevance of the work is due to the accelerated pace of development of beam technologies and the lack of a sufficient number of methods for diagnosing beams with new characteristics.

The section deals with dangerous and harmful audience factors No.243, 11 buildings Tomsk Polytechnic University, influencing the research process, legal and organizational issues, as well as measures to eliminate the consequences of accidents and emergencies.

5.1 Industrial safety

Harmful and dangerous factors of the room No. 243 educational building No. 11 of TPU and the regulatory documents regulating them are listed in Table 26.

Table 26 - Hazardous and harmful factors of the premisesNo. 243educational building No. 11 of TPU and a list of relevant regulatory documents

Factors (GOST12.0.003-2015 [60])	Regulations
1. Microclimate	GOST 30494-2011 Zdaniya zhilye i obshchestvennye. Parametry mikroklimata v pomeshcheniyah [61]
2. Illumination of the working area	SP 52.13330.2016 Estestvennoe i iskusstvennoe osveshchenie [62]
3. Noise and vibration	SanPiN 1.2.3685-21 Gigienicheskie normativy i trebovaniya k obespecheniyu bezopasnosti i (ili) bezvrednosti dlya cheloveka faktorov sredy obitaniya [63]
4.Fire and explosion safety	SP 12.13130.2009 Opredelenie kategorij pomeshchenij, zdanij i naruzhnyh ustanovok po vzryvopozharnoj i pozharnoj opasnosti [64] GOST 12.1.004-91. Sistema standartov bezopasnosti truda. Pozharnaya bezopasnost'. Obshchie trebovaniya [65]
5. Electrical safety	GOST12.1.009-2017 Sistema standartov bezopasnosti truda. Elektrobezopasnost'. Terminy i definition [66] GOST 12.1.019-2017 Elektrobezopasnost'. Obshchie trebovaniya i nomenklatura vidov zashchity [67] GOST R 58698-2019 (MEK 61140:2016). Zashchita ot porazheniya elektricheskim tokom. Obshchie polozheniya dlya elektroustanovok i elektrooborudovaniya [68]
6. Radiation safety	SP 2.2.3670-20 Sanitary-epidemiologicheskie trebovaniya k usloviyam truda [69] SanPiN 2.6.1.2523-09 Normy radiation safety NRB-99/2009 [70]

5.2 Microclimate

The indicators characterizing the microclimate are [61, 63]:

- air temperature;

- relative humidity;

- air speed;

- intensity of thermal radiation.

Each of the microclimate parameters affects a person, and together they can increase the negative impact on the body if these parameters deviate from the permissible norm [63].

All works have their own categories and their corresponding optimal and permissible values of microclimate characteristics. This work with a PC belongs to the category of light physical work (1b).

Optimal values for temperature, air velocity and humidity are given in Table 27 [61].

Table 27 - Optimal microclimate parameters (category 1b)

Period of the year	Temperature, °C	Relative humidity, %	Air speed, m/s
Cold	21-23	40-60	0.1
Warm	22-24	40-60	0.1

Since in cold and warm periods, without additional means of cooling and heating, the temperature in the room may go beyond the required norms, it is necessary to take measures to control methods and means of protection against high and low temperatures, heating systems, ventilation, etc.

ForTo maintain these sanitary standards, it is necessary to have a local fully air-conditioned air conditioner that ensures the constancy of temperature, relative humidity, speed and air purity.

To calculate the required fan performance W in an office space with a volume of V = 70 m3 (S = 20 m2, h = 3.5 m), which will circulate air masses in auditorium No. 243, 11 of the TPU building, we use the formula [71]:

$$W = V \cdot k,$$

where k is the normalized air exchange rate (for an office space, k = 2) [63].

Substituting the data into formula (5.1), we obtain the required fan performance value:

$$W = 70 \cdot 2 = 140 \ \frac{\text{м}^3}{\text{ч}}.$$

Thus, it is necessary to install a VARP Alpha318×150 fan with a capacity of 55 to 318 m3/h in the auditorium [72].

A central heating system is also required to provide a given temperature level in winter according to [73]. In winter, a water heating system is used in the

auditorium to maintain the required temperature. This system is reliable in operation and provides the ability to control the temperature over a wide range. When installing a ventilation and air conditioning system in the auditorium, certain fire safety requirements must be observed. In winter, a heating system must be provided in the room. It must provide sufficient, constant and uniform heating of the air.

To protect the researcher from the action of the harmful factor of deviation of the microclimate indicators of the room No. 243, 11 of the TPU building, microclimatic conditions are created by heating, exchange ventilation and air conditioning according to [71, 73].

5.3 Noise and vibration

Exceeding the noise level occurs during the operation of mechanical and electromechanical products.

To assess the noise environment, it is allowed to use a numerical characteristic called the sound level (measured in dB). In accordance with [74], the permissible noise level during work that requires concentration, work with increased requirements for the processes of monitoring and remote control of production cycles at workplaces in rooms with noisy equipment is 75 dB. Zones with a sound level of 80 dB must be marked with safety signs according to [75].

In room 243, the main sources of noise are the Acer TrevelMate P259 laptop (cooling system).

According to the specification on the Acer TravelMate P259 laptop, the noise level of the processor cooling device is 15-20 dB, the rest of the elements are passive and their noise level is not taken into account. The noise caused by the operation of the optical drive is also not taken into account, since it is used in operation for a slightly short time.

In the auditorium in question, additional sound insulation is not required, since the limit value of the noise level is not reached.

To bring the noise level to sanitary standards, the following rules should be followed when organizing work in the room:

- the indoor unit of the air conditioner should be located away from people engaged in creative activities (programmers), and not used at full capacity if climatic conditions allow;

- timely carry out preventive maintenance of computer system units (dust removal and lubrication of moving parts of cooling units, replacement of excessively noisy components).

Protection against increased levels of noise and vibration in the auditorium No. 243, 11 of the TPU building is carried out by methods of its reduction in the source of formation and on the path of propagation, the installation of screens and sound-absorbing linings, personal protective equipment according to [63, 74].

5.4 Lighting

Insufficient illumination of the working area is also considered one of the factors affecting human performance. For industrial enterprises, the optimal illumination of the territory and premises is an important and difficult technical task, the solution of which provides normal hygienic conditions for working personnel. Properly selected light sources and their design create conditions for production work, the correct execution of technological operations, compliance with rules and safety precautions.

The main task of lighting calculations for artificial lighting is to determine the required power of an electric lighting installation to create a given illumination.

Indoors, according to the method of placing lamps and the distribution of illumination, the following systems of artificial lighting are distinguished: general and combined.

General lighting is called, the lamps of which illuminate the entire area of \u200b\u200bthe room, both occupied by equipment or workplaces, and auxiliary. Depending on the location of the fixtures, uniform and localized general lighting are distinguished. With general uniform illumination, the luminaires are located evenly in the upper zone of the room, thereby ensuring the same illumination of the entire room. It is used, as a rule, when the location of the working areas during the design is unknown or with a flexible layout. With general localized lighting, luminaires are

placed taking into account the location of technological equipment, creating the required level of illumination on individual surfaces.

The combined lighting system consists of general and local lighting. General lighting is designed to illuminate passages and areas where work is not performed, as well as to equalize the brightness in the field of view of workers. Local lighting is provided by lamps located directly at the workplace. It should be preferred if different visual tasks are to be solved in several working areas of the room and therefore they require different levels of illumination. It is also necessary when workplaces are geographically distant from each other. At the same time, it should be borne in mind that the device of only local lighting is unacceptable, since it creates a large difference in the illumination of working surfaces and the surrounding space, which adversely affects vision [62].

When taking into account the peculiarities of the work process on the computer, it is allowed to use a system of general uniform lighting.

For general lighting, gas discharge lamps are used: daylight (LD), cold white (LHB), warm white (LTB) and white color (LB).

The computer room has the following options:
- room height: H= 350 cm;
- distance of fixtures from ceiling: hc = 35 cm;
- calculate the height of the lamp above the floor, the height of the suspension:

$$h_n = H - h_c = 350 - 35 = 315 \ \textit{см} ;$$

height of the working surface above the floor: hрп = 75 cm;
calculate the height of the lamp above the work surface:

$$h = h_n - h_{pn} = 315 - 75 = 260 \ \textit{см} .$$

When lighting a working room with two-lamp OD luminaires with a single installation or with continuous rows of single luminaires, in accordance with the requirements, the smallest permissible suspension height above the floor is 3.5 m. The calculated value h = 2.6 m does not meet the requirements.

- distance between adjacent lamps: L= 3.75 cm;
- distance from the end lamps to the wall: l = 0.9 cm.

This distance from the outermost fixtures to the wall is suitable, since the required value is:

$$\frac{L}{3} = \frac{3,75}{3} = 1,25 \ \text{см}.$$

The integral criterion for the optimal location of fixtures is a value equal to:

$$\lambda = \frac{L}{h}.$$

This value should be 1.4 with the best and high-quality arrangement of fixtures. Calculate the optimal distance between the lamps:

$$L = \lambda \cdot h = 1,4 \cdot 2,6 = 3,64 \ \text{м}.$$

This value is fully consistent with the current location of the fixtures.

Calculation of the general uniform artificial illumination of a horizontal working surface is carried out using the luminous flux coefficient method: φ

$$\varphi = \frac{E_{\text{н}} \cdot S \cdot K_s \cdot Z}{N \cdot n}$$

where the normalized minimum illumination, according to [62]: En = 200 Lm (visual work category VI: very low accuracy);area of the illuminated room: S = 20 m2; safety factor that takes into account the pollution of the lamp, the presence of smoke, dust in the atmosphere: Ks = 1.5 (room with low dust emission); coefficient of illumination unevenness: Z = 1.1 (for fluorescent lamps); number of lamps in the room: N = 4; luminous flux utilization factor: n = 0.5.

Then the luminous flux is:

$$\varphi = \frac{200 \cdot 20 \cdot 1,5 \cdot 1,1}{4 \cdot 0,5} = 3300 \ \text{Лм}.$$

In accordance with the value of the calculated luminous flux = 3300 Lm, for auditorium No. 243, 11 of the TPU building, the nearest light fluorescent lamp is a lamp of the LB40-1 type with an electric power of the lighting system of 40 W, which complies with the standards [62]. φ

5.5 Electromagnetic fields

The main harmful factor in the use of computers is electromagnetic radiation from the constituent parts of devices. An increased level of electromagnetic radiation can negatively affect the human body, namely, lead to nervous disorders, sleep disturbance, a significant deterioration in visual activity, a weakened immune system, and disorders of the cardiovascular system.

Electromagnetic fields are controlled in the following ranges: 50 Hz (power frequency) and from 30 kHz to 300 GHz. Measurements are carried out at the workplaces of users of stationary and portable personal computers. The following parameters are controlled: the strength of the electric and magnetic fields, the strength of the electrostatic field.

The norms of maximum permissible levels (MPL) of electromagnetic radiation, established in the document [63], are shown in tables 28 and 29.

Table 28 - Maximum permissible levels of electric and magnetic fields of industrial frequency 50 Hz

N p / p	Impact type	Electric field strength, kV/m	Induction (magnetic field strength), µT (A/m)
1	In residential buildings, children's, preschool, school, educational institutions	0.5	5.0(4.0)
2	In public buildings	0.5	10.0 (8.0)
3	On the residential area	1.0	10.0 (8.0)

Table 29 - EMI limits for the frequency range 30 kHz-300 GHz

Frequency range	30-300 kHz	0.3-3 MHz	3-30 MHz	30-300 MHz	0.3-300 GHz
Normalized parameter	Electric field strength, E (V/m)				Energy flux density, PES (µW/cm)
Maximum permissible levels	25	15	10	3	10 25 for cases of exposure from antennas operating in the circular view or scanning mode

This laptop model generates electromagnetic radiation with a frequency of 144 Hz, which is not controlled [63].

5.6 Fire and explosion protection

Depending on the characteristics of the substances and materials in the room, according to the explosion and fire hazard, the rooms are divided into categories A, B, C1-C4, D and E in accordance with [64].The room under consideration is classified as category B, as it contains solid combustible substances in a cold state. Possible causes of fire:

- work with open electrical equipment;

- short circuits in power supplies;

- non-compliance with fire safety rules.

In order to reduce the risk of a fire and minimize possible damage, preventive measures are taken, which are divided into: organizational and technical, operational and regime. Organizational and technical measures consist in conducting regular briefings for employees responsible for fire safety, training employees in the proper operation of equipment and the necessary actions in the event of a fire, certification of substances, materials and products in terms of ensuring fire safety, manufacturing and use of visual agitation to ensure fire safety [65]. Operational measures include preventive inspections of equipment. Regime measures include the establishment of rules for the organization of work and compliance with fire prevention measures.

- maintenance of premises in accordance with fire safety requirements;

- proper operation of the equipment (correct connection of the equipment to the power supply network, control of equipment heating);

- training of production personnel in fire safety rules;

- availability, proper placement and use of fire extinguishing equipment.

In a room with electrical equipment, in order to avoid electric shock, it is advisable to use carbon dioxide or powder fire extinguishers. These fire extinguishers are designed to extinguish fires of various substances and materials, electrical installations under voltage up to 1000 V, flammable liquids. Chemical and foam fire extinguishers are not allowed. Fire extinguishers should be located on the protected object in accordance with the requirements so that they are protected from direct sunlight, heat fluxes, mechanical influences and other adverse factors

(vibration, aggressive environment, high humidity, etc.). They must be clearly visible and easily accessible in the event of a fire. It is preferable to place fire extinguishers near the places of the most likely occurrence of a fire, along the paths of passage, and also near the exit from the premises. On the floor whereauditorium No. 243, building 11 of TPUthere are 2 fire extinguishers OP-3 (portable powder fire extinguishers), flights of stairs are equipped with hydrants, there is a fire alarm button, which corresponds to [64, 65].

5.7 Electrical safety

Electrical safety is a system of organizational and technical measures and means that ensure the protection of people from the harmful and dangerous effects of electric current, electric arc, electromagnetic field and static electricity according to [66, 67]. Electric current, passing through the human body, produces thermal, chemical and biological effects, thereby disrupting normal life. Workers hired to perform work in electrical installations must have professional training appropriate to the nature of the work.

An electric shock occurs when you come into contact with an electrical circuit in which there are sources of voltage and / or current sources that can cause current to flow through the energized part of the body. Usually sensitive to a person is the passage of a current of more than 1 mA. In addition, at high voltage installations, an electric shock is possible without touching the current-carrying elements, as a result of current leakage or breakdown of the air gap with the formation of an electric arc [67].

As part of the current work, contacts with open sources of electric current were not made. The current flowing in computer peripherals (computer mouse, keyboard) does not pose a significant danger to human health. According to the classification, this auditorium is suitable for class 1 rooms, in which operating voltages do not exceed 1000 V [66, 68].

5.8 Radiation safety

Due to the specifics of the educational program of the author, in theory, inauditorium No. 243, building 11 of TPUsources of ionizing radiation are possible.

Hazardous and harmful production factors associated with an increased level of ionizing radiation include the following types of radiation [70]:

a) short-wave electromagnetic radiation - X-ray and gamma radiation;

b) particle flows:

- beta particles;

- alpha particles;

- neutrons;

- protons, other ions, muons, etc.;

- fission fragments.

c) radiation caused by radioactive contamination (above the natural background), including contamination with technogenic radionuclides:

- radioactive contamination of the air of the working area (due to the presence of radioactive gases of radon, thoron, actinon, their radioactive decay products, aerosols containing radionuclides);

- radioactive contamination of surfaces and materials of the production environment, including protective equipment for workers and their skin.

However, in the course of a scientific study involving theoretical calculations using a computer and no more thanauditorium No. 243, building 11 of TPU, work with sources of ionizing radiation has not been carried out [69, 70].

5.9 Safety in emergencies and emergencies

An emergency (emergency) situation is a situation in a certain territory that has developed as a result of an accident, a natural hazard, a catastrophe, a natural or other disaster that may or have caused human casualties, damage to human health or the natural environment, significant material losses and violation living conditions of people [76]. There are two main types of emergencies: man-made and natural.

Technogenic situations include fires, explosions, sabotage, and releases of toxic substances. To natural - natural disasters. Fires are the most probable technogenic situation.

Accident hazards include a sudden and uncontrolled source of energy: a moving object, uncontrolled movement or energy.

The research work was carried out in the auditorium No. 243 of the educational building No. 11 of TPU on the computer. Consider possible emergency situations, namely:

- the occurrence of a fire;

- electric shock;

- falling from a height of one's own height;

- falling down the stairs.

Emergency and emergenciesand measures for their prevention and elimination of consequences are presented in table 30.

Table 30 - Emergency and emergency situationsand measures for their prevention and elimination of consequences

No.	Emergency / emergency	Measures to prevent accidents and emergencies	Measures to eliminate the consequences of accidents and emergencies
1	Injury due to a fall from a height corresponding growth	1. Keeping the premises in proper order. 2. Restriction of the working space. 3. Timely briefing.	1. Examine or interrogate the victim; 2. If necessary - call an ambulance (112); 3. Stop bleeding, if any; 4. If there is a suspicion that the victim has a broken spine, it is necessary to provide the victim with complete rest in the supine position until qualified medical assistance is provided.
2	Injury due to falling down stairs	1. Installation of handrails on the stairs. 2. Covering the stairs with an anti-slip coating. 3. Timely briefing.	1. Call an ambulance (112); 2. Stop bleeding, if any; 3. If there is a suspicion that the victim has a broken spine (sharp pain in the spine at the slightest movement), it is necessary to provide the victim with complete rest in the supine position until qualified medical assistance is provided.
3	Injury due to electric shock	1. Grounding of all electrical installations. 2. Restriction of the working space. 3. Ensuring the inaccessibility of current-carrying parts of the equipment. 4. Timely briefing.	1. Quickly release the victim from the action of electric current [68]; 2. Call an ambulance (112); 3. If the victim has lost consciousness, but breathing has been preserved, he should be comfortably laid down, unbuttoned tight clothes, create an influx of fresh air and ensure complete rest; 4. The victim should be allowed to smell ammonia, sprinkle his face with water, rub and warm the body;

			5. In the absence of breathing, artificial respiration and heart massage should be done immediately.
4	Fire	1. Timely briefing. 2. Installation of automatic fire extinguishing equipment in the premises. 3. Installation of smoke and fire detectors. 4. Ensuring escape routes and maintaining them in proper condition. 4. Control of the operation of electrical appliances.	1. De-energize the room, stop the air supply; 2. Call firefighters or call emergency services (112); 3. Immediately report the fire to the duty officer or to the security post; 4. If possible, take measures to evacuate people, extinguish a fire and save property.

This section discusses potential emergencies and emergency situations that may arise when working in classroom No. 243, 11 of the TPU academic building. Measures to prevent and eliminate the consequences of these situations are considered, according to [68, 76].

5.10 Section Conclusions

The chapter discussesharmful and dangerous factors:

- microclimate [61, 63, 71, 73];

- noise and vibration [63, 74, 75];

- illumination [62];

- fire and explosion safety [64, 65];

- electrical safety [66-68];

- electromagnetic radiation [63];

- radiation safety [69, 70].

Room No. 243, 11 of the TPU buildingassigned to class B in terms of fire and explosion safety [64, 65] and to class 1on electrical safety [66, 67].

In addition, emergency and emergency situations, measures to prevent them, and measures to eliminate their consequences are considered [76]. The radiation

safety of work and the potential danger from electromagnetic radiation were considered separately.

All means of protection, prevention of exposure and methods for minimizing the factors of various situations are described in the relevant sections of the work.

CONCLUSION

The presented work is part of a project to develop a method of coherent radiation interferometry and is divided into three chapters. The first one is devoted to the formulation and development of the theoretical apparatus and the mathematical model describing in tandem the physical foundations of the method. Here attention is paid to the description of the created programs for modeling the behavior of the autocorrelation function on the interferogram. In the second chapter, the created model is tested on the data of real experiments. Its working and predictive ability is demonstrated. The third and final chapter presents the results of the analysis of the influence of the values of the parameters of a uniform sequence of electron bunches on the nature of the patterns of the interference pattern.

Chapter 1 is the most voluminous in content, because. solves 3 tasks at once, set in the work. In the first part, the author introduces the reader to the concept of interferometry, giving definitions to each new object and concept that arise on the way to understanding the physical process. Taken separately, by themselves, neither the concepts nor the description of phenomena are a new word in science. However, putting them together and considering them within the proposed methodology demonstrates the author's understanding of the physics behind the mathematics discussed in Chapter 2. The second part focuses on deriving the mathematical expression for the detector's signal function. At the very beginning, a general expression for the signal intensity is given. The following is the derivation of the most important factor for thinning its type of mathematical expression - the spectral-angular distribution of radiation, and its submultiplier, the electron beam form factor. As the work progresses, this parameter acquires more and more refinements, moving away from particular cases of beam configuration to the most general expression for sequences of electron bunches. Some of these refinements were not used in the modeling in this work. However, when developing a method for diagnosing beams, it is necessary to be prepared for different options for the distribution of bunches in space, since the conditions for conducting real experiments may be far from ideal cases. The last part of Chapter 1 describes the

computer programs that were created. The purpose of their creation was to facilitate the signal modeling process during the work described in chapters 2 and 3. The created programs, in addition to modeling the interference signal, and the emission spectrum display on the working screen a three-dimensional scheme of the electron beam, the geometry of the target and the detector, designed to be a visual demonstration of changes in the parameters of the conditions of the simulated experiment. Two versions of the program have been implemented. In the first case, the beam and experiment parameters are known in advance and are input in the form of a prepared list. In the second, uniform sequences are considered, it is possible to set the parameters of the bunch and experiment, dynamically change them. The first option is used in Chapter 2 when conditions of real experiments are simulated. The second option is in Chapter 3, when it is necessary to highlight the general patterns of the influence of beam parameters on the interferogram. Two versions of the program have been implemented. In the first case, the beam and experiment parameters are known in advance and are input in the form of a prepared list. In the second, uniform sequences are considered, it is possible to set the parameters of the bunch and experiment, dynamically change them. The first option is used in Chapter 2 when conditions of real experiments are simulated. The second option is in Chapter 3, when it is necessary to highlight the general patterns of the influence of beam parameters on the interferogram. Two versions of the program have been implemented. In the first case, the beam and experiment parameters are known in advance and are input in the form of a prepared list. In the second, uniform sequences are considered, it is possible to set the parameters of the bunch and experiment, dynamically change them. The first option is used in Chapter 2 when conditions of real experiments are simulated. The second option is in Chapter 3, when it is necessary to highlight the general patterns of the influence of beam parameters on the interferogram. when the conditions of real experiments are simulated. The second option is in Chapter 3, when it is necessary to highlight the general patterns of the influence of beam parameters on the interferogram. when the conditions of real experiments are simulated. The second option is in Chapter 3, when it is

necessary to highlight the general patterns of the influence of beam parameters on the interferogram.

In Chapter 2, the constructed model is tested on the data of 3 real experiments in which interferometry methods were used for various purposes. The first data for comparison were taken from articles [50, 51], which describe experiments carried out on the TPU microtoron. Comparison of the model and interferograms of a real experiment allows us to conclude that the model predicts the position and number of interference peaks with great accuracy. Nevertheless, this example fails to explain the discrepancy in the amplitude of the peaks of the model and experimental interferograms. An assumption is made about insufficient knowledge of the exact characteristics of instruments and equipment. The second stage considers the data of the experiment described in [52]. Modeling of this case was complicated by the need to take into account the throughput characteristics of the equipment. Step by step, leveling the influence of these factors, a certain agreement between the model and experiment was achieved, which once again confirmed the predictive potential of the model. In addition, this case was useful for consideration, since it affected parameters previously not taken into account in the model, related to the reality of the experiments being carried out. That is, there was the very transition from pure mathematical abstraction to the need to take into account the influence of the materials from which the devices are made. In addition, the uneven nature of the sequence was taken into account. In the third paragraph of Chapter 2, the interferograms obtained in the experiment at the LUCX accelerator [53] are simulated. Since the specifics of the LUCX experiments implied a set of interferogram data with an increase in the distance between the bunches, we can talk about two problems, posed before the analysis of this particular case. It was necessary, firstly, to demonstrate the agreement between the model and experiment, and secondly, to take advantage of the chance and trace the dynamics of changes in the characteristics of the interferogram. Let us also say that it was these data that became the starting point for the idea of the diagnostic method developed in this work. The results obtained, as well as the 2 previous cases, confirmed the operability

of the model and demonstrated the regularity of the influence of the bunch length on the distance between oscillation packets in the interferogram. Thus, this paragraph concludes chapter 2 and sets the stage for reading chapter 3. that it was these data that became the starting point for the idea of the diagnostic method developed in this work. The results obtained, as well as the 2 previous cases, confirmed the operability of the model and demonstrated the regularity of the influence of the bunch length on the distance between oscillation packets in the interferogram. Thus, this paragraph concludes chapter 2 and sets the stage for reading chapter 3. that it was these data that became the starting point for the idea of the diagnostic method developed in this work. The results obtained, as well as the 2 previous cases, confirmed the operability of the model and demonstrated the regularity of the influence of the bunch length on the distance between oscillation packets in the interferogram. Thus, this paragraph concludes chapter 2 and sets the stage for reading chapter 3.

In the course of the analysis of the third chapter, the reader is invited to get acquainted with the results of the analysis of the influence of the beam parameters on the form of the interferogram. This part is not tied to a specific experiment and allows a number of simplifications. In this way, only uniform sequences of beams are considered, and the detector sensitivity is assumed to be constant over the entire aperture. A list is given of which parameter of the autocorrelation function is affected by a change in the characteristic of the distribution of bunches in space and how this parameter is manipulated.

In the future, it is necessary to automate the process of reading information about beams from interferograms, since when the diagnostic method is implemented on real accelerators, a high data processing speed will be required. To manually count, for example, packets of oscillations, if their number reaches hundreds, becomes a difficult, inconvenient and thankless task. Special attention deserves the development of an algorithm for fitting the autocorrelation function. It will be important to analyze the influence of various kinds of irregularities in the beam on the interferogram and further strive to include reality factors in the model. For example, consider the influence of the radiation propagation medium, the influence

of the tilt of the beam splitter in the interferometer, the material and shape of the polarizer, if one is used in front of the detector, shape of the detector sensitivity function, etc. It is also important to continue to develop the formalism of the form factor as a key parameter that describes the formation and transformation of the signal. And although in this work only coherent radiation was considered, the incoherent form factor should be included in the theory. The description of the process of calculating the emission spectrum from a single electron should get its place. Those. it is necessary to carry out work on the generalization and refinement of the general theory of polarization radiation, and to improve methodological prescriptions. It is also necessary to study in more detail the methods of optical interferometry and the possibility of adapting to the developed technique. The work is addressed to the community involved in beam diagnostics and we hope it will find its application at accelerator facilities in Russia and the world with a well-thought-out technical implementation.

List of used sources and literature

1. Bhandari RK Applications of Accelerator Technology and its Relevance to NuclearTechnology / RK Bhandari, MK Dey. – Text : electronic // Energy Procedia. - 2011. - Vol. 7. - P. 577-588. – DOI: 10.1016/j.egypro.2011.06.078

2. IAEA Nuclear Energy SeriesNo.NW-T-2.9, Decommissioning of Particle Accelerators/ International Atomic Energy Agency. -Vienna: International Atomic Energy Agency, 2020. - ISBN 978-92-0-102419-0.-Text : direct.

3. Amaldi U. Cancer Therapy with Particle Accelerators / U. Amaldi. - Text : electronic // Nuclear Physics A. - 1999. - Vol. 654. – P. 375c-399c – DOI: 10.1016/S0375-9474(99)00264-X

4. Chernyaev AP Radiation Technology in Medicine: Part 1. Medical Accelerators / AP Chernyaev, MA Kolyvanova, P. Yu. Borshchegovskaya. – Text : electronic // Moscow University Physics Bulletin. - 2015. - Vol. 70, No. 6. - P. 457-465. – DOI: 10.3103/S0027134915060090

5. Chernyaev AP Radiation Technology in Medicine: Part 2. Using Isotopes in Nuclear Medicine / AP Chernyaev, MA Kolyvanova, P. Yu. Borshchegovskaya [et al.]. – Text : electronic // Moscow University Physics Bulletin. - 2016. - Vol. 71, No. 4. - P. 339-348. – DOI: 10.3103/S0027134916040044

6. Rubenstein E. Synchrotron Radiation for Angiography / E. Rubenstein. – Text : electronic // Annual Review of Biophysics and Biophysical Chemistry. - 1987. - Vol. 16. – P.161-174. – DOI: 10.1146/annurev.bb.16.060187.001113

7. Castelli E. Mammography with Synchrotron Radiation: First Clinical Experience with Phase-Detection Technique / E. Castelli, M. Tonutti, F. Arfelli[et al.].– Text : electronic // Radiology. - 2011. - Vol.259, No. 3. - P.684-694. – DOI:10.1148/radiol.11100745

8. Bayat S. Functional Lung Imaging with Synchrotron Radiation: Methods and Preclinical Applications / S. Bayat, L. Porra, P. Suortti [et al.]– Text :

electronic //Physica Medica. – 2020.-Vol. 79. – P.22-35. – DOI: 10.1016/j.ejmp.2020.10.001

9.   Patera V. Biomedical Research Programs at Present and Future High-Energy Particle Accelerators / V. Patera, Y. Prezado, F. Azaiez [et al.] – Text :electronic // Frontiers in Physics. - 2020. - Vol. 8. – P.1-16. – DOI: 10.3389/fphy.2020.00380

10.   FLASH. The Free-Electron Laser in Hamburg. - Text :electronic // flash.desy.de.   –   2007.   –   URL: https://flash.desy.de/sites2009/site_vuvfel/content/e395/e2188/FLASH-Broschrefrs_web.pdf(usage date: 06/04/2023).

11.   Enlightening Science. European XFEL. - Text :electronic // xfel.eu. – 2017.   – URL:https://www.xfel.eu/sites/sites_custom/site_xfel/content/e35178/e56171/e56378/xfel_file56379/Broschuere_XFEL_EN_17168_web_eng.pdf   (usage   date: 06/04/2023).

12.   Shenoy G.Basic Characteristics of Synchrotron Radiation / G. Shenoy. - Text :electronic //structural chemistry. - 2003. - Vol. 14,No.1. - P.3-14. – DOI:10.1023/A:1021656723964

13.   Synchrotron Light Sources and Free-Electron Lasers /EJ Jaeschke, S. Khan,JR Schneider [et al.]. - Berlin : Springer, 2020. - 2538 p. -ISBN 13:978-3030232009. -Text : direct.

14.   Neutze R. Time-resolved structural studies at synchrotrons and X-ray free electron lasers: opportunities and challenges / R. Neutze, K. Moffat. – Text : electronic // Current Opinion in Structural Biology. - 2012. - Vol. 22,No.5. - P.651-659. – DOI:10.1016/j.sbi.2012.08.006

15.   Yamamoto M. Protein microcrystallography using synchrotron radiation / M. Yamamoto, K. Hirata, K. Yamashita. – Text : electronic // International Union of Crystallography Journal. - 2017. - Vol. 4. - P.529-539. – DOI: 10.1107/S2052252517008193

16.   Wagner H. Pharmaceuticals Developed with Synchrotrons / H. Wagner – Text : electronic // Synchrotron Radiation News. - 2021. - Vol. 34,No.5. – P.2-2. – DOI: 10.1080/08940886.2021.1994316

17.   Willumeit-Römer R. Visualization of Implant Failure by Synchrotron Tomography / R. Willumeit-Römer, J. Moosmann, B. Zeller-Plumhoff [et al.].-Text : electronic // TMS 2018 147th Annual Meeting & Exhibition Supplemental Proceedings. - 2018. - P.275-284.– DOI: 10.1007/978-3-319-72526-0_25

18.   Accelerator-driven Medical Sterilization to Replace Co-60 Sources / TK Kroc, JCT Thangaraj, RT Penning [et al.]. - Batavia : Fermilab, 2017. - 38 p. – FERMILAB-PUB-17-314-DI.-Text : electronic

19.   IAEAAccelerator   Knowledge   Portal.-   Text   :electronic   // nucleus.iaea.org.   –   2023.   – URL:https://nucleus.iaea.org/sites/accelerators/Pages/default.aspx   (usage   date: 06/04/2023).

20.   Gorlova EN Current Aspects of Legal Personality in the Framework of Mega-Science Projects / EN Gorlova. – Text : electronic // Lex Russica. - 2020. - Vol. 73,No.7. – P.137-145. – DOI: 10.17803/1729-5920.2020.164.7.137-145

21.   Oficialnoe opublikovanie pravovyh aktov. Postanovlenie Pravitel'stva Rossiiskoi Federacii dated March 16, 2020 No. 287 "Ob utverjdenii Federal'noi nauchno-technicheskoi programmy razvitiya sinhrotronnyh i neitronnyh issledovanii i issledovatelskoi infrastruktury na 2019 - 2027 year".- Text :electronic //   publication.pravo.gov.ru.   –   2020.   – URL:http://publication.pravo.gov.ru/Document/View/0001202003260022   (usage date: 06/04/2023).

22.   Yan L. Ultrashort Electron Bunch Train Production by UV Laser Pulse Stacking / L. Yan, Y. Du, C. Liao [et al.]. - Text :electronic // Proceedings of IPAC'10.   -   2010.   -   P.3210-3212.   – URL:http://ir.ihep.ac.cn/handle/311005/231244(usage date: 06/04/2023).

23.   Andreev AA Effective Generation of Attosecond Pulses at The Interaction of Intense Laser Radiation with Ultrathin Targets / AA Andreev, K. Yu.

Platonov. - Text :electronic //Optics and Spectroscopy. - 2022. - Vol. 130,No. 6. - P.943-956. – DOI: 10.21883/EOS.2022.06.54713.2231-21

24.   Sears CMS Production and Characterization of Attosecond Electron Bunch Trains / CMS Sears, E. Colby, R. Ischebeck[et al.].- Text :electronic //Physical Review Special Topics - Accelerators and Beams. - 2008. - Vol. eleven,No. 6.– P.061301.– DOI: 10.1103/PhysRevSTAB.11.061301

25.   Nees J. Relativistic generation of isolated attosecond pulses a different route to extreme intensity / J. Nees, N. Naumova, E. Power [et al.]. – Text : electronic // Journal Of Modern Optics. - 2005. - Vol. 52, no. 2-3. - P.305-319. – DOI: 10.1080/0950034042000297285

26.   Smaluk VV Diagnostika puchkov zaryazhennyh chastic v uskoritelyah / VV Smaluk. - Novosibirsk : Parallel, 2009. - 294 p. -ISBN 978-5-98901-063-9. - Text : direct.

27.   Ko JH Electron Bunch Length Measurement Using Coherent Radiation Source of fs-THz Accelerator at Pohang Accelerator Laboratory / JH Ko, IS Ko, SH Jung [et al.]. – Text : electronic // Proceedings of IPAC2016. - 2016. - P.235-237. – URL:https://accelconf.web.cern.ch/ipac2016/papers/mopmr003.pdf(usage   date: 06/04/2023).

28.   Yang X. Interferometric Bunch Length Measurements of 3 MeV Picocoulomb Electron Beams / X. Yang, LH Yu, V. Smaluk [et al.]. – Text : electronic // Journal of Applied Physics. - 2022. - Vol. 131. – P. 084901. – DOI: 10.1063/5.0076593

29.   Lihn H.Measurement of subpicosecond electron bunch lengths/ H. Lihn, D. Bocek, P. Kung[et al.]. – Text : electronic //AIP Conference Proceedings. - 1996. - Vol. 367. – P. 435-444. – DOI:10.1063/1.50282

30.   Thangaraj J. Demonstration of a real-time interferometer as a bunch-length monitor in a high-current electron beam accelerator / J. Thangaraj, G. Andonian, R. Thurman-Keup [et al.]. – Text : electronic // Review of Scientific Instruments.- 2012. - Vol. 83,No. 4.– P.043302. – DOI:10.1063/1.3698388

31. Ginzburg VL Radiation by uniformly moving sources (Vavilov-Cherenkov effect, transition radiation, and other phenomena) / VL Ginzburg. – Text : electronic // Physics-Uspekhi. - 1996. - Vol. 39, No. 10. - P. 973-982. – DOI: 10.1070/PU1996v039n10ABEH000171

32. Konkov AS Harakteristiki Polyarizacionnogo Izlucheniya Zaryazhennyh Chastic i Magnitnyh Momentov : dis. …cand. tech. nauk / Anatoly Sergeevich Konkov. – Tomsk, 2015.– 134 p.– Text : direct.

33. Ginzburg VL Radiation of a uniformly moving electron due to its transition from one medium into another / VL Ginzburg, IM Frank. – Text : direct // Journal of Physics USSR. - 1945. - Vol. 9. - P. 353-362.

34. Goldsmith P. Optical transition radiation from protons entering metal surfaces / P. Goldsmith, JV Jelley. – Text : electronic // Philosophical Magazine. - 1959. - Vol. 4, No. 43.- P. 836-844. -DOI:10.1080/14786435908238241

35. Trudy FIAN. Yadernaya Fizika i Vzaimodejstvie Chastic s Veshestvom. – Text : electronic //http://proceedings.lebedev.ru. - 1969. - URL: http://proceedings.lebedev.ru/0044-1969(usage date: 06/04/2023).

36. Ter-Mikhaelyan ML Vliyanie Sredy na Elektromagnitnye Processy pri Vysokih Energiyah / ML Ter-Mikhaelyan. - Yerevan : Publishing house Akademii Nauk Armyanskoj SSR, 1969. - 460 p.-Text : direct.

37. Potylitsyn AP Spatial Coherence in Transition Radiation from Short Electron Bunches / AP Potylitsyn. – Text : electronic // Journal of Experimental and Theoretical Physics Letters. - 2016. - Vol. 103, No. 11. - P. 669-673. – DOI: 10.1134/S0021364016110102

38. Kalinin BN Measurement of the Angular Characteristics of Transition Radiation in Near and Far Zones/ BN Kalinin, GA Naumenko, AP Potylitsyn [et al.]. – Text : electronic // Journal of Experimental and Theoretical Physics Letters.- 2006. - Vol. 84,No. 3.– P.110-114. – DOI:10.1134/S0021364006150021

39. Naumenko GA Characteristics of Smith-Purcell radiation in millimeter wavelength region / GA Naumenko, AP Potylitsyn, P. Karataev[et al.]. – Text :

electronic // Journal of Physics: Conference Series.- 2016. - Vol. 732.– P.012018. – DOI:10.1088/1742-6596/732/1/012018

40.   Bunch B. The History of Science and Technology / B. Bunch, A. Hellemans. - Boston : Houghton Mifflin Harcourt, 2004. - 768 p.-ISBN-10: 0618221239.-Text : direct.

41.   Naumenko GA Form-factors of Relativistic Electron Bunches in Polarization Radiation / GA Naumenko.– Text : electronic // Advanced Materials Research.-   2015.   -   Vol.   1084.–   P.138-146.   – DOI:10.4028/www.scientific.net/AMR.1084.138

42.   Tryasuchev VA Kvantovaya Mehanika dlya Studentov Tehnicheskih Vuzov / VA Tryasuchev. - Tomsk: Tomsk Polytechnic University, 2017. - 156 p. – ISBN 978-5-4387-0746-2.-Text : direct.

43.   Tishchenko AA Incoherent Form Factor in Diffraction and Smith–Purcell Radiations / AA Tishchenko, D. Yu. Sergeeva. – Text : electronic // Journal of Experimental and Theoretical Physics Letters.- 2019. - Vol. 110No. 10.– P.638-645. – DOI:10.1134/S0021364019220120

44.   wolfram mathematica.- Text :electronic // wolfram.com. – 2023. – URL: https://www.wolfram.com/mathematica(usage date: 06/04/2023).

45.   Gradshteyn IS Table of Integrals, Series, and Products / IS Gradshteyn, IM Ryzhik.-Cambridge: Academic Press, 2007. - 1163 p.– ISBN-13: 978-0-12-373637-6.-Text : direct.

46.   Nagornyi VA Uglovye harakteristiki kogerentnogo perehodnogo izlucheniya ot sgustkov ultrarelyativistskih elektronov razlichnoi formy / VA Nagornyi,A.P. Potylitsyn.– Text : direct //Bulletin of the Tomsk Polytechnic University. - 2004. - Vol. 307,No. 1.– P.15-23.

47.   Sukhikh LG Focusing of Optical Transition and Diffraction Radiation by a Spherical Target / LG Sukhikh, GA Naumenko, AP Potylitsyn [et al.]. – Text : electronic // Proceedings of DIPAC. - 2007. - P. 259-261. – URL: https://accelconf.web.cern.ch/d07/papers/wepb13.pdf(usage date: 06/04/2023).

48.   Shkitov DA Code for Simulation of Diffraction Radiation from Flat Finite Surfaces / DA Shkitov.– Text : electronic // Proceedings of RuPAC.– 2018. – P.510-513. – DOI:10.18429/JACoW-RUPAC2018-THPSC56

49.   ASTR. A Space Charge Tracking Algorithm.- Text :electronic // design.de. – 2017. – URL: https://www.desy.de/~mpyflo(usage date: 06/04/2023).

50.   Naumenko GA Spectrum of Coherent Transition Radiation Generated by a Modulated Electron Beam/ GA Naumenko, AP Potylitsyn, PV Karataev[et al.].– Text : electronic // Journal of Experimental and Theoretical Physics Letters.- 2017. - Vol. 106No. 2.– P.127-130. – DOI:10.1134/S0021364017140089

51.   Naumenko G. Monochromatic coherent transition and diffraction radiation from a relativistic electron bunch train / G. Naumenko,A. Potylitsyn, M. Shevelev [et al.]. – Text : electronic // Journal of Instrumentation. - 2018. - Vol. 13. - P. C04007. – DOI: 10.1088/1748-0221/13/04/C04007

52.   Shen Y. Tunable Few-Cycle and Multicycle Coherent Terahertz Radiation from Relativistic Electrons / Y. Shen, X. Yang, GL Carr [et al.]. – Text : electronic // Physical Review Letters. - 2011. - Vol. 107. – P. 204801. – DOI: 10.1103/PhysRevLett.107.204801

53.   Shevelev Mihail Viktorovich. - Text :electronic // up.tpu.ru. – 2023. – URL: https://up.tpu.ru/en/ruk-oop/view.html?id=2605(usage date: 06/04/2023).

54.   Karlovets DV Generalized Surface Current Method in The Macroscopic Theory of Diffraction Radiation / DV Karlovets, AP Potylitsyn. – Text : electronic // Physics Letters A. – 2009. – Vol. 373. - P. 1988-1996. – DOI: 10.1016/j.physleta.2009.03.060

55.   Toktaganova M. Simulation of The Coherent Radiation Interferometry for The Beam Temporal Structure Diagnostics / M. Toktaganova, D. Shkitov, M. Shevelev[et al.]. – Text : electronic // Proceedings of RuPAC.– 2021. – P.413-416. – DOI:10.18429/JACoW-RuPAC2021-WEPSC36

56.   UQG Optics. 'Z' Cut Quartz Windows & Plates. – Text : electronic // uqgoptics.com. – 2023. – URL: https://www.uqgoptics.com/catalogue/optical-windows/fused-quartz/z-cut-quartz-windows(usage date: 06/04/2023).

57. Rowell NLBilayer free-standing beam splitter for Fourier transform infrared spectrometry/ NL Rowell, EA Wang.– Text : electronic //Applied Optics.- 1996. - Vol. 35, No. 16. - P. 2927-2933. – DOI:10.1364/AO.35.002927

58. web plot digitizer. Web based tool to extract data from plots, images, and maps. – Text : electronic // automeris.io. – 2022. – URL: https://automeris.io/WebPlotDigitizer(usage date: 06/04/2023).

59. Infrared Laboratories. Bolometers & IR Detector Systems.– Text : electronic // irlabs.com. – 2023. – URL:https://www.irlabs.com/products/bolometers (usage date: 06/04/2023).

60. GOST 12.0.003-2015 Sistema standartov bezopasnosti truda (SSBT). Opasnye i vrednye proizvodstvennye faktory. Classification: data vvedeniya 2017-03-01. – URL: https://docs.cntd.ru/document/1200136071/ (usage date: 04/20/2023). -Text : electronic.

61. GOST 30494-2011 Zdaniya zhilye i obshchestvennye. Parametry mikroklimata v pomeshcheniyah: data vvedeniya 2013-01-01. – URL: https://docs.cntd.ru/document/1200095053 (usage date: 04/20/2023). – Text: electronic.

62. SP 52.13330.2016 Estestvennoe i iskusstvennoe osveshchenie: data vvedeniya 2017-05-08 – URL: https://docs.cntd.ru/document/456054197 (data obrashcheniya: 20.04.2023). – Text: electronic.

63. SanPiN 1.2.3685-21 Gigienicheskie normativy i trebovaniya k obeSPecheniyu bezopasnosti i (ili) bezvrednosti dlya cheloveka faktorov sredy obitaniya: data vvedeniya 2021-01-28. – URL: https://docs.cntd.ru/document/573500115 (usage date: 04/20/2023). – Text: electronic.

64. SP 12.13130.2009. Opredelenie kategorij pomeshchenij, zdanij i naruzhnyh ustanovok po vzryvopozharnoj i pozharnoj opasnosti (v red. izm. No. 1, utv. prikazom MCHS Rossii dated 09.12.2010 No. 643): data vvedeniya 2009-05-01. – URL: https://docs.cntd.ru/document/1200071156 (usage date: 04/20/2023). – Text: electronic.

65.   GOST 12.1.004-91 Sistema standartov bezopasnosti truda. Pozharnaya bezopasnost'. Obshchie trebovaniya: data vvedeniya 1992-07-01. – URL: https://docs.cntd.ru/document/9051953 (usage date: 04/20/2023). – Text: electronic.

66.   GOST 12.1.009-2017 Sistema standartov bezopasnosti truda. Elektrobezopasnost'. Terminy i opredeleniya: data vvedeniya 2019-01-01. – URL: https://docs.cntd.ru/document/1200161311 (usage date: 04/20/2023). – Text: electronic.

67.   GOST 12.1.019-2017 Sistema standartov bezopasnosti truda. Elektrobezopasnost'. Obshchie trebovaniya i nomenklatura vidov zashchity: data vvedeniya 2019-01-01. – URL: https://docs.cntd.ru/document/1200161238 (usage date: 04/20/2023). – Text: electronic.

68.   GOST R 58698-2019 (MEK 61140:2016). Zashchita ot porazheniya elektricheskim tokom. Obshchie polozheniya dlya elektroustanovok i elektrooborudovaniya: data vvedeniya 2020-06-01. – URL: https://docs.cntd.ru/document/1200170001 (usage date: 04/20/2023). – Text: electronic.

69.   SP 2.2.3670-20 Sanitary-epidemiologicheskie trebovaniya k usloviyam truda: data vvedeniya 2020-12-01. – URL: https://docs.cntd.ru/document/573230583 (usage date: 04/20/2023). – Text: electronic.

70.   SanPiN 2.6.1.2523-09 Normy radiation safety NRB-99/2009: data vvedeniya 2009-07-07. – URL: https://docs.cntd.ru/document/902170553 (usage date: 04/20/2023). – Text: electronic.

71.   GOST 32548-2013 Vozduhoraspredelitel'nye ustrojstva. Obshchie tekhnicheskie usloviya: data vvedeniya 2015-01-01. – URL: https://docs.cntd.ru/document/1200110084 (usage date: 04/20/2023). – Text: electronic.

72.   Vihrevye vozduhoduvki LLC "Invers-Engineering": oficial'nyj site. – URL: https://varp.pro/vozduhoduvki/vihrevye/varp-alpha-420x170 (usage date: 04/20/2023). – Text: electronic.

73. SNiP 41-01-2003 Otoplenie, ventilyaciya i kondicionirovanie: data vvedeniya 2004-01-01 – URL: http://docs.cntd.ru/document/1200035579 (usage date: 04/20/2023). – Text: electronic.

74. SP 51.13330.2011 Zashchita ot shuma. Aktualizirovannaya redakciya SNiP 23-03-2003: data vvedeniya 2011-05-20. – URL: https://docs.cntd.ru/document/1200084097 (usage date: 04/20/2023). – Text: electronic.

75. GOST 12.4.026-2015 Sistema standartov bezopasnosti truda. Cveta signal'nye i znaki bezopasnosti: data vedeniya 2017-03-01. – URL: https://docs.cntd.ru/document/1200136061 (usage date: 04/20/2023). – Text: electronic.

76. GOST R 22.0.02-2016 Bezopasnost' v chrezvychajnyh situaciyah. Terminy i opredeleniya: data vvedeniya 2017-01-01. – URL: https://docs.cntd.ru/document/1200139176 (usage date: 04/20/2023). – Text: electronic.

APPENDIX A

Conferences

- *52st International Tulinov Conference on Physics of Interactions of Charged Particles with Crystals*Moscow, Russia, 2023
- *14thInternational Scientific Seminar in Memory of Professor VP Sarantsev "Problems of Colliders and Accelerators of Charged Particles",*Alushta, Russia, 2022
- *51st International Tulinov Conference on Physics of Interactions of Charged Particles with Crystals*Moscow, Russia, 2022
- *19th International Conference of Students and Young Scientists "Prospects of Fundamental Sciences Development"*, Tomsk, Russia, 2022
- *27th Russian Particle Accelerator Conference (RuPAC-2021)*, Alushta, Russia, 2021
- *18th International Conference of Students and Young Scientists "Prospects of Fundamental Sciences Development"*, Tomsk, Russia, 2021
- *59th International Scientific Students Conference*, Novosibirsk, Russia, 2021
- *18th International Conference on Advances in IT and Robotics*, Tomsk, Russia, 2021

Articles

Shkitov D., Toktaganova M., Naumenko G., Shevelev M."Comparison of the Results of Simulation and Measurements of Interference Patterns of Coherent Transition Radiation.", in*Journal of Surface Investigation: X-ray, Synchrotron and Neutron Techniques*, vol. 7, no. 2, 2023, pp. 252-258.

Conference materials

- Shkitov D., Toktaganova M., Naumenko G., Shevelev M. "Comparison of the Results of Simulation and Measurements of Interferograms of Coherent Transition Radiation", in Collection of abstracts of 51st International Tulinov Conference on Physics of Interactions of Charged Particles with Crystals , Moscow, Russia, 2022, p. 89.

- Toktaganova M., Shevelev M., "Simulation of the coherent pulse addition in the interferometer and comparison with measurement data", in Proc. 19th International Conference of Students and Young Scientists "Prospects of Fundamental Sciences Development", Tomsk, Russia, 2022, pp. 185-187.

- Toktaganova M., Shkitov D., Shevelev M., Stuchebrov S., "Simulation of the coherent radiation interferometry for the beam temporal structure diagnostics", in Proc. 27th Russian Particle Accelerator Conference (RuPAC-2021), Alushta, Russia, 2021, pp. 413-416. https://doi.org/10.18429/JACoW-RuPAC2021-WEPSC36

- Toktaganova M., Shevelev M., "Non-gaussian effects of bunch charge distribution in generating coherent transition radiation" in Proc. 18th International Conference of Students and Young Scientists "Prospects of Fundamental Sciences Development", Tomsk, Russia, 2021, pp. 340-342.

- Toktaganova M., "Development of a method for diagnosing the distance between electron bunches of THz repetition rate based on transition radiation", in Proc. 59th International Scientific Students Conference, Novosibirsk, Russia, 2021, p. 281.

- Toktaganova M., Shkitov D., "Experimental facilities for potential studies of polarization radiation in Russia" in Proc. 18th International Conference on Advances in IT and Robotics, Tomsk, Russia, 2021, pp. 172-173.

Internet project

Shkitov D., Toktaganova M. "Coherent Transition Radiation from Bunches of Charged Particles", WOLFRAM Demonstrations Project, 2020
http://demonstrations.wolfram.com/CoherentTransitionRadiationFromBunchesOfCharged Particles/

In work

- Coherent polarization radiation from a beam of charged particlesstudy guide
- Measurement of an electron microbunches spacing via coherent transition radiation, article
- Russian Electrons accelerators for scientific purpose, review and internet portal

APPENDIX B

```
Manipulate[{Graphics3D[
{(*Axis*)
Black,Arrowheads[0.02],
{Thickness[0.002],Arrow[Tube[{{0,0,0},{2.5,0,0}}]]},
{Thickness[0.002],Arrow[Tube[{{0,0,0},{0,2.5,0}}]]},
{Thickness[0.002],Arrow[Tube[{{0,0,0},{0,0,2.5}}]]},
(*Axis labels*)
Text[Style[ "X",Large,25],{2.7 ,0,0}],
Text[Style["Y",Large,25],{0,2.7,0}],
Text[Style["Z",Large,25],{0,0,2.7}],
(*Wavevector1*)
{Red,Thickness[0.003],Arrowheads[.03],Arrow[Tube[{{0,0,0},l{Cos[\[Theta]y]*Co
s[\[Theta]x],Cos[\ [Theta]y]*Sin[\[Theta]x],Sin[\[Theta]y]}}]]},
Text[Style[ "Overscript[k,
\[RightVector]]",Red,Large,Italic,25],l{Cos[\[Theta]y]*Cos[\[Theta]x]+0.3,Cos
[\ [Theta]y]*Sin[\[Theta]x],Sin[\[Theta]y]}],
(*Wavevector2*)
{Red,Thickness[0.003],Arrowheads[.03],Arrow[Tube[{{x,y,x/Tan[\[Theta]0]},{l*C
os[\[Theta]y]*Cos[
\[Theta]x]+x,l*Cos[\[Theta]y]*Sin[\[Theta]x]+y,l*Sin[\[Theta]y]+x/Tan[\[Theta
] 0]}}]]},
Text[Style[ "Overscript[k,
\[RightVector]]",Red,Large,Italic,25],{l*Cos[\[Theta]y]*Cos[\[Theta]x]+x+0.3,
l*Cos[\[Theta]y]*Sin[\[Theta]x]+y,l*Sin[\[Theta]y]+x/Tan[\[Theta]0]}],
(*Target*)
Rotate[{Opacity[0.5],Blue,Parallelepiped[{-2,2,0},{{4,0,0},{0,-
4,0}}]},\[Theta]0-90 \ [Degree],{0,1,0}],
(*Clot1*)
{Red,Ellipsoid[{0,0,-1.5},{0.05,0.05,0.1}]},
{Red,Dashed,Thickness[0.002],Line[{{0,0,-1.5},{0,0,0}}]},
Text[Style[ "e^-",Red,Large,Italic,25],{0.3,0,-1.5}],
(*clot2*)
{Red,Ellipsoid[{x,y,-2.5},{0.05,0.05,0.1}]},
{Red,Dashed,Thickness[0.002],Line[{{x,y,-2.5},{x,y,x/Tan[\[Theta]0]}}]},
Text[Style[ "e^-",Red,Large,Italic,25],{x+0.3,y,-2.5}],
(*Lines*)
{Thickness[0.004],Arrow[{{0,0,0},{x,y,x/Tan[\[Theta]0]}}]},
{Thickness[0.008],Darker[Darker[Green]],Line[{{x,y,x/Tan[\[
Theta]y] (-Cos[\[ Theta]x] (y Cos[\[Theta]y] Sin[\[Theta]x]+x Cot[\[Theta]0]
Sin[\[Theta]y])+x (Cos[\[Theta] y] Sin[\[Theta]x]^2+Sin[\[Theta]y]
Tan[\[Theta]y]))),(Cos[\[Theta]x] Cos[\[Theta]y] ^2 (y Cos[\[Theta]x]-x
Sin[\[Theta]x])-x Cos[\[Theta]y] Cot[\[Theta]0] Sin[\[Theta]x] Sin
[\[Theta]y]+y Sin[\[Theta]y]^2),(Cos[\[Theta]y] (x Cos[\[Theta]y]
Cot[\[Theta]0]-Cos [\[Theta]x] Sin[\[Theta]y] (x+y Tan[\[Theta]x])))}}]},
{Thickness[0.008],Darker[Darker[Green]],Line[{{0,0,0},-{(Cos[\[Theta]y] (-
Cos[\[Theta]x] (y Cos[ \[Theta]y] Sin[\[Theta]x]+x Cot[\[Theta]0]
Sin[\[Theta]y])+x (Cos[\[Theta]y] Sin[\[Theta] x]^2+Sin[\[Theta]y]
Tan[\[Theta]y])))-x,(Cos[\[Theta]x] Cos[\[Theta]y]^2 (y Cos[ \[Theta]x]-x
Sin[\[Theta]x])-x Cos[\[Theta]y] Cot[\[Theta]0] Sin[\[Theta]x] Sin[\[Theta]y
]+y Sin[\[Theta]y]^2)-y,(Cos[\[Theta]y] (x Cos[\[Theta]y] Cot[\[Theta]0]-
Cos[\[Theta ]x] Sin[\[Theta]y] (x+y Tan[\[Theta]x])))-x/Tan[\[Theta]0]}}]},
{Dashed,Thickness[0.004],Line[{{0,0,0},{(Cos[\[Theta]y] (-Cos[\[Theta]x] (y
Cos[\[Theta]y] Sin [\[Theta]x]+x Cot[\[Theta]0] Sin[\[Theta]y])+x
(Cos[\[Theta]y] Sin[\[Theta]x]^2+Sin[ \[Theta]y]
Tan[\[Theta]y]))),(Cos[\[Theta]x] Cos[\[Theta]y]^2 (y Cos[\[Theta]x]-x Sin
[\[Theta]x])-x Cos[\[Theta]y] Cot[\[Theta]0] Sin[\[Theta]x] Sin[\[Theta]y]+y
Sin[\[Theta] y]^2),(Cos[\[Theta]y] (x Cos[\[Theta]y] Cot[\[Theta]0]-
Cos[\[Theta]x] Sin[\[Theta]y] (x+y Tan[\[Theta]x])))}}]},
{Dashed,Thickness[0.004],Line[{-{(Cos[\[Theta]y] (-Cos[\[Theta]x] (y
Cos[\[Theta]y] Sin[\[Theta]x] +x Cot[\[Theta]0] Sin[\[Theta]y])+x
(Cos[\[Theta]y] Sin[\[Theta]x]^2+Sin[\[Theta]y] Tan [\[Theta]y])))-
```

```
x,(Cos[\[Theta]x] Cos[\[Theta]y]^2 (y Cos[\[Theta]x]-x Sin[\[Theta] x])-x
Cos[\[Theta]y] Cot[\[Theta]0] Sin[\[Theta]x] Sin[\[Theta]y]+y
Sin[\[Theta]y]^2) -y,(Cos[\[Theta]y] (x Cos[\[Theta]y] Cot[\[Theta]0]-
Cos[\[Theta]x] Sin[\[Theta]y] (x+ y Tan[\[Theta]x])))-
x/Tan[\[Theta]0]},{x,y,x/Tan[\[Theta]0]}}]},
Text[Style[ "Overscript[r,
\[RightVector]]",Black,Bold,Large,Italic,25],{x/2,y/2+0.3,x/(2 Tan[\[Theta]0]
)-0.2}],
{Blue,Thickness[0.002],BezierCurve[{{0,0,-1},{-0.4,0,-1.3},{-
Tan[\[Theta]0],0,-1}}]]},
Rotate[{Blue,Thickness[0.003],Line[{{0,0,0},{0,0,-2}}]]},\[Theta]0,{0,1,0}],
Text[Style[ "Subscript[\[Theta], 0]",Blue,Bold,Large,Italic,23],{-0.4,0,-1.4
}]]},
ImageSize->{500,500},PlotRange->{{-3,3},{-3,3},{-3,3}},Boxed->False],
-x Cos[\[Theta]x] Cos[\[Theta]y]-y Cos[\[Theta]y] Sin[\[Theta]x]-x
Cot[\[Theta]0] Sin[\[ Theta]y]},
{{x,0.5},0,3},
{{y,1.5},0,3},
{{\[Theta]0.30 \[Degree]},0.90 \[Degree]},
{{\[Theta]y,30 \[Degree]},0.360 \[Degree]},
{{\[Theta]x,30 \[Degree]},0.360 \[Degree]},
{{l,2},1,3}]
```

APPENDIX C

```
<<(NotebookDirectory[]<>"E$all_spectra_rupac_Auto.txt");
W$TR=Interpolation[dataTRspectra2,InterpolationOrder->2, Method->"Spline"];
Wy$DR=Interpolation[dataDRspectra2,InterpolationOrder->2, Method->"Spline"];
c1=300;
F1[m_,\[Lambda]_,ee_,\[Theta]0_,
\[Theta]y_,\[Theta]x_,\[Sigma]x1_,\[Sigma]y1_,\[Sigma]z1_,\[
Sigma]x2_,\[Sigma]y2_,\[Sigma]z2_,\[Sigma]x3_,\[Sigma]y3_,\[Sigma]z3_,\[Sigma
]x4_,\[Sigma]y4_,\[Sigma
]z4_,\[Sigma]x5_,\[Sigma]y5_,\[Sigma]z5_,\[Sigma]x6_,\[Sigma]y6_,\[Sigma]z6_,\
[Sigma]x7_,\[Sigma]y7_,
\[Sigma]z7_,\[Sigma]x8_,\[Sigma]y8_,\[Sigma]z8_,\[Sigma]x9_,\[Sigma]y9_,\[Sig
ma]z9_,\[Sigma]x10_,\[
Sigma]y10_,\[Sigma]z10_,x01_,y01_,z01_,x02_,y02_,z02_,x03_,y03_,z03_,x04_,y04
_,z04_,x05_,y05_,z05_,x06_,y06_,z06_,x07_,y07_,
z07_,x08_,y08_,z08_,x09_,y09_,z09_,x010_,y010_,z010_,\[Mu]1_,\[Mu]2_,\[Mu]3_,
\[Mu]4_,\[Mu]5_, \[Mu]6_,\[Mu]7_,\[Mu]8_,\[Mu]9_,\[Mu]10_,spectraswitch_]:=
Module[{\[Nu],\[Beta],a,b,c,\[Sigma],cor0,\[Mu]},
\[Sigma]={{\[Sigma]x1,\[Sigma]y1,\[Sigma]z1},{\[Sigma]x2,\[Sigma]y2,\[Sigma]z
2},{\[Sigma
]x3,\[Sigma]y3,\[Sigma]z3},{\[Sigma]x4,\[Sigma]y4,\[Sigma]z4},{\[Sigma]x5,\[S
igma]y5,\
[Sigma]z5},{\[Sigma]x6,\[Sigma]y6,\[Sigma]z6},{\[Sigma]x7,\[Sigma]y7,\[Sigma]
z7},{\[Sigma
]x8,\[Sigma]y8,\[Sigma]z8},{\[Sigma]x9,\[Sigma]y9,\[Sigma]z9},{\[Sigma]x10,\[
Sigma]y10,\ [Sigma]z10}};
cor0={{x01,y01,z01},{x02,y02,z02},{x03,y03,z03},{x04,y04,z04},{x05,y05,z05},{
x06,y06,z06} ,{x07,y07,z07},{x08,y08,z08},{x09,y09,z09},{x010,y010,z010}};
\[Mu]={\[Mu]1,\[Mu]2,\[Mu]3,\[Mu]4,\[Mu]5,\[Mu]6,\[Mu]7,\[
Mu]8,\[Mu]9,\[Mu]10};
a=0;
b=0;
c=1/\[Beta];
\[Beta]=Sqrt[1-(0.511)^2/ee^2];
\[Lambda]=c1/\[Nu];
(Abs[Total[\[Mu][[#]]Exp[-((2\[Pi]^2)/\[Lambda]^2)(\[Sigma][[#]][[1]] ^2
a^2+\[Sigma][[#]][[2]]^2 b^2+\[Sigma][[#]][[3]]^2 c^2)]Exp[- I
(2\[Pi])/\[Lambda] (cor0[[#]][[1]]a+cor0[[#]][[2]]b+cor0[[#]][[3]
]c)]&/@Range[m]]])^2*If[spectraswitch=="on",Wy$DR,1]]
c1=300;
F[m_,\[Lambda]_,ee_,\[Theta]0_,
\[Theta]y_,\[Theta]x_,\[Sigma]x1_,\[Sigma]y1_,\[Sigma]z1_,\[
Sigma]x2_,\[Sigma]y2_,\[Sigma]z2_,\[Sigma]x3_,\[Sigma]y3_,\[Sigma]z3_,\[Sigma
]x4_,\[Sigma]y4_,\[Sigma
]z4_,\[Sigma]x5_,\[Sigma]y5_,\[Sigma]z5_,\[Sigma]x6_,\[Sigma]y6_,\[Sigma]z6_,\
[Sigma]x7_,\[Sigma]y7_,
\[Sigma]z7_,\[Sigma]x8_,\[Sigma]y8_,\[Sigma]z8_,\[Sigma]x9_,\[Sigma]y9_,\[Sig
ma]z9_,\[Sigma]x10_,\[
Sigma]y10_,\[Sigma]z10_,x01_,y01_,z01_,x02_,y02_,z02_,x03_,y03_,z03_,x04_,y04
_,z04_,x05_,y05_,z05_,x06_,y06_,z06_,x07_,y07_,
z07_,x08_,y08_,z08_,x09_,y09_,z09_,x010_,y010_,z010_,\[Mu]1_,\[Mu]2_,\[Mu]3_,
\[Mu]4_,\[Mu]5_, \[Mu]6_,\[Mu]7_,\[Mu]8_,\[Mu]9_,\[Mu]10_,spectraswitch_]:=
Module[{\[Nu],\[Beta],a,b,c,\[Sigma],cor0,\[Mu]},
\[Sigma]={{\[Sigma]x1,\[Sigma]y1,\[Sigma]z1},{\[Sigma]x2,\[Sigma]y2,\[Sigma]z
2},{\[Sigma
]x3,\[Sigma]y3,\[Sigma]z3},{\[Sigma]x4,\[Sigma]y4,\[Sigma]z4},{\[Sigma]x5,\[S
igma]y5,\
[Sigma]z5},{\[Sigma]x6,\[Sigma]y6,\[Sigma]z6},{\[Sigma]x7,\[Sigma]y7,\[Sigma]
z7},{\[Sigma
]x8,\[Sigma]y8,\[Sigma]z8},{\[Sigma]x9,\[Sigma]y9,\[Sigma]z9},{\[Sigma]x10,\[
Sigma]y10,\ [Sigma]z10}};
```

```
cor0={{x01,y01,z01},{x02,y02,z02},{x03,y03,z03},{x04,y04,z04},{x05,y05,z05},{
x06,y06,z06} ,{x07,y07,z07},{x08,y08,z08},{x09,y09,z09},{x010,y010,z010}};
\[Mu]={\[Mu]1,\[Mu]2,\[Mu]3,\[Mu]4,\[Mu]5,\[Mu]6,\[Mu]7,\[
Mu]8,\[Mu]9,\[Mu]10};
a=-Cos[\[Theta]x]Cos[\[Theta]y]-(Sin[\[Theta]y]-(Sqrt[1-(0.511)^2/ee^2])^-1)
/Tan[\[Theta]0];
b=-Cos[\[Theta]y]Sin[\[Theta]x];
c=-(Sqrt[1-(0.511)^2/ee^2])^-1;
\[Lambda]=c1/\[Nu];
(Abs[Total[\[Mu][[#]]Exp[-((2\[Pi]^2)/\[Lambda]^2)(\[Sigma][[#]][[1]] ^2
a^2+\[Sigma][[#]][[2]]^2 b^2+\[Sigma][[#]][[3]]^2 c^2)]Exp[- I
(2\[Pi])/\[Lambda] (cor0[[#]][[1]]a+cor0[[#]][[2]]b+cor0[[#]][[3]
]c)]&/@Range[m]])^2 If[spectraswitch=="on",Wy$TR,1]]
trainDistribution3D[m_,l_,\[Sigma]x1_,\[Sigma]y1_,\[Sigma]z1_,\[Sigma]x2_,\[S
igma]y2_,\[Sigma]z2_,\[Sigma]x3_,\[
Sigma]y3_,\[Sigma]z3_,\[Sigma]x4_,\[Sigma]y4_,\[Sigma]z4_,\[Sigma]x5_,\[Sigma
]y5_,\[Sigma]z5_,\[Sigma]
x6_,\[Sigma]y6_,\[Sigma]z6_,\[Sigma]x7_,\[Sigma]y7_,\[Sigma]z7_,\[Sigma]x8_,\
[Sigma]y8_,\[Sigma]z8_,
\[Sigma]x9_,\[Sigma]y9_,\[Sigma]z9_,\[Sigma]x10_,\[Sigma]y10_,\[Sigma]z10_,x0
1_,y01_,z01_,x02_,y02_,z02_,x03_,
y03_,z03_,x04_,y04_,z04_,x05_,y05_,z05_,x06_,y06_,z06_,x07_,y07_,z07_,x08_,y0
8_,z08_,x09_,y09_,z09_,x010_,y010_,z010_]:=
Module[{\[Sigma],cor0},
\[Sigma]={{\[Sigma]x1,\[Sigma]y1,\[Sigma]z1},{\[Sigma]x2,\[Sigma]y2,\[Sigma]z
2},{\[Sigma
]x3,\[Sigma]y3,\[Sigma]z3},{\[Sigma]x4,\[Sigma]y4,\[Sigma]z4},{\[Sigma]x5,\[S
igma]y5,\
[Sigma]z5},{\[Sigma]x6,\[Sigma]y6,\[Sigma]z6},{\[Sigma]x7,\[Sigma]y7,\[Sigma]
z7},{\[Sigma
]x8,\[Sigma]y8,\[Sigma]z8},{\[Sigma]x9,\[Sigma]y9,\[Sigma]z9},{\[Sigma]x10,\[
Sigma]y10,\ [Sigma]z10}};
cor0={{x01,y01,z01},{x02,y02,z02},{x03,y03,z03},{x04,y04,z04},{x05,y05,z05},{
x06,y06,z06} ,{x07,y07,z07},{x08,y08,z08},{x09,y09,z09},{x010,y010,z010}};
Ellipsoid[{cor0[[#]][[1]],cor0[[#]][[2]],-cor0[[#]][[3]]+l},{3\[Sigma][
[#]][[1]],3\[Sigma][[#]][[2]],3\[Sigma][[#]][[3]]}]&/@Range[m] ]
trainDistribution3D1[m_,Ne_,l_,\[Sigma]x1_,\[Sigma]y1_,\[Sigma]z1_,\[Sigma]x2
_,\[Sigma]y2_,\[Sigma]z2_,\[Sigma]x3_,
\[Sigma]y3_,\[Sigma]z3_,\[Sigma]x4_,\[Sigma]y4_,\[Sigma]z4_,\[Sigma]x5_,\[Sig
ma]y5_,\[Sigma]z5_,\[
Sigma]x6_,\[Sigma]y6_,\[Sigma]z6_,\[Sigma]x7_,\[Sigma]y7_,\[Sigma]z7_,\[Sigma
]x8_,\[Sigma]y8_,\[Sigma]
z8_,\[Sigma]x9_,\[Sigma]y9_,\[Sigma]z9_,\[Sigma]x10_,\[Sigma]y10_,\[Sigma]z10
_,x01_,y01_,z01_,x02_,y02_,z02_,
x03_,y03_,z03_,x04_,y04_,z04_,x05_,y05_,z05_,x06_,y06_,z06_,x07_,y07_,z07_,x0
8_,y08_,z08_,x09_,y09_,z09_,x010_,y010_,z010_ ,\[
Mu]1_,\[Mu]2_,\[Mu]3_,\[Mu]4_,\[Mu]5_,\[Mu]6_,\[Mu]7_,\[Mu]8_,\[Mu]
9_,\[Mu]10_]:=
Module[{gaussDistribution1bunch,\[Sigma],cor0,\[Mu]},
\[Sigma]={{\[Sigma]x1,\[Sigma]y1,\[Sigma]z1},{\[Sigma]x2,\[Sigma]y2,\[Sigma]z
2},{\[Sigma
]x3,\[Sigma]y3,\[Sigma]z3},{\[Sigma]x4,\[Sigma]y4,\[Sigma]z4},{\[Sigma]x5,\[S
igma]y5,\
[Sigma]z5},{\[Sigma]x6,\[Sigma]y6,\[Sigma]z6},{\[Sigma]x7,\[Sigma]y7,\[Sigma]
z7},{\[Sigma
]x8,\[Sigma]y8,\[Sigma]z8},{\[Sigma]x9,\[Sigma]y9,\[Sigma]z9},{\[Sigma]x10,\[
Sigma]y10,\ [Sigma]z10}};
cor0={{x01,y01,z01},{x02,y02,z02},{x03,y03,z03},{x04,y04,z04},{x05,y05,z05},{
x06,y06,z06} ,{x07,y07,z07},{x08,y08,z08},{x09,y09,z09},{x010,y010,z010}};
\[Mu]={\[Mu]1,\[Mu]2,\[Mu]3,\[Mu]4,\[Mu]5,\[Mu]6,\[Mu]7,\[
Mu]8,\[Mu]9,\[Mu]10};
```

```
gaussDistribution1bunch=MultinormalDistribution[{cor0[[#]][[1]],cor0[[#]][[2]
],-cor0[[#]][[3]]+l},{{\[Sigma
][[#]][[1]]^2,0,0},{0,\[Sigma][[#]][[2]]^2,0},{0,0,\[Sigma ][[#]][[3]]^2}}]&;
RandomReal[gaussDistribution1bunch[#],IntegerPart[k*\[Mu][[#]]]]&/@Range[m]]
(*Interferogram*)
Interferogram[m_,ee_,\[Theta]0_,
\[Theta]y_,\[Theta]x_,\[Sigma]x1_,\[Sigma]y1_,\[Sigma]z1_,\[Sigma]x2_,\[
Sigma]y2_,\[Sigma]z2_,\[Sigma]x3_,\[Sigma]y3_,\[Sigma]z3_,\[Sigma]x4_,\[Sigma
]y4_,\[Sigma]z4_,\[Sigma]
x5_,\[Sigma]y5_,\[Sigma]z5_,\[Sigma]x6_,\[Sigma]y6_,\[Sigma]z6_,\[Sigma]x7_,\
[Sigma]y7_,\[Sigma]z7_,
\[Sigma]x8_,\[Sigma]y8_,\[Sigma]z8_,\[Sigma]x9_,\[Sigma]y9_,\[Sigma]z9_,\[Sig
ma]x10_,\[Sigma]y10_,\[
Sigma]z10_,x01_,y01_,z01_,x02_,y02_,z02_,x03_,y03_,z03_,x04_,y04_,z04_,x05_,y
05_,z05_,x06_,y06_,z06_,x07_,y07_,z07_,x08_,y08_ ,
z08_,x09_,y09_,z09_,x010_,y010_,z010_,\[Mu]1_,\[Mu]2_,\[Mu]3_,\[Mu]4_,\[Mu]5_
,\[Mu]6_,
\[Mu]7_,\[Mu]8_,\[Mu]9_,\[Mu]10_,lmin_,lmax_,lstep_,\[Nu]minD_,\[Nu]maxD_,\[N
u]min_,\[
Nu]max_,Ne_,spectraswitch_]:=Module[{\[Lambda],a,b,c,BunchSeqFactor,Multiplie
rInt,SensDet,\[Nu],\[CapitalDelta]l,\[Beta],\[Sigma] ,cor0,\[Mu]},
\[Sigma]={{\[Sigma]x1,\[Sigma]y1,\[Sigma]z1},{\[Sigma]x2,\[Sigma]y2,\[Sigma]z
2},{\[Sigma
]x3,\[Sigma]y3,\[Sigma]z3},{\[Sigma]x4,\[Sigma]y4,\[Sigma]z4},{\[Sigma]x5,\[S
igma]y5,\
[Sigma]z5},{\[Sigma]x6,\[Sigma]y6,\[Sigma]z6},{\[Sigma]x7,\[Sigma]y7,\[Sigma]
z7},{\[Sigma
]x8,\[Sigma]y8,\[Sigma]z8},{\[Sigma]x9,\[Sigma]y9,\[Sigma]z9},{\[Sigma]x10,\[
Sigma]y10,\ [Sigma]z10}};
cor0={{x01,y01,z01},{x02,y02,z02},{x03,y03,z03},{x04,y04,z04},{x05,y05,z05},{
x06,y06,z06} ,{x07,y07,z07},{x08,y08,z08},{x09,y09,z09},{x010,y010,z010}};
\[Mu]={\[Mu]1,\[Mu]2,\[Mu]3,\[Mu]4,\[Mu]5,\[Mu]6,\[Mu]7,\[
Mu]8,\[Mu]9,\[Mu]10};
a=-Cos[\[Theta]x]Cos[\[Theta]y]-(Sin[\[Theta]y]-(Sqrt[1-(0.511)^2/ee^2])^-1)
/Tan[\[Theta]0];
b=-Cos[\[Theta]y]Sin[\[Theta]x];
c=-(Sqrt[1-(0.511)^2/ee^2])^-1;
\[Lambda]=c1/\[Nu];(*radiation wave length*)
BunchSeqFactor=Ne+Ne(Ne-1)(Abs[Total[\[Mu][[#]]Exp[-
((2\[Pi]^2)/\[Lambda]^2)(\[Sigma] [[#]][[1]]^2 a^2+\[Sigma][[#]][[2]]^2
b^2+\[Sigma][[#]][[3]] ^2 c^2)]Exp[-I (2\[Pi])/\[Lambda]
(cor0[[#]][[1]]a+cor0[[#]][[2]]b+
cor0[[#]][[3]]c)]&/@Range[m]])^2*If[spectraswitch=="on",Wy$TR,1];(*factor of
train*)
MultiplierInt=Abs[1+Exp[-((I*2\[Pi]*\[CapitalDelta]l)/\[Lambda])]]^2;(*factor
of interferometer*)
SensDet=Piecewise[{{1,\[Nu]minD<\[Nu]<\[Nu]maxD},{0,\[Nu]minD<\[Nu]&&\[Nu]>\[
Nu]maxD }}];(*sensitivity of detector*)
Table[{\[CapitalDelta]l,NIntegrate[BunchSeqFactor*SensDet*MultiplierInt,{\[Nu
],\[Nu]min,\[Nu]max},Method->{Automatic,"SymbolicProcessing"->False}]
},{\[CapitalDelta]l,lmin,lmax,lstep}]]
(*Interferogram*)
Interferogram1[m_,ee_,\[Theta]0_,
\[Theta]y_,\[Theta]x_,\[Sigma]x1_,\[Sigma]y1_,\[Sigma]z1_,\[Sigma]x2_,\[
Sigma]y2_,\[Sigma]z2_,\[Sigma]x3_,\[Sigma]y3_,\[Sigma]z3_,\[Sigma]x4_,\[Sigma
]y4_,\[Sigma]z4_,\[Sigma]
x5_,\[Sigma]y5_,\[Sigma]z5_,\[Sigma]x6_,\[Sigma]y6_,\[Sigma]z6_,\[Sigma]x7_,\
[Sigma]y7_,\[Sigma]z7_,
\[Sigma]x8_,\[Sigma]y8_,\[Sigma]z8_,\[Sigma]x9_,\[Sigma]y9_,\[Sigma]z9_,\[Sig
ma]x10_,\[Sigma]y10_,\[
Sigma]z10_,x01_,y01_,z01_,x02_,y02_,z02_,x03_,y03_,z03_,x04_,y04_,z04_,x05_,y
05_,z05_,x06_,y06_,z06_,x07_,y07_,z07_,x08_,y08_ ,
z08_,x09_,y09_,z09_,x010_,y010_,z010_,\[Mu]1_,\[Mu]2_,\[Mu]3_,\[Mu]4_,\[Mu]5_
```

```
,\[Mu]6_,
\[Mu]7_,\[Mu]8_,\[Mu]9_,\[Mu]10_,lmin_,lmax_,lstep_,\[Nu]minD_,\[Nu]maxD_,\[N
u]min_,\[
Nu]max_,Ne_,spectraswitch_]:=Module[{\[Lambda],a,b,c,BunchSeqFactor,Multiplie
rInt,SensDet,\[Nu],\[CapitalDelta]l,\[Beta],\[Sigma] ,cor0,\[Mu]},
\[Sigma]={{\[Sigma]x1,\[Sigma]y1,\[Sigma]z1},{\[Sigma]x2,\[Sigma]y2,\[Sigma]z
2},{\[Sigma
]x3,\[Sigma]y3,\[Sigma]z3},{\[Sigma]x4,\[Sigma]y4,\[Sigma]z4},{\[Sigma]x5,\[S
igma]y5,\
[Sigma]z5},{\[Sigma]x6,\[Sigma]y6,\[Sigma]z6},{\[Sigma]x7,\[Sigma]y7,\[Sigma]
z7},{\[Sigma
]x8,\[Sigma]y8,\[Sigma]z8},{\[Sigma]x9,\[Sigma]y9,\[Sigma]z9},{\[Sigma]x10,\[
Sigma]y10,\ [Sigma]z10}};
cor0={{x01,y01,z01},{x02,y02,z02},{x03,y03,z03},{x04,y04,z04},{x05,y05,z05},{
x06,y06,z06} ,{x07,y07,z07},{x08,y08,z08},{x09,y09,z09},{x010,y010,z010}};
\[Mu]={\[Mu]1,\[Mu]2,\[Mu]3,\[Mu]4,\[Mu]5,\[Mu]6,\[Mu]7,\[
Mu]8,\[Mu]9,\[Mu]10};
a=0;
b=0;
c=-(Sqrt[1-(0.511)^2/ee^2])^-1;
\[Lambda]=c1/\[Nu];(*radiation wave length*)

BunchSeqFactor=Ne+Ne(Ne-1)(Abs[Total[\[Mu]][[#]]Exp[-
((2\[Pi]^2)/\[Lambda]^2)(\[Sigma] [[#]][[1]]^2 a^2+\[Sigma][[#]][[2]]^2
b^2+\[Sigma][[#]][[3]] ^2 c^2)]Exp[-I (2\[Pi])/\[Lambda]
(cor0[[#]][[1]]a+cor0[[#]][[2]]b+
cor0[[#]][[3]]c)]&/@Range[m]])^2*If[spectraswitch=="on",Wy$DR,1];(*factor of
train*)
MultiplierInt=Abs[1+Exp[-((I*2\[Pi]*\[CapitalDelta]l)/\[Lambda])]]^2;(*factor
of interferometer*)
SensDet=Piecewise[{{1,\[Nu]minD<\[Nu]<\[Nu]maxD},{0,\[Nu]minD<\[Nu]&&\[Nu]>\[
Nu]maxD }}];(*sensitivity of detector*)
Table[{\[CapitalDelta]l,NIntegrate[BunchSeqFactor*SensDet*MultiplierInt,{\[Nu
],\[Nu]min,\[Nu]max},Method->{Automatic,"SymbolicProcessing"->False}]
},{\[CapitalDelta]l,lmin,lmax,lstep}]]
Framed[Manipulate[
Quiet[Grid@{{If[q=="TR",
Grid@{{If[t=="F(\[Lambda])",
Labeled[Plot[F[m,\[Lambda],ee,\[Theta]0 \[Degree], \[Theta]y
\[Degree],\[Theta]x \[Degree],\[Sigma]x1
,\[Sigma]y1,\[Sigma]z1,\[Sigma]x2,\[Sigma]y2,\[Sigma]z2,\[Sigma]x3,\[Sigma]y3
,\[Sigma]z3,\
[Sigma]x4,\[Sigma]y4,\[Sigma]z4,\[Sigma]x5,\[Sigma]y5,\[Sigma]z5,\[Sigma]x6,\
[Sigma]y6,\[Sigma
]z6,\[Sigma]x7,\[Sigma]y7,\[Sigma]z7,\[Sigma]x8,\[Sigma]y8,\[Sigma]z8,\[Sigma
]x9,\[Sigma]y9
,\[Sigma]z9,\[Sigma]x10,\[Sigma]y10,\[Sigma]z10,x01,y01,z01,x02,y02,z02,x03,y
03,z03,x04,y04,z04,x05
,y05,z05,x06,y06,z06,x07,y07,z07,x08,y08,z08,x09,y09,z09,x010,y010,z010,\[Mu]
1,\[Mu]2,\[Mu ]3,\[Mu]4,\[Mu]5,\[Mu]6,\[Mu]7,\[Mu]8,\[Mu]9,\[Mu]10,{\[Lambda
],\[Lambda]min,\[Lambda]max},
Frame->True,FrameLabel->{"\[Lambda], mm","F(\[Lambda]), rel. units."},
PlotStyle->{Thickness[.0035],Red},PlotRange->{0,1},
ImageSize->600,AxesStyle->{{Black,Thick},{Black,Thick}},
LabelStyle->{Large,Black,FontFamily->"Times"},
PlotPoints->pp,MaxRecursion->mr,ImagePadding->All],
"Form-factor and detector sensitivity function\nvs radiation
wavelength",Top,LabelStyle->{Large,Black,FontFamily->"Times"}],
Labeled[Plot[{Piecewise[{{1,\[Nu]minD<\[Nu]<\[Nu]maxD},{0,\[Nu]minD<\[Nu]&&\[
Nu]>\[ Nu]maxD}}],F[m,c1/\[Nu],ee,\[Theta]0 \[Degree], \[Theta]y
\[Degree],\[Theta]x \[Degree],
\[Sigma]x1,\[Sigma]y1,\[Sigma]z1,\[Sigma]x2,\[Sigma]y2,\[Sigma]z2,\[Sigma]x3,
\[Sigma]y3,\[
```

```
Sigma]z3,\[Sigma]x4,\[Sigma]y4,\[Sigma]z4,\[Sigma]x5,\[Sigma]y5,\[Sigma]z5,\[
Sigma]x6,\[Sigma]
y6,\[Sigma]z6,\[Sigma]x7,\[Sigma]y7,\[Sigma]z7,\[Sigma]x8,\[Sigma]y8,\[Sigma]
z8,\[Sigma]x9,
\[Sigma]y9,\[Sigma]z9,\[Sigma]x10,\[Sigma]y10,\[Sigma]z10,x01,y01,z01,x02,y02
,z02,x03,y03,z03,x04,
y04,z04,x05,y05,z05,x06,y06,z06,x07,y07,z07,x08,y08,z08,x09,y09,z09,x010,y010
,z010,\[Mu]1,\[Mu]
2,\[Mu]3,\[Mu]4,\[Mu]5,\[Mu]6,\[Mu]7,\[Mu]8,\[Mu]9,\[Mu]10,
spectraswitch]},{\[Nu],\[Nu]min,\[Nu]max},
Exclusions->None,
Frame->True,FrameLabel->{"\[Nu], GHz","F(\[Nu]), au"},
PlotStyle->{{Black,Dashed},{Thickness[.0035],Red}},PlotRange->{0,1.05},
PlotLegends->Placed[{Style[Text["detector
sensitivity"],Small],Style[Text["form-factor"],Small]},{Right,Center}],
ImageSize->600,AxesStyle->{{Black,Thick},{Black,Thick}},
LabelStyle->{Large,Black,FontFamily->"Times"},
PlotPoints->pp,MaxRecursion->mr,ImagePadding->All],
"Form-factor and detector sensitivity function\nvs radiation
frequency",Top,LabelStyle->{Large,Black,FontFamily->"Times"}]],
joy=Interferogram[m,ee,\[Theta]0 \[Degree], \[Theta]y \[Degree],\[Theta]x
\[Degree],\[Sigma]x1,\[Sigma]y1,
\[Sigma]z1,\[Sigma]x2,\[Sigma]y2,\[Sigma]z2,\[Sigma]x3,\[Sigma]y3,\[Sigma]z3,
\[Sigma]x4,\[
Sigma]y4,\[Sigma]z4,\[Sigma]x5,\[Sigma]y5,\[Sigma]z5,\[Sigma]x6,\[Sigma]y6,\[
Sigma]z6,\[Sigma]
x7,\[Sigma]y7,\[Sigma]z7,\[Sigma]x8,\[Sigma]y8,\[Sigma]z8,\[Sigma]x9,\[Sigma]
y9,\[Sigma]z9,
\[Sigma]x10,\[Sigma]y10,\[Sigma]z10,x01,y01,z01,x02,y02,z02,x03,y03,z03,x04,y
04,z04,x05,y05,z05,x06,
y06,z06,x07,y07,z07,x08,y08,z08,x09,y09,z09,x010,y010,z010,\[Mu]1,\[Mu]2,\[Mu
]3,\[Mu]
4,\[Mu]5,\[Mu]6,\[Mu]7,\[Mu]8,\[Mu]9,\[Mu]10,lmin,lmax,lstep,\[Nu]minD,
\[Nu]maxD,\[Nu]min,\[Nu]max,Ne,spectraswitch];
joy1=Transpose[{joy[[#]][[1]]&/@Range[Length[joy]],joy[[#]][[2]]&/@Range[Leng
th[joy]]/( joy[[#]][[2]]&/@Range[Length[joy]]//Max)}];
Labeled[ListLinePlot[joy1,
InterpolationOrder->2,AspectRatio->1/2,
PlotStyle->{{Blue},{Thick,Dashed, Darker@Red }},
Frame->True,FrameLabel->{"\[CapitalDelta]l, mm","Intensity, au"},
LabelStyle->{Large,Black,FontFamily->"Times"},
ImageSize->700,PlotRange->All],"Interferogram",Top,LabelStyle-
>{Large,Black,FontFamily->"Times"}]
}},
Grid@{{If[t=="F(\[Lambda])",
Labeled[Plot[F1[m,\[Lambda],ee,\[Theta]0 \[Degree], \[Theta]y
\[Degree],\[Theta]x \[Degree],\[Sigma]x1
,\[Sigma]y1,\[Sigma]z1,\[Sigma]x2,\[Sigma]y2,\[Sigma]z2,\[Sigma]x3,\[Sigma]y3
,\[Sigma]z3,\
[Sigma]x4,\[Sigma]y4,\[Sigma]z4,\[Sigma]x5,\[Sigma]y5,\[Sigma]z5,\[Sigma]x6,\
[Sigma]y6,\[Sigma
]z6,\[Sigma]x7,\[Sigma]y7,\[Sigma]z7,\[Sigma]x8,\[Sigma]y8,\[Sigma]z8,\[Sigma
]x9,\[Sigma]y9
,\[Sigma]z9,\[Sigma]x10,\[Sigma]y10,\[Sigma]z10,x01,y01,z01,x02,y02,z02,x03,y
03,z03,x04,y04,z04,x05
,y05,z05,x06,y06,z06,x07,y07,z07,x08,y08,z08,x09,y09,z09,x010,y010,z010,\[Mu]
1,\[Mu]2,\[Mu ]3,\[Mu]4,\[Mu]5,\[Mu]6,\[Mu]7,\[Mu]8,\[Mu]9,\[Mu]10,{\[Lambda
],\[Lambda]min,\[Lambda]max},
Frame->True,FrameLabel->{"\[Lambda], mm","F(\[Lambda]), rel. units."},
PlotStyle->{Thickness[.0035],Red},PlotRange->{0,1},
ImageSize->600,AxesStyle->{{Black,Thick},{Black,Thick}},
LabelStyle->{Large,Black,FontFamily->"Times"},
PlotPoints->pp,MaxRecursion->mr,ImagePadding->All],
```

```
"Form-factor and detector sensitivity function\nvs radiation
wavelength",Top,LabelStyle->{Large,Black,FontFamily->"Times"}],
Labeled[Plot[{Piecewise[{{1,\[Nu]minD<\[Nu]<\[Nu]maxD},{0,\[Nu]minD<\[
Nu]&&\[ Nu]>\[ Nu]maxD}}],F1[m,c1/\[Nu],ee,\[Theta]0 \[Degree], \[Theta]y
\[Degree],\[Theta]x \[Degree],
\[Sigma]x1,\[Sigma]y1,\[Sigma]z1,\[Sigma]x2,\[Sigma]y2,\[Sigma]z2,\[Sigma]x3,
\[Sigma]y3,\[
Sigma]z3,\[Sigma]x4,\[Sigma]y4,\[Sigma]z4,\[Sigma]x5,\[Sigma]y5,\[Sigma]z5,\[
Sigma]x6,\[Sigma]
y6,\[Sigma]z6,\[Sigma]x7,\[Sigma]y7,\[Sigma]z7,\[Sigma]x8,\[Sigma]y8,\[Sigma]
z8,\[Sigma]x9,
\[Sigma]y9,\[Sigma]z9,\[Sigma]x10,\[Sigma]y10,\[Sigma]z10,x01,y01,z01,x02,y02
,z02,x03,y03,z03,x04,
y04,z04,x05,y05,z05,x06,y06,z06,x07,y07,z07,x08,y08,z08,x09,y09,z09,x010,y010
,z010,\[Mu]1,\[Mu]
2,\[Mu]3,\[Mu]4,\[Mu]5,\[Mu]6,\[Mu]7,\[Mu]8,\[Mu]9,\[Mu]10,
spectraswitch]},{\[Nu],\[Nu]min,\[Nu]max},
Exclusions->None,
Frame->True,FrameLabel->{"\[Nu], GHz","F(\[Nu]), au"},
PlotStyle->{{Black,Dashed},{Thickness[.0035],Red}},PlotRange->{0,1.05},
PlotLegends->Placed[{Style[Text["detector
sensitivity"],Small],Style[Text["form-factor"],Small]},{Right,Center}],
ImageSize->600,AxesStyle->{{Black,Thick},{Black,Thick}},
LabelStyle->{Large,Black,FontFamily->"Times"},
PlotPoints->pp,MaxRecursion->mr,ImagePadding->All],
"Form-factor and detector sensitivity function\nvs radiation
frequency",Top,LabelStyle->{Large,Black,FontFamily->"Times"}]],

joy=Interferogram1[m,ee,\[Theta]0 \[Degree], \[Theta]y \[Degree],\[Theta]x
\[Degree],\[Sigma]x1,\[Sigma]y1,
\[Sigma]z1,\[Sigma]x2,\[Sigma]y2,\[Sigma]z2,\[Sigma]x3,\[Sigma]y3,\[Sigma]z3,
\[Sigma]x4,\[
Sigma]y4,\[Sigma]z4,\[Sigma]x5,\[Sigma]y5,\[Sigma]z5,\[Sigma]x6,\[Sigma]y6,\[
Sigma]z6,\[Sigma]
x7,\[Sigma]y7,\[Sigma]z7,\[Sigma]x8,\[Sigma]y8,\[Sigma]z8,\[Sigma]x9,\[Sigma]
y9,\[Sigma]z9,
\[Sigma]x10,\[Sigma]y10,\[Sigma]z10,x01,y01,z01,x02,y02,z02,x03,y03,z03,x04,y
04,z04,x05,y05,z05,x06,
y06,z06,x07,y07,z07,x08,y08,z08,x09,y09,z09,x010,y010,z010,\[Mu]1,\[Mu]2,\[Mu
]3,\[Mu]
4,\[Mu]5,\[Mu]6,\[Mu]7,\[Mu]8,\[Mu]9,\[Mu]10,lmin,lmax,lstep,\[Nu]minD,
\[Nu]maxD,\[Nu]min,\[Nu]max,Ne,spectraswitch];
joy1=Transpose[{joy[[#]][[1]]&/@Range[Length[joy]],joy[[#]][[2]]&/@Range[Leng
th[joy]]/( joy[[#]][[2]]&/@Range[Length[joy]]//Max)}];
Labeled[ListLinePlot[joy1,
InterpolationOrder->2,AspectRatio->1/2,
PlotStyle->{{Blue},{Thick,Dashed, Darker@Red }},
Frame->True,FrameLabel->{"\[CapitalDelta]l, mm","Intensity, au"},
LabelStyle->{Large,Black,FontFamily->"Times"},
ImageSize->700,PlotRange->All],"Interferogram",Top,LabelStyle-
>{Large,Black,FontFamily->"Times"}]]}}
]},
{
Labeled[Graphics3D[{
Black,Arrowheads[Large],{Arrow[{{0,0,0},{1.5*tar1,0,0}}],
Arrow[{{0,0,0},{0,1.5*tar1,0}}],
Arrow[{{0,0,-(m+3)*tar1},{0,0,1.5*tar1}}]},
Text[Style[ "X",Large,18],{2 *tar1,0,0}],
Text[Style[ "Y",Large,18],{0,2 *tar1,0}],
Text[Style[ "Z",Large,18],{0,0,2 *tar1}],
If[q=="TR",Rotate[{Green,Parallelepiped[{-tar1,-
tar1,0},{{2*tar1,0,0},{0,2*tar1,0}}]}, (90-\[Theta]0) \[Degree],{0,-1,0}]],
```

```
Rotate[Rotate[{Yellow,Polygon[{{r,0.2tar1,0.2tar1},{r,0.2tar1,-0.2tar1},{r,-
0.2tar1,-0.2tar1},{r,-0.2tar1, 0.2tar1}}]}],\[Theta]y \[Degree],{0,-
1,0}],\[Theta]x \[Degree],{0,0,1}],
If[l>0,{Blue,Rotate[Cone[{{l,0,0},{0,0,0}},0.05l],-(90-2\[Theta]0)\[Degree]
,{0,1,0}]}],Nothing],
If[u=="points",{Opacity[.9],Hue[ee/1500],( Point@trainDistribution3D1
[m,Ne,l,\[Sigma]x1,\[Sigma]y1,\[Sigma]
z1,\[Sigma]x2,\[Sigma]y2,\[Sigma]z2,\[Sigma]x3,\[Sigma]y3,\[Sigma]z3,\[Sigma]
x4,\[Sigma]y4,
\[Sigma]z4,\[Sigma]x5,\[Sigma]y5,\[Sigma]z5,\[Sigma]x6,\[Sigma]y6,\[Sigma]z6,
\[Sigma]x7,\[
Sigma]y7,\[Sigma]z7,\[Sigma]x8,\[Sigma]y8,\[Sigma]z8,\[Sigma]x9,\[Sigma]y9,\[
Sigma]z9,\[Sigma]
x10,\[Sigma]y10,\[Sigma]z10,x01,y01,z01,x02,y02,z02,x03,y03,z03,x04,y04,z04,x
05,y05,z05,x06,y06,z06,
x07,y07,z07,x08,y08,z08,x09,y09,z09,x010,y010,z010,\[Mu]1,\[Mu]2,\[Mu]3,\[Mu]
4,\[ Mu]5,\[Mu]6,\[Mu]7,\[Mu]8,\[Mu]9,\[Mu]10][[#]])&/@Range[m]},
{Opacity[.9],Hue[ee/1500],trainDistribution3D[m,l,\[Sigma]x1,\[Sigma]y1,\[Sig
ma]z1,\[Sigma]x2,\[Sigma]y2,
\[Sigma]z2,\[Sigma]x3,\[Sigma]y3,\[Sigma]z3,\[Sigma]x4,\[Sigma]y4,\[Sigma]z4,
\[Sigma]x5,\[
Sigma]y5,\[Sigma]z5,\[Sigma]x6,\[Sigma]y6,\[Sigma]z6,\[Sigma]x7,\[Sigma]y7,\[
Sigma]z7,\[Sigma]
x8,\[Sigma]y8,\[Sigma]z8,\[Sigma]x9,\[Sigma]y9,\[Sigma]z9,\[Sigma]x10,\[Sigma
]y10,\[Sigma]z10,
x01,y01,z01,x02,y02,z02,x03,y03,z03,x04,y04,z04,x05,y05,z05,x06,y06,z06,x07,y
07,z07,x08,y08,z08,x09, y09,z09,x010,y010,z010]}]
},
ImageSize->{1000,500},PlotRange->{{-1.05 r,1.05 r},{-1.05 r,1.05 r},{1.05 r,-
1.05 r-(m+1.5)*tar1}},PlotRangePadding ->0.001,
ViewVertical->{-1,0,0},ViewVector->{{x,y,z},{0,0,0}},Axes->False,AxesLabel-
>{"mm","mm", "mm"},AxesStyle-
>{Directive[Black,12],Directive[Black,12],Directive[Black,12]},AxesEdge-
>{{1,-1},{-1,1},{ -1.1}}],
"3D scheme of electron bunch train",Top,LabelStyle->{Large,Black,FontFamily-
>"Times"}]
}}],
Style["Form-factor parameters",Bold,18,Red],Delimiter,
Control[{{spectraswitch,"off",Style["single electron spectra
switcher",Bold,18]},{"on","off"},RadioButton}],Delimiter,
Control[{{q,"TR",Style["radiation
type",Bold,18]},{"TR","DR"},RadioButton}],Delimiter,
Control[{{t,"F(\[Nu])",Style["form-factor
vs",Bold,18]},{"F(\[Lambda])","F(\[Nu]) "},RadioButton}],Delimiter,
Style["train parameters",Bold,18],
{{Ne,1000,Style["number of electrons",18]},1000,10000,1000,Appearance-
>"Open"},
{{m,2,Style["number of bunches",18]},1,10,1,Appearance->"Open"},
{{ee,10,Style["energy [MeV]",18]},1,1000,Appearance->"Open"},Delimiter,
Column[{Style["bunches sizes",Bold,18],
Row@{
Column@{
Column[{Control[{{\[Sigma]x1,0.1,Style["Subscript[\[Sigma],
x1][mm]",18]}}],Control[{{\[Sigma]y1,0.1, Style["Subscript[\[Sigma],
y1][mm]",18]}}],Control[{{\[Sigma]z1,0.12,Style["Subscript[\[Sigma], z1][mm]
",18]}}]}],Spacer[50],
Column[{Control[{{\[Sigma]x2,0.1,Style["Subscript[\[Sigma],
x2][mm]",18]}}],Control[{{\[Sigma]y2,0.1, Style["Subscript[\[Sigma],
y2][mm]",18]}}],Control[{{\[Sigma]z2,0.12,Style["Subscript[\[Sigma], z2][mm]
",18]}}]}],Spacer[50],
Column[{Control[{{\[Sigma]x3,0.01,Style["Subscript[\[Sigma],
x3][mm]",18]}}],Control[{{\[Sigma]y3,0.01, Style["Subscript[\[Sigma],
```

```
y3][mm]",18]}}]),Control[{{\[Sigma]z3,0.01,Style["Subscript[\[Sigma], z3][mm]
",18]}}]}]}],Spacer[50],
Column[{Control[{{\[Sigma]x4,0.01,Style["Subscript[\[Sigma],
x4][mm]",18]}}]),Control[{{\[Sigma]y4,0.01, Style["Subscript[\[Sigma],
y4][mm]",18]}}]),Control[{{\[Sigma]z4,0.01,Style["Subscript[\[Sigma], z4][mm]
",18]}}]}]}],Spacer[50],
Column[{Control[{{\[Sigma]x5,0.01,Style["Subscript[\[Sigma],
x5][mm]",18]}}]),Control[{{\[Sigma]y5,0.01, Style["Subscript[\[Sigma],
y5][mm]",18]}}]),Control[{{\[Sigma]z5,0.01,Style["Subscript[\[Sigma], z5][mm]
",18]}}]}]}]}],Spacer[50],
Column@{
Column[{Control[{{\[Sigma]x6,0.01,Style["Subscript[\[Sigma],
x6][mm]",18]}}]),Control[{{\[Sigma]y6,0.01, Style["Subscript[\[Sigma],
y6][mm]",18]}}]),Control[{{\[Sigma]z6,0.01,Style["Subscript[\[Sigma], z6][mm]
",18]}}]}]}],Spacer[50],
Column[{Control[{{\[Sigma]x7,0.01,Style["Subscript[\[Sigma],
x7][mm]",18]}}]),Control[{{\[Sigma]y7,0.01, Style["Subscript[\[Sigma],
y7][mm]",18]}}]),Control[{{\[Sigma]z7,0.01,Style["Subscript[\[Sigma], z7][mm]
",18]}}]}]}],Spacer[50],
Column[{Control[{{\[Sigma]x8,0.01,Style["Subscript[\[Sigma],
x8][mm]",18]}}]),Control[{{\[Sigma]y8,0.01, Style["Subscript[\[Sigma],
y8][mm]",18]}}]),Control[{{\[Sigma]z8,0.01,Style["Subscript[\[Sigma], z8][mm]
",18]}}]}]}],Spacer[50],
Column[{Control[{{\[Sigma]x9,0.01,Style["Subscript[\[Sigma],
x9][mm]",18]}}]),Control[{{\[Sigma]y9,0.01, Style["Subscript[\[Sigma],
y9][mm]",18]}}]),Control[{{\[Sigma]z9,0.01,Style["Subscript[\[Sigma], z9][mm]
",18]}}]}]}],Spacer[50],
Column[{Control[{{\[Sigma]x10,0.01,Style["Subscript[\[Sigma],
x10][mm]",18]}}]),Control[{{\[Sigma]y10,0.01, Style["Subscript[\[Sigma],
y10][mm]",18]}}]),Control[{{\[Sigma]z10,0.01,Style["Subscript[\[Sigma],
z10][mm] ",18]}}]}]}]}]}}}]],Delimiter,
Column[{Style["bunches displacement",Bold,18],
Row@{
Column@{
Column[{Control[{{x01,0,Style["Subscript[x,
1][mm]",18]}}]),Control[{{y01,0,Style["Subscript[y, 1][mm
]",18]}}]),Control[{{z01,0,Style["Subscript[z, 1][mm]",18]}}]}],Spacer[50],
Column[{Control[{{x02,0,Style["Subscript[x,
2][mm]",18]}}]),Control[{{y02,0,Style["Subscript[y, 2][mm
]",18]}}]),Control[{{z02,3.6,Style["Subscript[z, 2][mm]",18]}}]}],Spacer[50],
Column[{Control[{{x03,0,Style["Subscript[x,
3][mm]",18]}}]),Control[{{y03,0,Style["Subscript[y, 3][mm
]",18]}}]),Control[{{z03,0.2,Style["Subscript[z, 3][mm]",18]}}]}],Spacer[50],
Column[{Control[{{x04,0,Style["Subscript[x,
4][mm]",18]}}]),Control[{{y04,0,Style["Subscript[y, 4][mm
]",18]}}]),Control[{{z04,0.3,Style["Subscript[z, 4][mm]",18]}}]}],Spacer[50],
Column[{Control[{{x05,0,Style["Subscript[x,
5][mm]",18]}}]),Control[{{y05,0,Style["Subscript[y, 5][mm
]",18]}}]),Control[{{z05,0.4,Style["Subscript[z, 5][mm]",18]}}]}]}],Spacer[50],
Column@{
Column[{Control[{{x06,0,Style["Subscript[x,
6][mm]",18]}}]),Control[{{y06,0,Style["Subscript[y, 6][mm
]",18]}}]),Control[{{z06,0.5,Style["Subscript[z, 6][mm]",18]}}]}],Spacer[50],
Column[{Control[{{x07,0,Style["Subscript[x,
7][mm]",18]}}]),Control[{{y07,0,Style["Subscript[y, 7][mm
]",18]}}]),Control[{{z07,0.6,Style["Subscript[z, 7][mm]",18]}}]}],Spacer[50],
Column[{Control[{{x08,0,Style["Subscript[x,
8][mm]",18]}}]),Control[{{y08,0,Style["Subscript[y, 8][mm
]",18]}}]),Control[{{z08,0.7,Style["Subscript[z, 8][mm]",18]}}]}],Spacer[50],
Column[{Control[{{x09,0,Style["Subscript[x,
9][mm]",18]}}]),Control[{{y09,0,Style["Subscript[y, 9][mm
]",18]}}]),Control[{{z09,0.8,Style["Subscript[z, 9][mm]",18]}}]}],Spacer[50],
```

```
Column[{Control[{{x010,0,Style["Subscript[x,
10][mm]",18]}}],Control[{{y010,0,Style["Subscript[y, 10][mm
]",18]}}],Control[{{z010,0.9,Style["Subscript[z,
10][mm]",18]}}]}]}]}}],Delimiter,
Column[{Style["train's charge ratio",Bold,18],
Row@{
Column[{Control[{{\[Mu]1,0.5,Style["Subscript[\[Mu], 1]",18]},0,1,Appearance-
>"Open"}],Control[{{ \[Mu]2,0.5,Style["Subscript[\[Mu],
2]",18]},0,1,Appearance->"Open"}],Control[{{\[Mu]3,0.1
,Style["Subscript[\[Mu], 3]",18]},0,1,Appearance-
>"Open"}],Control[{{\[Mu]4,0.1,Style["Subscript[\ [Mu],
4]",18]},0,1,Appearance-
>"Open"}],Control[{{\[Mu]5,0.1,Style["Subscript[\[Mu], 5]"
,18]},0,1,Appearance->"Open"}]}],
Column[{Control[{{\[Mu]6,0.1,Style["Subscript[\[Mu], 6]",18]},0,1,Appearance-
>"Open"}],Control[{{ \[Mu]7,0.1,Style["Subscript[\[Mu],
7]",18]},0,1,Appearance->"Open"}],Control[{{\[Mu]8,0.1
,Style["Subscript[\[Mu], 8]",18]},0,1,Appearance-
>"Open"}],Control[{{\[Mu]9,0.1,Style["Subscript[\ [Mu],
9]",18]},0,1,Appearance-
>"Open"}],Control[{{\[Mu]10,0.1,Style["Subscript[\[Mu], 10]"
,18]},0,1,Appearance->"Open"}]}]}]}}],Delimiter,

Style["target tilt",Bold,18],
{{\[Theta]0.45,Style["Subscript[\[Theta], 0] [Degree]",18]},0,
90.5,Appearance->"Open"},Delimiter,
Style["detector position",Bold,18],
Row@{
Control[{{\[Theta]x,0,Style["Subscript[\[Theta], x] [Degree]",18]},-90,
90.5,Appearance->"Open"}],Spacer [60],
Control[{{\[Theta]y,0,Style["Subscript[\[Theta], y] [Degree]",18]},-90,
90.5,Appearance->"Open"}]}, delimiter,
Style["spectra range",Bold,18],
Row@{
Column[{Control[{{\[Lambda]min,0.003,Style["Subscript[\[Lambda],
min][mm]",18]},0,100,Appearance->"Open"}],Control[{
{\[Lambda]max,0.5,Style["Subscript[\[Lambda],
max][mm]",18]},0.05,101,Appearance->"Open"}]}],Spacer[50],
Column[{Control[{{\[Nu]min,0.001,Style["Subscript[\[Nu],
min][GHz]",18]},0.001,9,Appearance->"Open"}],Control
[{{\[Nu]max,800,Style["Subscript[\[Nu], max][GHz]",18]},0.1,10000,Appearance-
>"Open"}]}]},
delimiter,
Style["Precision",Bold,18],
{{pp,2,Style["PlotPoints ",18]},{2,4,5,8,10}},
{{mr,10,Style["MaxRecursion ",18]},{2,4,5,8,10}},
delimiter,
Style["3D scheme parameters",Bold,18,Red],Delimiter,
Control[{{u,"ellipsoids",Style["3D bunch
representation",Bold,18]},{"points","ellipsoids"},RadioButton}],Delimiter,
{{tar1,1,Style["target size[mm]",18]},0.09,2.7,Appearance->"Open"},
{{r,2.3tar1,Style["distance between target and detector[mm]",18]},2
tar1,4tar1,Appearance->"Open"},
{{l,-1.5 tar1,Style["bunch movement",18]},-1.5 tar1,(m+1.5)*tar1,Appearance-
>"Open"},
delimiter,
Style["Camera",Bold,18],
{{z,5,Style["Z position",18]},-100,100,1},
{{y,-16,Style["Y position",18]},-100,100,1},
{{x,-3,Style["X position",18]},-100,100,1},
delimiter,
Style["Detector sensitivity range",Bold,18,Red],
```

```
{{\[Nu]minD,500,Style["Subscript[Detector, min]
[GHz]",18]},0.001,10000,Appearance->"Open"},{{\[Nu]maxD,700,
Style["Subscript[Detector, max] [GHz]",18]},0.001,10000,Appearance->"Open"},
delimiter,
Style["Interferogram settings",Bold,18,Red],
{{lmin,-20,Style["Subscript[\[CapitalDelta]l, min] [mm]",18]}, -
40,0,5,Appearance->"Open"},{{lmax,20, Style["Subscript[\[CapitalDelta]l, max]
[mm]",18]},-40,40,Appearance->"Open"},
{{lstep,0.1,Style["Inerferogamme plotting step [mm]",18]},0.1,2,Appearance-
>"Open"},
ControlPlacement->Flatten[{Table[Left,36],Table[Right,21]}],SaveDefinitions-
>True]]
```

APPENDIX D

```
ListOfCoordinates[k_,m_,l_,\[Sigma]x_,\[Sigma]y_,\[Sigma]z_]:=Partition[Flatt
en[Table[RandomVariate[MultinormalDistribution[{0,0,zi},({\[
Sigma]x^2,0,0},{0,\[Sigma]y^2,0},{0,0,\[Sigma]z^2}}],k],{zi,Table[l
*o,{o,1,m}]}]],3];
r=ListOfCoordinates[100,2,3.6,0.1,0.1,0.12];
n=Length[r]
c1=300.;
ee=10.;
\[Theta]x=0.degree;
\[Theta]y=0.degree;
\[Theta]0=45. degree;
a=-Cos[\[Theta]x]Cos[\[Theta]y]-(Sin[\[Theta]y]-(Sqrt[1-(0.511)^2/ee^2])^-1)
/Tan[\[Theta]0];
b=-Cos[\[Theta]y]Sin[\[Theta]x];
c=-(Sqrt[1-(0.511)^2/ee^2])^-1;
s={a,b,c};
Graphics3D[Point[r]]
DiscreteFormFactor1[\[Nu]_]:=Module[{f},f[x_]:=Re[Exp[I (2\[Pi] \[Nu])/c1
s.(r[[#]]- x)]]&/@Range[n];
(Total[ParallelMap[f,r],2]-n)/(n(n-1))]
DiscreteFormFactor2[\[Nu]_]:=(Abs[ParallelSum[Exp[I (2\[Pi]
\[Nu])/c1*s.(r[[i]]-r[[j]])] ,{i,1,n},{j,1,n}]]-n)/(n(n-1));
TableOfDiscreteFormFactor=Table[{\[Nu],DiscreteFormFactor1[\[Nu]]},{\[Nu],1,1
001.,5}]
ListLinePlot[TableOfDiscreteFormFactor]
```